Multi Three-Cluster Coupling Model of Nuclear Reactions

Kazuya Miyagawa

(February, 1987)

Department of Applied Mathematics
Faculty of Engineering Science
Osaka University
Toyonaka, Osaka 560, Japan

Abstract

Two alternative versions of practicable connected kernel theories of nuclear reactions are proposed. The basic assumption is that the state of a many-body system can be approximated by a superposition of two- and three-cluster states corresponding to various possible reaction processes. The approach is based on the concept of transitions due to particle exchange as in the Amado-Lovelace (AL) formalism. All important three-cluster partitions can be incorporated via multi-channel couplings in two-cluster subsystems. The simpler of two models, which is called the Multi Three-Cluster Coupling (MTCC) model, is a direct extension of the AL formalism. Using the separable representation of two-cluster potentials, the AL type coupled equations among reaction amplitudes are postulated. The basic assumption in this model, as well as in the AL and AGS theories, is shown to contain some degree of inconsistency regarding the treatment of bound state pole parts of interacting pairs. This is remedied in the other model, which we call the Multi Two- and Three-Cluster coupling (MTTC) model. This model can treat all possible processes within the limitation of two- and three-cluster approximation.

In the first stage of the application to nuclear reactions, we employ a simpler version of the MTCC model that is represented by only one three-cluster partition, but that involves absorption effects in the two-cluster subsystems. We name it the absorption model. The absorption model and the MTCC model are applied to

the d-α elastic scattering at E_d= 21 and 56 MeV. The results of the analyses suggest that the explicit couplings among the three-cluster partitions (n,p,α), (n,d,^{3}He) and (p,d,^{3}H) give rise to the conspicuous structures in the tensor analyzing powers at 56 MeV that have not been resolved by any other reaction theories.

Contents

§ 1 Introduction

1.1 General scope of three-body and many-body scattering theories

Conventional nuclear reaction theories such as the Distorted Wave Born Approximation (DWBA) and the Coupled Reacton Channel (CRC) method have been applied successfully to reactions that are essentially describable as two-body problems with phenomenological optical potentials[1,2]. These treatments lose their validity in reactions where processes more complcated than two-body are strongly coupled, because such processes cannot be treated in terms of the two-body Lippmann-Schwinger (LS) equations even if optical potential parameters are phenomenologically adjusted.

In order to treat nuclear reactions as three-body problems but still within the conventional treatments, two approaches based on the CRC method have been proposed, which are called the Coupled Continuum Channel method[3], and the Coupled Discretised Continuum Channel method[4]. However, as shown in Ref. 5, in these approaches, either a model space must be assumed or some sort of an L^2 discretization has to be introduced in order to be able to solve a three-body LS equation. As is made clear in Ref. 5, such procedures either do not give a convergent solution, or else affect breakup amplitudes in a serious manner by destroying phase relations among three particles. Futhermore, in these conventional treatments, there can be no rearrangement channel components in the asymptotic region. In other words, the

three-body LS equation can not satisfy all possible three-body boundary conditions. This fact is closely related to the non-uniqueness problem of a single three-body LS equation (a review of this problem is given in Ref. 5). To obtain a solution which satisfies all three-body boundary conditions correctly in compliance with the unitarity requirement, the theory must be founded on the Faddeev formalism[6] or some equivalent connected kernel theories[7].

The quantum theory of scattering of three-body systems based on rigorous mathematical treatments was eatablished by Faddeev[6]. Since then, this theory has been extended by many authors[7]. In particular, Alt, Grassberger and Sandhas (AGS) treat scattering amplitudes directly in operator form, and obtain a set of coupled integral equations for amplitudes with the Faddeev kernel[8]. These theories have been applied successfuly to three nucleon problems, but there have been only a few application to nuclear reactions. For example, the analyses on d-α[9~13] scatterings have revealed a lot of reaction mechanisms which are inherent in many-body scattering processes. However, the theory has been applied only to reactions where the scattering states can be approximately described by only one three-cluster partition, and where each of the three clusters can be regarded as inert. This restriction is due mainly to the fact that practical methods of treating effects other than purely three-body partition have not been established.

Obviously, we must develop a theory that can meet the current interests in remarkably advanced experiments that concern

with such many-body effects. Let us compare, for example, the result of a purely three-body Faddeev calculation[14] with the experimental data on the tensor analyzing powers in $\alpha(\vec{d},d)\alpha$ mesured at E_d=20 MeV[15] and 56 MeV[16]. At both energies, optical model analyses demand strong tensor terms in the potentials which exceed the folding model values. The authors in Ref. 16 describe that the tensor potential at 56 MeV is roughly in accordance with the one at 20 MeV. They suggest that the anomalies in both cases are of the same physical origins. However, our analyses[14] with no adjustable parameters at the same energies yield different conclusions. The observables at 20 MeV are well reproduced by the three-body model represnted by the partition (N, N,α). However, the data for tensor analyzing powers at 56 MeV are not reproduced at all by this model. This fact means that the structures in the tensor analyzing powers at 56 MeV reflect the more complex mechanisms than the purely three-body one. This shows that we have to construct approaches more sophisticated than either the Faddeev or the conventional ones.

There exist the so-called N-body connected kernel theories[17,18] that are the generalizations of the three-body Faddeev formalism for many-body systems. These theories, however, are difficult to apply to nuclear reactions because of their complicated representations. Some efforts have been made to generate effective approximation schemes to these theories. Greben and Levin reduce the Channel Coupling Array (CCA) theory[18], one of the many-body scattering theories, to a set of two-body equations and assess the validity of the DWBA and CRC

schemes[19]. They introduce the bound state approximation into the channel Green functions to avoid disconnected diagrams. Thus, breakup effects can not be incorporated. Without the bound state apprximation, the CCA equation can not be solved. Hence it seems hard to extend it to more complicated scatterings.

Another approximation scheme has been proposed by Redish[20] based on his connected kernel equations. He decomposes the equations into a hierachy of nested equations in increasingly many variables. The first equation is a set of LS equations coupling together all two-cluster channels, the second is a two-variable integral equations for the effective interactions appearing in the first equation, and so on. The hierachy can be truncated at any level as one wishes, and particular partitions can be selected within each level. This treatment offers a fine perspective of the many-body scattering and provides a framework for extending usual direct reaction pictures. However, here again, for realistic analyses, it seems inevitable to introduce further approximations or effective phenomenological stands.

In view of the discussions presented above, we conclude that a practicable yet divergence-free connected kernel method has to be established which embodies many-body effects reflected in recent experimental results in a unified manner and which complies with the unitarity requirement.

1.2 Outline of the present work

In this paper, we propose two alternative versions of connected kernel theories that possess both practicability and versatility. We name these models the Multi Three-Cluster Coupling (MTCC) model and the Multi Two- and Three-Cluster coupling (MTTC) model. The basic assumption is that the state of a many-body system can be approximated by a superposition of two- and three-cluster states corresponding to various possible reaction processes. We intend to study those nuclear direct reaction processes that concern with a few degrees of freedom, in view of high experimental interests in the present-day stage relating to three-body or, at most, four-body effects. We utilize separable two-cluster interactions to formulate the scattering processes in a simple set of one-variable integral equations. This makes the formalism practicable. On this basic stand, we introduce various three-cluster partitions in addition to the original one in order to cope with a wide class of nuclear reactions.

In the MTCC model, various three-cluster partitions that cause strong influence on scattering processes are explicitly taken into accont by means of the method proposed by Ueda in his study of πNN and ρNN systems[21]. These partitions are coupled to one another via possible rearragement processes between two-cluster subsystems. Each of three-cluster partitions is treated as a Faddeev system. All reaction processes that are expected to be only weakly coupled to the scattering state are not considered explicitly but are incorporated into the

two-cluster processes as absorption effects. The conception as mentioned above are formulated in a set of coupled integral equations for scattering amplitudes in a manner similar to the Amado-Lovelace (AL) formalism[22], in which transitions between particle channels are assumed to be due to particle exchanges.

The MTTC model is an extention of the MTCC model. It incorporates sequential transfer processes that are missing from the MTCC as well as the Faddeev approaches. It can be shown that such processes amount to inducing new couplimg schemes between three-cluster partitions in the MTCC model. As a result, the MTTC model can treat all possible processes within the limitation of two- and three-cluster approximation.

As mentioned above, in our models, we introduce absorption effects into two-cluster subsystems in order to simulate weak-coupling processes or processes more complicated than three-cluster one. However, how to treat absorption effects in two-cluser subsytems in a three-cluster model has been a unsettled theoretical problem. A straightforward manner to incorporate absorption effects is the use of a phenomenological optical potential[23]. However, this method contains a serious problem of not knowing how to extend the complex potential to off-shell energy regions analytically. In this regard, a multi-channel two-body interactions has advantage. In our models, we introduce multi-channel separable interactions into two-cluster subsystems. The first channel is assigned to the two-cluster elastic channel and the second one to an inelastic channel, and so on. We also include a dummy channel to reprsent

the effects of various reaction channels that are not considered explicitly. The t-matrix for this multi-channel interaction is determined by fitting various scattering data to be considerd explicitly as well as by reproducing bound state poles. In three-cluster calculations, when the components of the t-matrix other than that of the dummy channel are utilized as inputs, it can be shown that such treatment is equivalent to using the optical potential obtained by eliminating the dummy reaction channel from coupled Schrödinger equations. Therefore, it gives rise to absorptions.

Our basic tool throughout the present work is a multi-channel two-cluster interaction of separable form. This interaction has all required properties in the MTCC and MTTC model, i.e. not only representing the rearrangement processes that connect various three-cluster partitions, but also simulating absorption effects by the perturbative treatment as mentioned above. Furthermore, the separable representation in the two-cluster interaction enables us to deal with a set of simple one-variable integral equations.

The simplest version of the MTCC model is to restrict to the initial three-cluster partition only, but with the effects of other three-cluster partitions, together with other many-body effects, contained in two-cluster t-matrices as absorption effects. This restricted version of the MTCC model is a relatively simple three-cluster model but it differs from the Faddeev theory by the inclusion of the absorption effects. Therefore, we name this model the absorption model. Thus, the

absorption model is an immediate extension of the Faddeev theory. We expect the model to be applicable to a wide class of nuclear collisions which can be characterized by three-body features.

In this paper, we apply the absorption model and the MTCC model to d-α elastic scatterings at relatively high incident energies, and discuss many-body effects reflected in the scattering observables. The organization of this paper is as follows. In § 2, we formulate the multi-channel two-body t-matrix of separable form. The property of the t-matrix is investigated in the negative energy region as well as in the scattering region. The exclusion of the Pauli forbidden states by the orthogonal projection method is also discussed. Further we explain the conditions to be imposed upon the analytic property of the t-matrix for the contour deformation method in three-cluster calculations. In § 3, we describe the absorption model as a restricted version of the MTCC model. Absorption effects are simulated by using the multi-channel t-matrix proposed in § 2. This model is applied to the d-α elastic scatterings at E_d= 21 and 56 MeV. The disagreement with the experiments at 56 MeV forces us to introduce the three-cluster partitions (n,d,^{3}He) and (p,d,^{3}H) in addition to (n,p,α). In § 4, we present the MTCC model, where the scattering processes are represented by various three-cluster partitions. According to the spirit of the AL formalism, it is formulated in a set of one-variable integral equations for scattering amplitudes. We apply it to the d-α elastic scattering at E_d= 56 MeV, where the three-cluster partitions (n,p,α), (n,d,^{3}He) and (p,d,^{3}H) are

taken into account explicitly. At the end of section 4, we mention the MTTC model as an extention of the MTCC model. Summary and discussions are given in § 5.

§ 2 Two-body separable t-matrix with channel-coupling effects

Our basic tool throughout the present work is a multi-channel two-body interaction of separable form. The two-body t-matrix obtained by the interaction is used as an input to three-body calculations in the following sections. First, the two-body t-matrix is derived by solving coupled Lippmann-Schwinger equations. Some remarks are given for the case that non-orthogonal channels exist. Next, we investigate the bound state problem and extract spectroscopic factors in channels. In § 2.2, we describe a treatment of Pauli forbidden states, which are projected away to infinite energy by the orthogonal projection method[24]. In § 2.3, the analytic property of a multi-channel t-matrix is discussed that is needed for the contour deformation in three-body calculations.

2.1 Multi-channel formulation of a separable t-matrix

We consider the system which is constructed by two composite particles. The Hamiltonian of this system is denoted by

$$H = H_\alpha + V_\alpha + K_\alpha \quad , \tag{2.1}$$

where H_α is the cluster-internal Hamiltonian, V_α is the cluster-external interaction and K_α is the relative kinetic energy operator between the center-of-mass of two clusters in two-cluster partition α. First, we consider the case where no rearrangement channels exist. Thus, there is only one

two-cluster partition to be considered and the operators H_α, V_α and K_α are defined uniquely. (The case when rearrangement processes exist will be discussed later.)

Now, we introduce a model space expanded by the eigenstates of H_α, $\{|\chi_i\rangle \mid i=1,N\}$, which specify the internal bound states of two clusters. Here, these states satisfy with the orthogonality relations,

$$\langle\chi_i|\chi_j\rangle = \delta_{ij} \quad (i,j=1,N) \quad . \tag{2.2}$$

Hence, the problem amounts to the multi-channel two-body problem where the channels are defined according to the internal states of two clusters. The two-body coupling potential V is expressed as N×N matrix, the components of which are

$$V_{ij} = \langle\chi_i| V_\alpha |\chi_j\rangle \quad (i,j=1,N) \quad . \tag{2.3}$$

The Lippmann-Schwinger equation for the t-matrix of this coupled two-body system is represented by

$$t(e) = V + V\, G_0(e)\, t(e) \quad , \tag{2.4}$$

where V, $G_0(e)$ and t(e) are N×N matrices and the matrix $G_0(e)$ is diagonal by the requirement of Eq. (2.2).

Now, a two-body multi-channel separable potential is introduced,

$$V = |g\rangle \lambda \langle g| \quad . \tag{2.5}$$

Here, λ is the strength parameter and $|g\rangle$ is the form factor which are expressed by the column vector corresponding to the multi-channel couplings,

$$|g\rangle = \begin{pmatrix} |g_1\rangle \\ |g_2\rangle \\ \vdots \\ |g_N\rangle \end{pmatrix} \quad . \tag{2.6}$$

The components $|g_i\rangle$ (i=1,N) describe the relative motion of two clusters in channel i. For example, for a p-α system, they can be assigned to the channels such as p-α(the ground state) and p-α^*(a excited state). If needed, higer-rank interactions can be employed but we shall maintain the form of rank-1 for simplicity. The Lippmann-Schwinger equation, Eq. (2.4), can be solved for the interaction given by Eq. (2.5) so that the t-matrix is represented by the following separable form,

$$t(e) = |g\rangle \tau(e) \langle g| \quad . \tag{2.7}$$

Here, $\tau(e)$ describes the propagation of two interacting clusters and is given by

$$\tau(e) = \left[\lambda^{-1} - \sum_{i=1}^{N} \langle g_i | G_0^{(i)}(e) | g_i \rangle \right]^{-1} \quad . \tag{2.8}$$

$G_0^{(i)}(e)$ is the free Green function in channel i,

$$G_0^{(i)}(e) = \left((e-E_i) - K_\alpha + i\varepsilon \right)^{-1} , \qquad (2.9)$$

where E_i is the sum of the internal energies of two clusters in channel i. The summation on i in Eq. (2.8) shows the channel-coupling effects.

Now, we discuss an important extension of this formalism to treat a wide class of two-cluster processes. When rearramgement channels exist, the Hamiltonian H in Eq. (2.1) must be defined to each channel in a different manner. Therefore, the orthogonality relations between internal states in the channels as given by Eq. (2.2) are no longer valid. Hence, one might consider that serious modifications have to be brought into our formalism. However, it is not necessary. The detailed explanation will be deferred to Appendix A, and here only the essential points are mentioned. In this case, the coupled channel equations contain the non-orthogonality terms, namely the overlap integrals between the wave functions of non-orthogonal channels which include only the kinetic energy operators but no interactions between two clusters. If we define the coupling potential between the channels in terms of only cluster-external interactions such as in Eq. (2.3), then not only that it becomes non-hermitian but the free Green function contains non-diagonal elements. Such treatment gives rise to troubles in our approach. However, in our point of view, the non-orthogonality terms should be regarded as a part of the coupling interaction. This is natural and reasonable because they arise due to the overlaps between the

wave functions of non-orthogonal channels. As a result of including the non-orthogonality terms in the coupling interaction, the free Green function becomes diagonal and the coupling interaction hermitian. In this treatment, the two-body t-matrix takes the usual form expressed by Eqs. (2.7)∿(2.9), and the effects of the non-orthogonality terms are incorporated into the off-shell components of the coupling potential V. In the determination of the two-body t-matrix as an input to three-body calculations, we take a phenomenological stand that they are simulated by experimental data, i.e. information at on-shell region.

Next, we shall investigate the bound state problem with the channel-coupling potential and extract a spectroscopic factor in each channel. Here, we restrict ourselves to the case where rearrangement channels do not exist. For the Hamiltonian defined by Eq. (2.1), the Schrödinger equation is written down as

$$(e_B - H_\alpha - K_\alpha)|\Psi_B\rangle = V_\alpha|\Psi_B\rangle \quad , \tag{2.10}$$

where e_B and $|\Psi_B\rangle$ represent a binding energy and a bound state in two-cluster system, respectively. Projecting Eq. (2.10) on the i-th internal state of two clusters , $|\chi_i\rangle$, and substituting the coupling interaction V in Eq. (2.5) into the equation, we obtain

$$(e_B - E_i - K_\alpha)|\psi_i\rangle = A|g_i\rangle \quad , \tag{2.11}$$

where $|\psi_i\rangle$ is the i-th projection of $|\Psi_B\rangle$ and the factor A is

defined by

$$A = \sum_{j=1}^{N} \lambda \langle g_j | \psi_j \rangle \quad . \tag{2.12}$$

Therfore, from Eq. (2.11) the i-th component of $|\Psi_B\rangle$ is expressed as

$$|\psi_j\rangle = A\, G_0^{(i)}(e_B)\, |g_i\rangle \quad . \tag{2.13}$$

The factor A is determined by the normalization condition,

$$1 = \langle \Psi_B | \Psi_B \rangle = \sum_{i=1}^{N} \langle \psi_i | \psi_i \rangle \quad , \tag{2.14}$$

where

$$\langle \psi_i | \psi_i \rangle = A^2 \langle g_i |\, G_0^{(i)}(e_B)\, G_0^{(i)}(e_B)\, |g_i\rangle \quad . \tag{2.15}$$

Here, we find that the overlap $\langle \psi_i | \psi_i \rangle$ is the probability strength of the i-th component of the bound state $|\psi_B\rangle$ and its square root corresponds to the spectroscopic factor of the component.

2.2 Exclusion of Pauli forbidden states

In this subsection, we describe a method of excluding Pauli forbidden states in two-cluster subsystems. One of the shortcomings in the three-body Faddeev calculation has been that the effects of the Pauli exclusion can not be treated correctly. Indeed, two-cluster t-matrices as inputs to the calculation may have the bound state poles corresponding to Pauli forbidden states in the negative energy region. However, the orthogonal projection method which has been introduced by Kukulin et al.[24] enables us to treat two-cluster systems in the subspace which is orthogonal to forbidden states. This method is handy in our practice because a forbidden state can be projcted away to infinite energy by incorporating an additional potential of separable form.

Let us consider the bound state supported by the two-cluster separable interaction (2.5), which should be forbidden by the Pauli principle. We denote this state by $|\Psi_B\rangle$. Following the prescription of the orthogonal projection method, we introduce a pseudo-potential of a rank-2 separable form,

$$V_\Lambda = |g\rangle\lambda\langle g| + |\Psi_B\rangle\Lambda\langle\Psi_B| \quad , \tag{2.16}$$

where $|g\rangle\lambda\langle g|$ is the original coupling potential and Λ is a parameter which will be made to become infinity in the final stage. Solving the modified Lippmann-Schwinger equation defined by

$$t_\Lambda(e) = V_\Lambda + V_\Lambda\, G_0(e)\, t_\Lambda(e) \quad , \tag{2.17}$$

we obtain the t-matrix for the pseudo-potential,

$$t_\Lambda(e) = \sum_{k,\ell=1,2} |h_k\rangle\, \tau_{\Lambda,k\ell}(e)\, \langle h_\ell| \quad , \tag{2.18}$$

where $|h_k\rangle$ is defined by

$$|h_k\rangle = \begin{cases} |g\rangle & (k=1) \\ |\Psi_B\rangle & (k=2) \end{cases} \quad , \tag{2.19}$$

and $\tau_{\Lambda,k\ell}(e)$ is the (k,ℓ) component of the 2×2 matrix $\tau_\Lambda(e)$,

$$\tau_\Lambda(e) = \left[\begin{pmatrix} \lambda^{-1} & 0 \\ 0 & \Lambda^{-1} \end{pmatrix} - \begin{pmatrix} \langle g|G_0(e)|g\rangle & \langle g|G_0(e)|\Psi_B\rangle \\ \langle \Psi_B|G_0(e)|g\rangle & \langle \Psi_B|G_0(e)|\Psi_B\rangle \end{pmatrix} \right]^{-1} . \tag{2.20}$$

Now, Turning to the limit $\Lambda\to\infty$, we obtain

$$\tau_\infty(e) = \left[\begin{pmatrix} \lambda^{-1} & 0 \\ 0 & 0 \end{pmatrix} - \begin{pmatrix} \langle g|G_0(e)|g\rangle & \langle g|G_0(e)|\Psi_B\rangle \\ \langle \Psi_B|G\ (e)|g\rangle & \langle \Psi_B|G\ (e)|\Psi_B\rangle \end{pmatrix} \right]^{-1} . \tag{2.21}$$

Since $|\Psi_B\rangle$ is orthogonal to scattering states, the introduction of pseudo-potential of (2.16) does not affect the scatteing state at all. Therefore, the sacttering observables remain exactly the same as before. Futhermore, the bound state is shifted by Λ so that by letting $\Lambda\to\infty$ the Pauli forbidden bound state is projected

away to infinity. Thus we can construct the two-clustr t-matrix,

$$t_{\infty}(e) = \sum_{k,\ell=1,2} |h_k\rangle \, \tau_{\infty,k\ell}(e) \, \langle h_\ell| \qquad (2.22)$$

in which the effects of the Pauli forbiden state are excluded.

2.3 Analytic property of a multi-channel t-matrix

A major difficulty in three-body calculations is the treatment of singularities of the kernel in coupled integral equations. The rotated contour method introduced by Hetherington and Schick[25] solved this problem, and we can perform stable calculations on a complex integration path. However, the succesful application of this method requires us to have the knowledge of the analytic property of the kernel, which includes the two-body propagator $\tau(e)$ as a source of singularities. Therefore, in order to bring channel-coupling t-matrices into three-body calculations, we shall investigate their analytic properties conditioned by the rotated contour method.

In the single-channel case, the analytic property of the two-body t-matrix is discussed on the complex plane of the relative momentum between two clusters. However, it is not convenient in the case of many channels because the t-matrix is considered as the function of channel momenta which are dependent on one another. Therefore, we introduce another variable, as in Ref. 26, on which the t-matrix is continued analytically. we consider the two-channel case which is relatively simple. The relative momentum k_i between two clusters in channel i is defined by

$$\frac{k_i^2}{2\mu_i} = (e-E_i) \qquad (i=1,2) \quad , \tag{2.23}$$

where e is the total energy, μ_i is the reduced mass and E_i is the

internal energy of two clusters in channel i. By energy conservation, k_1 is related to k_2 by

$$\frac{k_1}{2\mu_1} - \frac{k_2}{2\mu_2} = E_2 - E_1 \quad . \tag{2.24}$$

Now, we introduce the variable z defined by

$$\Delta\, \mu_2^{1/2}\, z = \mu_2^{1/2}\, k_1 + \mu_1^{1/2}\, k_2 \quad , \tag{2.25}$$

or

$$\Delta\, \mu_2^{1/2}\, z^{-1} = \mu_2^{1/2}\, k_1 - \mu_1^{1/2}\, k_2 \quad , \tag{2.26}$$

where Δ is defined by

$$\Delta^2 = 2\mu_1(E_2-E_1) \quad . \tag{2.27}$$

According to Eqs. (2.25) and (2.26), we can write

$$k_1 = \Delta\, (z + z^{-1})/2 \quad , \tag{2.28}$$

and

$$k_2 = \Delta\, (\mu_2/\mu_1)^{1/2}\, (z - z^{-1})/2 \quad . \tag{2.29}$$

Eqs (2.28) and (2.29) constitute a mapping of the Riemann energy surface to the complex z plane. The mapping is shown in Fig. 1. The numbers in each square bracket indicate the quadrants to which k_1 and k_2 belong in each complex plane.

Now, we discuss the condition with which the two-channel t-matrix has to satisfy for the rotated contour method in three-body calculations. In such calculations, the contour is usually rotated into the fourth quadrant in the complex plane of the relative momentum between spectators and center-of-masses of interacting two clusters. Then, the energy e in the two-cluster system runs on a complex path, the imaginary value of which is positive. Therefore, in the complex z plane, the path is mapped into region [1,1]. As a result, the two-cluster t-matrix must be constructed with no singurality in the region [1,1].

§ 3 Three-body AGS theory with absorption effcts in tw-body subsystems

In this section, we propose a restricted form of the MTCC model, where the scattering processes are represented by only one three-cluster partition. However, it includes absorption effects in the two-cluster subsystems. Thus this model is an immediate extension of the three-body Faddeev approach. Therefore, We name this model the absorption model. In § 3.1, We simulate absorption effects in two-cluster subsystems by using the multi-channel separable interaction proposed in § 2. In § 3.2, the absorption model is applied to the d-α scatterings at E_d= 21 and 56 MeV. The scattering processes are represented by the three-cluster partition (N,N,α). In the (N,α) subsystem, absorption effects are included. The Pauli-forbidden state of $s_{1/2}$ in this subsystem is excuded by the orthogonal projection method. As expected, absorption effects are notable at E_d= 56 MeV. At the end of this section, the discrepancy between the theory and experiments at 56 MeV is discussed.

3.1 The absorption model

In addition to the N-d scattering, the three-body model can be introduced naturally to the reactions between loosely-bound projectiles and targets which are not easily excited. Now, let us consider the collision bwtween the deuteron and such a nucleus denoted by A for simplicity. The degree of freedom that should

be taken into account first of all is the three-body kinematics between N, N and A, which is accomplished by the Faddeev theory. The problem is how to treat effectively the many-body processes induced by the interaction between N and A. In real scatterings, there are two possible cases. One is that the elastic channel in the subsystem is coupled weakly to other reaction channels. The other is the case where there exist some conspicuous channels which bring strong reflections into the elastic one. In the former case, the treatment based on the concept of the optical model can be applied, namely the effect of reaction processes other than the elastic one is described by the disappearance of a part of flux from the elastic channel. However, in the latter, the more sophisticated approaches should be introduced. Putting off the latter to the following section, we shall investigate the former case and formulate our absorption model.

As mentioned in §1, the immediate introduction of a complex potential causes a serious problem how to extend the potential to off-shell energy regions analytically. In this regard, the multi-channel interaction proposed in §2 has advantage. Let us adopt the two-channel coupling potential of Eq. (2.5). The first channel is assigned to the elastic N-A channel, and the second to a hybrid channel which represents all reaction channels such as inelastic and rearrangement ones. The two-channel form factor of the expression (2.6) is writen as

$$|g\rangle = \begin{pmatrix} |g_1\rangle \\ |g_2\rangle \end{pmatrix} = \begin{pmatrix} \sqrt{1-\kappa}\,|f_1\rangle \\ \sqrt{\kappa}\,|f_2\rangle \end{pmatrix}, \qquad (3.1)$$

where κ is a coupling strength parameter. Then the two-body t-matrix for the coupling potential can be expressed by 2x2 matrix of Eq. (2.7). The elastic component t_{11} of the t-matrix is determined in each partial wave by fitting the energy of a bound state and on-shell experimental data of N-A elastic scatterings. (Taking a higher-rank potential, it is possible to reproduce plural bound states.) In the three-body equation, only the elastic component obtained by the above procedure is utilized in order to represent the two-body processes. This is justified by the assumption that the coupling between elastic and reaction channels are weak enough to be incorporated into the intermediate states only.

Now we demonstrate that our treatment amounts to replacing the N-A interaction by its optical potential V_{opt} and confirm that it produces absorption effects in the elastic channel. From Eq. (A.6) we obtain

$$V_{opt} = |g_1\rangle \left[\lambda^{-1} - \langle g_2| G_0^{(2)}(e)|g_2\rangle \right]^{-1} . \qquad (3.2)$$

This is derived in Appendix B. Notice that the denominator of V_{opt} is real below the reaction threshold while it is complex above it. On the other hand, t_{11} as an input to the three-body equations is the same as the t-matrix t_{opt} of this optical potential, which is also shown explicitly in Appendix B. Thus, we find that t_{11} produces absorption effects in the elastic channel.

3.2 An application to the d-α elastic scattering

The d-α scattering at relatively low incident energies have been studied well by a number of theoretical approsches[9~12,27]. Among them, the three-body Faddeev calculation has been most successful in reproducing the experimental data. Indeed, it explains surprisingly well cross sections and analyzing powers in breakup scatterings as well as elastic ones below $E_d \simeq$ 20 MeV (14 MeV CM). This fact means that the three-body effects by N,N,α play the main role in the energy region where α can be regarded as inert. At higher energies, however, there have been only a few analyses[13,28] and the effective approach has not yet been established. This is because the situation is rather complicated at higher energies. Aside from the deuteron breakup, the first reaction channel ^{3}H-^{3}He opens at the center-of-mass energy 14.3 MeV. The second channel that opens up is the ^{3}H-d-p channel at 19.8 MeV, which is followed by a number of individual reaction channels. For realistic analyses, it seems inevitable to take the effects of these channels into account in some ways. Now, we examine the validity of our absorption model by applying it in this energy region. We adopt the three-cluster partition (N,N,α) as a first approximation based on the success in lower energy scatterings. First, the two-body interaction in the n-α subsystem is constructed by the method mentioned in § 3.1. Then we analyze the elastic scatterings $\alpha(\vec{d},d)\alpha$ at E_d = 21 and 56 MeV.

3.2.1 Separable t-matrix for the N-α subsystem.

In the three-body calculations, we ignore the Coulomb force , which is expected not to exert serious influence on kinematical regions other than the forward scattering. Furthermore, we igonore the mass-difference between p and n. Therefore, we consider the p-α system and the n-α system as the same. Then, in this system, we find the first reaction channel d-^{3}He at 18.4 MeV in CM. The p-α^* and p-n-^{3}He channels closely follow it. To incorporate the effect of these and other reaction channels, we adopt the two-channel separable interaction of the form of Eq. (2.5) with form factor (3.1). All reaction channels are bunched together and are represented by a hybrid dummy channel. The first channel is assigned to the elastic p-α channel and the second channel to the dummy one. The threshold of the hybrid channel is fixed at E_2= 18.4 MeV, which is the threshold of the d-^{3}He channel as mentioned above. After partial wave decomposition, we adopt the Yamaguchi type form factor as $|f_i\rangle$ (i=1,2) in Eq. (3.1), namely

$$f_i(p) = p^{\ell i}/(p^2+\beta_i^2)^{\ell i+1} \quad (i=1,2) \ , \qquad (3.3)$$

where p is the relative momentum and ℓ_i is the orbital angular momentum of channel i. Then the input t_{11} to the three-body calculation contains the five parameters λ, κ, β_1, β_2 and ℓ_2 in each partial wave. Here the orbital angular momentum ℓ_2 of the hybrid channel takes only the values which would be satisfied with the total angular momentum and parity conservation if the

channel is regarded as one of reaction channels. The values of these parameters are searched to reproduce the p-α phase shifts and the absorption coefficients at E_p(lab)=0 to 55 MeV, in seven partial waves s1/2, p1/2, p3/2, d3/2, d5/2, f5/2 and f7/2[29].

The resulting values are shown in Table 1, and the fits to the data in Fig. 2. It is found that the simple rank-1 separable potential can reproduce surprisingly well the elastic scattering data over the wide range of proton incident energies. As shown in Fig. 2, the most striking feature of the phase shifts is the dominance of absorption above the inelastic threshold in even partial waves. We find that the threshold behavior of them strongly influences on the values of ℓ_2. The notable structure of $d_{3/2}$ is due to the well-known resonance, which is of almost pure d-^{3}He character[30]. Our fit to the structure is unsatisfactory but it is caused by the fact that we strain to obtain the overall best fit over a wide energy range with a simple rank-1 potential. However, we confirm that our potential of $d_{3/2}$ state has a pole in the region [1,3] of the complex z plane defined in § 2.3. This pole is near the inelatic threshold (z=1 and k_2=0) and gives rise to the structure in Fig. 2.

Finally, we mention the exclusion of a Pauli forbidden state. Our potential of $s_{1/2}$ supports a bound state at E_1= -13.09 MeV, which should be forbidden by the Pauli principle. To avoid such unphysical bound state, two kinds of potentials have previously been used, i.e. a repulsive and a strongly attractive potential[9,10]. However, as mentioned in § 2.2, it is now possible to exclude Pauli forbidden states explicitly by the

orthogonal projection method. We adopt this method and project the bound state of $s_{1/2}$ away to infinite energy.

3.2.2 The d-α elastic scattering

We calculate the d-α elastic scattering in terms of the Faddeev formalism. The scattering processes are represented by only one three-cluster partition (N,N,α), but absorption effects are included in the (N,α) subsytem, which is accomplished by utilizing the t-matrix mentioned in § 3.2.1. No Coulomb force is included. We start with the Alt-Grassberger-Sandhas (AGS) equation[8]:

$$U_{ij} = (1-\delta_{ij})(E-H_0) + \sum_{k=i} t_k G_0 U_{kj} \quad (i,j,k=1,2,3) \ , \qquad (3.4)$$

where particle channels 1, 2 and 3 are assigned to α(n,p), n(p,α) and p(n,α) respectively. The use of the two-body t-matrix of separable form enables us to reduce the AGS equation to the well-known Amado-Lovelace (AL) equation[22]:

$$X_{ij} = Z_{ij} + \sum_{k\neq i} Z_{ik} \tau_k X_{kj} \ , \qquad (3.5)$$

where X_{ij} and Z_{ij} denote the scattering amplitude and Born amplitude from particle channel j to i, respectively. The propagator of interacting pair in particle channel is denoted by τ_i. Notice that the labels which specify channel states are omitted. Since we neglect the Coulomb force, channel 3 is identical with channel 2 except for the isospin states. Then

Eq. (3.5) is reduced to

$$\begin{pmatrix} I_{11} \\ I_{21} \end{pmatrix} = \begin{pmatrix} 0 \\ Z_{21} \end{pmatrix} + \begin{pmatrix} 0 & Z_{12}\tau_2 \\ 2Z_{21}\,\tau_1 & -Z_{32}\,\tau_2 \end{pmatrix} \begin{pmatrix} I_{11} \\ I_{21} \end{pmatrix} , \quad (3.6)$$

where the amplitudes I_{11} and I_{12} are defined by

$$I_{11} = X_{11}/2 \quad , \quad I_{12} = (X_{21}-X_{31})/2 \quad . \quad (3.7)$$

The detailes of the reduction are described in Refs 9 and 10.

For the two-body interaction between two nucleons, we adopt the separable interactions of Doleshall[31], Phillips[32] and Cahill and Sloan[33]. We take into account only the coupled $^3S_1$-$^3D_1$ state. For the N-α subsystem, we employ the elastic component of the two-channel t-matrix constructed in § 3.2.1 which includes absorption effcts, and in which the Pauli forbidden state of $s_{1/2}$ is excluded.

In numerical calculations, we utilize the rotated contour method[25] to avoid singularities of the kernel of Eq. (3.7). Some remarks due to the introduction of the two-channel t-matrix has already been mentioned in § 2.3. In solving the equation, we employ the Pade approximant[34].

The results at E_d(Lab) = 21 and 56 MeV are shown in Figs. 3 and 4. The experiments have been performed in Tsukuba[35] and RCNP[16]. The solid lines indicate the calculations in which both effects of absorption and the Pauli exclusion are included. We adopt the YY7 potential of Phillips[32] as the N-N interaction,

which is rank-1 with 7 % deuteron D-state probability. As shown in Fig. 3, quite good agreements with the data are obtained in the analyzing powers as well as the cross section at E_d= 21 MeV, which improve the Charnomordic's results[9]. However, at E_d= 56 MeV the data can not be reproduced well, especially the analyzing powers at $\theta_{CM} > 90°$. The fact that our simple model succeeds at E_d= 21 Mev but fails at 56 MeV indicates the need to include more reaction channels at E_d= 56 MeV. The details will be discussed later.

The absorption effects due to the hybrid reaction channel at 18.4 MeV (CM) in the (N,α) subsystem are investigated. We re-adjust the potential parameters and construct a single-channel interaction which reproduces well the p-α phase shifts but has no absorption. The results of three-body calculations with this interaction are shown by the dashed lines in Figs. 3 and 4. At E_d= 21 MeV, the difference between the results with and without absorption effects are not appreciable. On the other hand, the effect of the coupling to the hybrid reaction channel is large at E_d= 56 MeV. This is to be expected because no reaction channel opens at E_d= 21 MeV, whereas the incident energy of E_d= 56 MeV, is well above the threshhold of the hybrid channel.

We also investigate the effects of the Pauli exclusion. The dashed-dot lines in Figs. 3 and 4 represent the calculations without the Pauli exclusion of the $s_{1/2}$ bound state in the (N,α) subsystem. Comparing with the results including the Pauli exclusion (solid lines), we find that the effect is relatively small at E_d= 21 MeV but it is large at 56 MeV. This fact can be

explained qualitatively by the following consideration. First, for the Pauli exclusion to be effective, the incident wave (prior to the application of the Pauli exclusion) has to penetrate to within the interaction region. The shallowness of the potential as evidenced by the smallness of the binding energy (-13.09 MeV) of this Pauli-forbidden state has the consequence that at high energies the mismatching of wave numbers inside and outside the potential is immaterial and hence the transmission to within the interaction region can occur relatively freely, while at low energies the mismatching is large and therefore the transmission is hindered. Therefore, we expect the effect of the Pauli projection to be small at E_d= 21 MeV but to become substantial at 56 MeV.

Next, we examine to what extent the results depend on the property of the N-N potentials utilized in the three-body calculations. In d-α scatterings below E_d= 21 MeV, the effect of the tensor force in the coupled $^3S_1$-$^3D_1$ partial wave has been discussed by a number of authors. Based on the three-body calculation of the elastic sacttering at E_d= 12 MeV, Charnomordic et al.[9] claim that the presence of the tensor force is not essential for both cross section and analyzing powers. On the other hand, the recent analyses of the breakup reactions at E_d= 12 and 21 MeV by Ishikawa et al.[36] indicate that the double differential cross section and the vector analyzing power are explainable without the tensor force, but for the tensor analyzing powers, the inclusion of the tensor force is essential. We perform the computations with a number of N-N interactions

beside the YY7 potentials. In Figs. 5 and 6, the dashed lines represent the results with the YY0 potential of Cahill and Sloan[33], which is rank-1 with no deuteron D state. The comparison with the results by YY7 (solid lines) shows that at E_d= 21 MeV the tensor force is indispensable for reproducing the data of the analyzing powers, T_{20} and T_{22}. At E_d= 56 MeV, results with YY0 are almost null for the tensor analyzing powers at forward angles $\theta_{CM} < 90°$ and fail to reproduce the experimental data.

We have also performed the calculation with the 2T4 potential of Doleshall[31] which is of rank-2 with 4% deuteron D-state probability and which reproduces the experimental $^3D_1$ phase shifts as well as $^3S_1$ phase shifts. As shown in Fig. 7, the difference between the results with YY7 and with 2T4 are not appreciable but in the tensor analyzing power T_{20}, the fit to the data by 2T4 is somewhat worse than the fit by YY7. This is puzzling and needs further investigation. we mention that at E_d= 56 MeV the results with other tensor potentials YY4[32](rank-1) and 2T7[31](rank-2) do not exhibit substantial changes in the results with YY7 in all observables.

Finally, in Fig. 8, we show the results with and without f-waves in the (N,α) subsystem at E_d= 56 MeV. The inclusion of the f-waves gives rise to a large contribution at large deuteron scattering angles. At E_d= 21 MeV, we find that the contribution of the f-waves is almost null.

§ 3.2.3 Discussions

In this section, we propose the absorption model, and apply it to the d-α elastic scatterings at E_d = 21 and 56 MeV. The reasons why we choose these two energies are the following:

(1) At 21 MeV, the three-body model with no absorption effects has previously shown to be successful. Hence, we can check the absorption model by comparing with the previous results.

(2) As mentioned already, at 56 MeV the situation is rather complicated, since there are various reaction channels such as ^{3}He +^{3}H, n+d+^{3}He and n+p+α* beside n+p+α. Therefore it is interesting to examine the validity of the absorption model.

As expected, at 21 MeV, the present results reproduce the experimental data well, and even improve previous results somewhat. The absorptive effects in the (N,α) system are found to be small. On the other hand, at 56 MeV absorption effects are notable. However, the conspicuous diffraction-like structures in the data of analyzing powers can not be reproduced.

In investigating the cause of the disagreement, we should recall the assumption imposed on the absorption model that the couplings between elastic and reaction channels in the (N,α) subsystem are weak enough to be incorporated as absorption effects. Now, we scrutinize this assumption. The fact that the resonance in the $d_{3/2}$ partial wave is almost purely d-^{3}He character, as mentioned in § 3.2.1, suggests that the coupling between the p-α and the d-^{3}He channel is not weak. Futhermore, the reaction cross sections of p+α → d+^{3}He above the threshold

amount to nearly 50 per cent of the total reaction cross sections of p+α scttarings[37]. In view of these data and the results of the present analyses, we consider that the validity of the above assumption is doubtful and that the effects of the d-^{3}He channel should be investigated explicitly. However, the explicit treatment of the d-^{3}He channel in the (n,α) subsytem forces us to introduce a new three-cluster partition (n,d,^{3}He). The method that is capable of treating various three-cluster partitions will be proposed in the next section, and the effects of the partition (n,d,^{3}He) will be investigated.

§ 4 The Multi Three-Cluster Coupling (MTCC) model

In the MTCC model, various three-cluster partitions in addition to the initial partition are introduced, corresponding to possible processes to be considered explicitly. They are coupled to one another via two-cluster rearrangement processes, and each of which is treated as a Faddeev system. This model is applied to the d-α elastic scattering at E_d= 56 MeV, where the absorption model is not successful. As we show, the MTCC effects are evident especially at large angles. Only process missing from the MTCC model within the limitation of the two- and three-cluster approximation is the process of sequential transfer. At the end of this section, we mention briefly the Multi Two- and Three-Cluster coupling (MTTC) model which succeeds in incorporating this process.

4.1 The MTCC model

The absorption model proposed in § 3 is the three-body model represented by only one three-cluster partition, although it includes the coupling between the elastic and reaction channels in the two-body subsystems as absorption effects. As discussed in § 3.2.3, the method lose the validity when the coupling between the elastic and reaction channels become strong because the weak-coupling assumption breaks down. The explicit consideration of such two-cluster reaction processes requires the introduction of new three-cluster partitions which differ from

the original one. The formulation of a practical unified theory of nuclear reactions in which scattering processes among various three-cluster partitions are coupled has not been reported to date. The MTCC model accomplishes this problem. The basic conception of the model may be described as follows. Various three-cluster partitions which are coupled strongly to one another are taken into account explicitly. Each of them is treated as a three-body Faddeev system and is coupled to other three-cluster partitions via interactions between two-cluster subsystems. Other reaction processes which do not affect the scattering state appreciably are incorporated into two-cluster processes as absorption effects.

We formulate the above concept in a manner similar to the Amado-Lovelace (AL) formalism[22]. For each three-cluster partitions, there is a triad of three-particle channels each consisting of an interacting pair of particles and a spectater particle. We impose two-basic rules for the MTCC approach.

Rule 1 In each Faddeev system, the transition between particle channels is due to particle exchange.

The only exception to Rule 1 is the Coulomb interaction which is not considered in the present work. If needed, the effect can be treated in an approximate manner.

Rule 2 Interacting pairs can break up into two clusters but spectator particles can not.

Under these rules, possible rearrangement or inelastic processes between interacting pairs which belong to various Faddeev systems generate the couplings between the Faddeev systems. The

scattering processes are represented by a superposition of various three-cluster processes. By the use of separable interactions, we arrive at a set of coupled integral equations among reaction amplitudes of the AL form.

The model may be best explained by means of the explicit example of the d-α scattering. In addition to (n,p,α), let us consider, for example, the three-cluster partitions (n,d,^{3}He) and (p,d,^{3}H). The three-cluster partition (n,d,^{3}He) can be coupled to the partition (n,p,α) via the rearrangement process between two-cluster channels (d,^{3}He) and (p,α). Similarly, the partitions (p,d,^{3}H) and (n,p,α) are coupled to each other via the two-cluster process (d,^{3}H)↔(n,α). We can also cosider the three-cluster partition (n,p,α^*) which can be coupled to (n,p,α) via the two-cluster inelastic process (p,α^*)↔(p,α). In this thesis, for simplicity, we consider only the partitions (n,d,^{3}He) and (p,d ^{3}H). The MTCC processes as mentioned above are presented schematically in Fig. 9. Each square box represents a Faddeev system, and each particle channel in the box is assigned a channel number. The interacting pairs are indicated inside parentheses. In the box on the left, the particles N_2 and N_3 symbolize the nucleon. Since we ignore the Coulomb force, and since the total isospin of this system is zero, the pair of N_2 and N_3 in each particle channel constructs the antisymmetric isospin state,

$$\frac{1}{\sqrt{2}} (pn - np) \quad . \tag{4.1}$$

In the box on the right in Fig. 9, the particle N represents the nucleon, and the particle A symbolizes the nuclei ^{3}He or ^{3}H. Similarly the pair of N and A in each particle channel constructs the isospin state, the eigen value of which is zero,

$$\frac{1}{\sqrt{2}} \left(p\ ^3H - n\ ^3He \right) \quad . \tag{4.2}$$

The interaction between each pair of particle channel in a box is due to the exchange of the particle shown along the double-pointed arrows. Each Faddeev system is connected to others via the two-cluster rearrangement processes $(N_2,\alpha)\leftrightarrow(A,d)$ and $(N_3,\alpha)\leftrightarrow(A,d)$ which are indicated by the dashed lines. Explicitly, they are the processes $(p,\alpha)\leftrightarrow(^3He,d)$ and $(n,\alpha)\leftrightarrow(^3H,d)$. If other three-cluster partitions are needed, they can be taken into account by adding corresponding Faddeev systems. In the above MTCC approach, the effect of all other reaction processes that are coupled weakly to the scattering state can be incorporated into the two-cluster subsystems as absorption effects.

Now we formulate the MTCC processes in a set of coupled equations. The dynamical inputs to the theory are two-cluster t-matrices. The separable multi-channel t-matrix introduced in § 2 has all required properties to described the MTCC processes. Not only it represents the rearrangement processes that connect various three-cluster partitions, but also it simulates absorption effects by the perturbative treatment as in the absorption model. By the use of the separable t-matrix, the

rules imposed upon the MTCC processes enable us to postulate the following AL type coupled channel equation among scattering amplitudes,

$$X_{\beta\alpha} = Z_{\beta\alpha} + \sum_{\gamma(\neq\beta)} \sum_{\delta} Z_{\beta\gamma}\tau_{\gamma\delta}X_{\delta\alpha} \quad , \tag{4.3}$$

where $X_{\beta\alpha}$ and $Z_{\beta\alpha}$ denote the scattering amplitude and the Born amplitude from particle channel α to β, respectively. The propagator $\tau_{\gamma\delta}$ represents the propagation of interacting two clusters where the transition takes place between the two-cluster subsystems in particle channels γ and δ. It is expressed explicitly by Eq. (2.8). Since τ is common to all reaction processes in coupled two-cluster systems, τ_{24}, for example, is the same as τ_{22} or τ_{44} for particle channel 2 and 4 shown in Fig. 9.

Eq. (4.3) can be depicted by the diagram shown in Fig. 10. The scattering amplitude X is represented by a large circle. The Born amplitude $Z_{\beta\alpha}$ is written explicitly as

$$Z_{\beta\alpha}(\vec{q}_\beta,\vec{q}_\alpha;E) = (1-\delta_{\beta\alpha})\langle\vec{q}_\beta|\langle g_\beta(\vec{p}_\beta)|G_0(E)|g_\alpha(\vec{p}_\alpha)\rangle|\vec{q}_\alpha\rangle \quad , \tag{4.4}$$

where $\vec{q}_\alpha$ is the momentum of the spectator relative to the centr-of-mass of the interacting pair in particle channel α. Similarly for $\vec{q}_\beta$. The two-body internal momenta $\vec{p}_\alpha$ and $\vec{p}_\beta$ are expressed as the linear combinations of $\vec{q}_\alpha$ and $\vec{q}_\beta$ in an usual manner[38]. The form factors $|g_\alpha\rangle$ and $|g_\beta\rangle$ are taken from the two-body t-matrices of particle channel α and β respectively,

which are explicitly shown in Eq. (2.7). They are depicted by the small semi-circles at both ends of the diagram representing the three-body free Green function $G_0(E)$. The two-body propagator $\tau_{\gamma\delta}$ is shown by two horizontal lines connecting $Z_{\beta\gamma}$ and $X_{\delta\alpha}$ with a twist to indicate the channel coupling between γ and δ.

For detailed discussions, we give the explicit expression of Eq. (4.3) for the d-α scattering depicted in Fig. 9. At first, it should be noticed that there are two possible particle channels inducing this reaction, channel 1 and channel 5. In the initial sate of particle channel 1, the deuteron is described as the bound state of p and n, and α as the spactator. On the other hand, in particle channel 5, the deuteron is the spactator and α is expressed as the bound state of p and ^{3}H, or n and ^{3}He. Denoting the initial particle channel by i (i=1,5), the equation (4.3) is written as the following matrix form,

$$\underset{\sim}{X}_i = \underset{\sim}{Z}_i + Z\,\tau\,\underset{\sim}{X}_i \quad , \tag{4.5}$$

where $\underset{\sim}{X}_i$ and $\underset{\sim}{Z}_i$ are column vectors, while Z and τ are square matrices. The matrices Z, τ and $\underset{\sim}{X}_i$ are given by

$$Z = \begin{pmatrix} 0 & Z_{12} & Z_{13} & 0 & 0 & 0 \\ Z_{21} & 0 & Z_{23} & 0 & 0 & 0 \\ Z_{31} & Z_{32} & 0 & 0 & 0 & 0 \\ 0 & 0 & 0 & 0 & Z_{45} & Z_{46} \\ 0 & 0 & 0 & Z_{54} & 0 & Z_{56} \\ 0 & 0 & 0 & Z_{64} & Z_{65} & 0 \end{pmatrix} , \tag{4.6}$$

$$\tau = \begin{pmatrix} \tau_{11} & 0 & 0 & 0 & 0 & 0 \\ 0 & \tau_{22} & 0 & \tau_{24} & 0 & 0 \\ 0 & 0 & \tau_{33} & \tau_{34} & 0 & 0 \\ 0 & \tau_{42} & \tau_{43} & \tau_{44} & 0 & 0 \\ 0 & 0 & 0 & 0 & \tau_{55} & 0 \\ 0 & 0 & 0 & 0 & 0 & \tau_{66} \end{pmatrix} , \qquad (4.7)$$

$$\underset{\sim}{X}_i = \begin{pmatrix} X_{1i} \\ X_{2i} \\ X_{3i} \\ X_{4i} \\ X_{5i} \\ X_{6i} \end{pmatrix} . \qquad (4.8)$$

For each initial particle channel, the column vector $\underset{\sim}{Z}_i$ composed by Born amplitudes is given by

$$\underset{\sim}{Z}_1 = \begin{pmatrix} 0 \\ Z_{21} \\ Z_{31} \\ 0 \\ 0 \\ 0 \end{pmatrix} , \qquad \underset{\sim}{Z}_5 = \begin{pmatrix} 0 \\ 0 \\ 0 \\ Z_{45} \\ 0 \\ Z_{65} \end{pmatrix} . \qquad (4.9)$$

Since Eq. (4.5) is linear, the full MTCC amplitude for the d-α scattering which we denote by $\underset{\sim}{X}$ is expressed as the superposition of the amplitudes originating from both initial particle channels, i= 1 and 5, namely

$$\underset{\sim}{X} = \underset{\sim}{X}_1 + \underset{\sim}{X}_5 \quad . \tag{4.10}$$

The full amplitude $\underset{\sim}{X}$ satisfies the integral equation,

$$\underset{\sim}{X} = \underset{\sim}{Z} + Z \; \tau \; \underset{\sim}{X} \quad , \tag{4.11}$$

where $\underset{\sim}{Z}$ is defined by

$$\underset{\sim}{Z} = \underset{\sim}{Z}_1 + \underset{\sim}{Z}_5 \quad . \tag{4.12}$$

In Fig. 11, we show the processes involved in particle channel 1 (process (a)) and particle channel 5 (process (b)). The deuteron in process (a) is represented as the bound state pole of the pair (p,n), while the α particle in process (b) is considered to be the bound state pole of the pair (n,^{3}He). By Rule 2, in process (a) the deuteron can break up into p and n but the α particle can not. On the other hand, in process (b) the α particle can break up into n and ^{3}He, but the deuteron can not. Hence, particle channel 1 and particle channel 5 are clearly distinguishable throughout the MTCC processes. However, due to this classification of the processes involving the d+α state according to Rule 2, the expressions of the elastic scattering observables become restricted to the sum of the individual transition probabilities corresponding to the d+α states in channel 1 and 5. Let us denote by X_k the k-th element of the column vector $\underset{\sim}{X}$ which is explicitly expressed as

$$X_k = X_{k1} + X_{k5} \quad (k=1\sim6) \quad . \tag{4.13}$$

In compliance with the unitarity requirement, the differential cross section of the elastic scattering is given by the sum of the individual cross sections to the final d+α states in channel 1 and 5, namely

$$\frac{d\sigma}{d\Omega} = |X_1|^2 + |X_5|^2 \quad , \tag{4.14}$$

where a kinematical factor is suppressed. The unitarity relation which demands Eq. (4.14) is explicitly shown in Appendix C.

Before closing this subsection, we resolve a question of double counting. In Fig. 12, we show one of the lowest order diagrams of transition from particle channel 1 to 6. The time runs from left to right. The neutron in the deuteron is denoted by n_1 and the neutron in the α particle by n_2. The two-cluster processes inside the square box is represented by the two-body t-matrix with the channel coupling $(p,\alpha)\leftrightarrow(d,{}^3He)$. As the t-matrix is determined from the p-α scattering data, the lowest order diagrams of the t-matrix contains the diagram shown in Fig. 13. When the square box of Fig. 12 is replaced by Fig. 13, we have the possibilities of Fig. 14 (a) and (b). The problem of double counting arises if both of these processes are present in Fig. 12 <u>and</u> in Z_{65} of the coupled system of the partition $(n,d,{}^3He)$. We assert that this is not the case since, as we explain below, Fig. 14(a) is not a part of Fig. 12 while Fig.

14(b) is not included in Z_{65}. In Fig. 14(a), the interaction of n_1 with p occurs at A between the interactions at B and C. Therefore, this process is not contained in Fig. 12 in which n_1 must remain free between the vertices B and C of Fig. 13. On the other hand, in Fig. 14(b) the interaction A occures before the vertex B, and n_2 is bound in the α particle at the time of interaction at A. This situation is completely excluded from Z_{65} since we determine the two-body t-matrix of particle channel 6 by the n_2-d scattering data where, in the initial state, n_2 has to be free prior to the last interaction at A between n_1 and p in the deuteron.

4.2 An application to the d-α elastic scattering

4.2.1 Formulation

In this subsection, we apply the MTCC model to the d-α elastic scattering at E_d= 56 MeV. As discussed in § 3.2.3, the analyses by the absorption model suggest that in addition to (n,p,α) the three-cluster partitions (n,d,^{3}He) and (p,d,^{3}H) exert strong influence on the scattering processes in this energy region. These effects can not be treated sufficiently in the absorption model because they can only be taken into account as absorption effects in the two-cluster subsystems. The MTCC model enables us to take into consideration various three-cluster partitions explicitly. Let us take the three-cluster partitions (n,p,α), (n,d,^{3}He) and (p,d,^{3}H) since these are the most important ones at this energy. Other reaction processes can be incorporated into the two-cluster subsystems as absorption effects. Since we neglect the Coulomb force and ignore the mass differences between p and n and between ^{3}He and H, the MTCC processes can be shown schematically by Fig. 9. The set of integral equations which describe these processes is given by Eq. (4.11). Written explicitly, this becomes

$$
\begin{aligned}
X_1 &= Z_{12}\tau_{22}X_2+Z_{13}\tau_{33}X_3+(Z_{12}\tau_{24}+Z_{13}\tau_{34})X_4 \\
X_2 &= Z_{21}+Z_{21}\tau_1X_1+ +Z_{23}\tau_{33}X_3+Z_{23}\tau_{34}X_4 \\
X_3 &= Z_{31}+Z_{31}\tau_1X_1+Z_{32}\tau_{22}X_2 +Z_{32}\tau_{24}X_4 \\
X_4 &= Z_{45} +Z_{45}\tau_5X_5+Z_{46}\tau_6X_6 \\
X_5 &= Z_{54}\tau_{42}X_2+Z_{54}\tau_{43}X_3+Z_{54}\tau_{44}X_4 +Z_{56}\tau_6X_6
\end{aligned}
$$

$$X_6 = Z_{65} + Z_{64}\tau_{42}X_2 + Z_{64}\tau_{43}X_3 + Z_{64}\tau_{44}X_4 + Z_{65}\tau_5 X_5 \tag{4.15}$$

where X_k is the transition amplitudes to particle channel k, which is explicitly shown in Eq. (4.13). The consideration of isospin states and the identity of nucleons N_2 and N_3 lead to the symmetric properties for Born amplitudes and propagators:

$$Z_{12} = -Z_{13} \quad , \quad \tau_{24} = -\tau_{34} \tag{4.16}$$

and

$$\tau_{22} = \tau_{33} \quad . \tag{4.17}$$

In Appendix D, the relations (4.16) are explicitly derived. Using Eqs. (4.16) and (4.17), the coupled equations (4.15) are reduced to the following set of equations.

$$\begin{aligned}
Y_1 &= Z_{12}\tau_{22}Y_2 + Z_{12}\tau_{24}X_4 \\
Y_2 &= Z_{21} + 2Z_{21}\tau_1 Y_1 - Z_{32}\tau_{22}Y_2 - Z_{32}\tau_{24}X_4 \\
X_4 &= Z_{45} + Z_{45}\tau_5 X_5 + Z_{46}\tau_6 X_6 \\
X_5 &= 2Z_{54}\tau_{42}Y_2 + Z_{54}\tau_{44}X_4 + Z_{56}\tau_6 X_6 \\
X_6 &= Z_{65} + 2Z_{64}\tau_{42}Y_2 + Z_{64}\tau_{44}X_4 + Z_{65}\tau_5 X_5
\end{aligned} \tag{4.18}$$

Here we have introduced the antisymmetric amplitudes:

$$Y_1 = X_1/2 \quad , \quad Y_2 = (X_2 - X_3)/2 \tag{4.19}$$

Eq. (4.18) is numerically solved. When the coupling between two Faddeev systems in Fig. 9 is turned off (the case of $\tau_{24}= \tau_{34}= 0$), Eq. (4.18) separates into two sets of integral equations, each of which represents the usual three-body AL equations. One of them is identified with Eq. (3.6). Therefore, numerical calculations are no more difficult than the pure three-body model and can be performed by the usual techniques, i.e. the contour deformation[25] and the Pade approximant[34]. As mentioned in § 4.1, the elastic scattering observables are represented by the sum of the individual transition probabilities to the final d+α states in channel 1 and channel 5. The differential cross section is given by Eq. (4.14), which is rewritten by using Eq. (4.13) as

$$\frac{d\sigma}{d\Omega} = |X_{11}+X_{15}|^2 + |X_{51}+X_{55}|^2 \quad . \tag{4.20}$$

The analyzing powers can also be expressed in a similar manner.

At the present stage of calculation, there remains an ambiguity as to the sign of τ_{24}. For explanation, let us look at the lowest order diagrams for the transitions from channel 1 to channel 1 and from channel 5 to channel 1. These processes are shown in Fig. 15. Both processes (a) and (b) are parts of the elastic scattering, which are superposed in Eq. (4.20). In process (a), the deuteron of initial particle channel 1 is described as the composite particle of nucleons N_2 and N_3, and its state is constructed by the interaction between N_2 and N_3. Here we denote it by d_1. On the other hand, in process (b), the

deuteron of inital particle channel 5 is the spectator, which we symbolize by d_5. The information of the internal state of d_5 is implicitly included in the values of two-cluster propagator τ_{24} which is determined by the experimental data corresponding to $A+d_5 \rightarrow N_3+\alpha$. Hence, the question arises how to define the relative phase of the state d_1 to d_5 in order to identify the initial state $d_1+\alpha$ in process (a) with the initial state $d_5+\alpha$ in process (b). The case is the same for the alpha particle of initial channel 1 in process (a) and of initial channel 5 in process (b). Thus, there exists an ambiguity of relative phase between the amplitudes corresponding to process (a) and process (b). However, this ambiguity ought not to exist, since the $d+\alpha$ state in particle channel 1 is related with the $d+\alpha$ state in particle channel 5 by the transition corresponding to Fig. 15(a) in itself. Indeed, the spectator deuteron in particle channel 5 is connected to the spectator α in particle channel 1 due to two-cluster propagator τ_{24}. The propagator τ_{24} in the coupled system $(A,d_5)\leftrightarrow(N_3,\alpha)$ takes real values below the lower thresholds of $A-d_5$ and $N_3-\alpha$, so that the ambiguity of relative phase is reduced to the ambiguity of relative sign only. Therefore, in order to remove completely the ambiguity as mentioned above, we must determine the sign of τ_{24}. However, this can not be performed in the present state of calculation, because τ_{24} is as an input to the MTCC calculation determined phenomenologically by the scattering observables in this coupled two-cluster subsystem. The sign of τ_{24} will be determined uniquely by investigating the interference between the amplitudes

of nuclear part and Coulomb part in $A+d_5 \rightarrow N_3+\alpha$ scattering, since we can obtain the Coulomb amplitude with no ambiguity. This is under investigation. In the present work, we calculate the elastic scattering observables for two possible cases according to the ambiguity of the sign of τ_{24}, which remains unresolved. Thus, the differential cross section is expressed either by Eq. (4.20) or by

$$\frac{d\sigma}{d\Omega} = |X_{11}-X_{15}|^2 + |X_{51}-X_{55}|^2 \quad . \tag{4.21}$$

4.2.2 Two-cluster interactions for the MTCC calculation

Before presenting results, we describe the two-cluster interactions used in the MTCC calculation. For the coupled (N_2,α) and (d,A) systems connecting particle channel 2 to 4 (or the coupled (N_3,α) and (d,A) systems connecting particle channel 3 to 4), we construct the multi-channel separable t-matrix by the following simplified procedures. In § 3.2.1, the two-body t-matrix for the coupled (N,α) system has been constructed, where the (N,α) channel is coupled to a second dummy channel. The dummy channel contains the effect of (d,A) and the rest of reaction channels. (Notice that the potential parameters have been determined by fitting only p-α elastic scattering data.) Here, we split this second channel into two, one for (d,A) with weight w and the other for the rest with weight 1-w. As discussed in § 3.2.3, in the p-α scattering the rearrangement process to the $(d,{}^3He)$ channel palys an important role above its

threshold. Futhermore, our main aim in the present calculation consists in investigating the effects of the partition (N,d,A) which is coupled to (N_2,N_3,α) through this rearrangement process. Therefore, for simplicity, we set w=1.0 and utilize the resulting two-channel t-matrix as an input to the MTCC calculation. For the (N_2,N_3) subsystem in particle channel 1, we take the coupled $^3S_1$-$^3D_1$ state into account and adopt the YY7 potential which is mentioned in § 3.2.2.

For the other two-cluster subsystems in particle channel 5 and 6, we also employ simplified interactions with the Yamaguchi type form factors. In the (N,d) system in particle channel 6, we consider only the $^2S_{1/2}$-$^4D_{1/2}$ partial waves where the bound states ^{3}He or ^{3}H exist. To describe the two-channel interaction, the same formulas as Eqs (2.5), (3.1) and (3.3) are adopted where the channel $^2S_{1/2}$ is assigned to the channel number 1 and the channel $^4D_{1/2}$ to the channel number 2. The potential parameters are searched to reproduce the binding energy as well as the phase shifts of $^2S_{1/2}$ and the mixing parameters[39] in low energy p-d scatterings. In Table 2, we list the resulting values of the parameters. This potential supports a bound state at the bound state energy of ^{3}H (E= -6.26 MeV relative to the threshold energy of n-d). The fits to the $^2S_{1/2}$ phase shifts and the mixing parameters are shown in Fig. 16. For the (N,A) subsystem in particle channel 5, we limit ourselves to only the $^1S_0$ partial wave which sustains the bound state α. We utilize the single-channel separable potential of rank-2, namely

$$V = \lambda_1 |g_1\rangle\langle g_1| + \lambda_2 |g_2\rangle\langle g_2| \quad , \tag{4.22}$$

with the Yamaguchi type form factor

$$g_i(p) = 1 / (p^2 + \beta_i^2) \qquad (i=1,2) \ . \tag{4.23}$$

The potential parameters λ_1, λ_2, β_1 and β_2 are determined by reproducing the binding energy 20.64 MeV of the α particle and by fitting the phase shifts[40] of low energy n-^{3}He scatterings. The resulting values of the parameters are shown in Table 3 and the fits to the phase shifts in Fig. 17.

4.2.3 Results and discussions

The results of preliminary calculation for the elastic scattering at E_d= 56 MeV are shown in Fig. 18. The solid and the dashed lines indicate the MTCC results corresponding to two possible choice of the sign of τ_{24} mentioned in § 4.2.1. The dot-dashed lines are pure three-body calculations without the couplings to the partitions (n,d,^{3}He) and (p,d,^{3}H), which are given in § 3.2.2 (with no absorption effects). In the cross section, the MTCC results represented by the solid lines are better than the result of the pure three-body model and reproduces the experimental data well up to $\theta_{CM} \simeq 150^\circ$. On the other hand, in the analyzing powers, the fits to the data are still poor, but the MTCC effects are seen to give rise to notable oscillations that can not be seen in the pure three-body calculations. The MTCC effects are evident at large angles and are caused by the processes such as shown in Fig. 15(b), which

are inhernt in this model. These facts mean that it is necessary to include the couplings among the three-cluster partitions (n,p,α), (n,d,^{3}He) and (p,d,^{3}H) in order to reproduce the experimental data, especially those conspicuous diffraction-like patterns in the analyzing powers.

The fits to the experimental data are rather poor for the tensor analyzing powers. In order to assess the quality of the fits to the data, it is important to remark two limitations in the present calculation. One is the practical limitation due to the use of the simplified two-cluster interactions. The other is fundamental that is concerned with the limitation of the MTCC model. First, we consider the former problem. As mentioned previously, for the coupled (N_2,α) and (d,A) system we utilize for simplicity a potential which is obtained by fitting only the p-α elastic scattering. In a full scale investigation, we should adopt the interaction which reproduces all available experimental data on N_2+α scattering. To see to what extent the present potential can reproduce the scattering data of p+α → d+^{3}He and d+^{3}He → d+^{3}He, we compare the result for the excitation function of the d+^{3}He → d+^{3}He scattering at 90° (CM) with the experimental data[41] in Fig. 19. The fit to the data is not good above E_p(Lab) ≃ 5 MeV. A similar situation exists for the p+α → d+^{3}He scattering also. For the (N,d) and (N,A) system, we also use the simplified potentials. In each of them, we consider only one partial wave which supports the bound state ^{3}H (^{3}He) or α, and therefore a number of partial waves which seem to exert important influence on the sacttering state are missing, for example, the

$^4S_{3/2}$ wave for the (N,d) system, or the $^3S_1$ wave for the (N,A) system. All these facts mean the importance of improving the two-cluster interactions.

We examine the other limitation which is inherent in the MTCC modl. Although the model can describe three-cluster processes where various three-cluster partitions are coupled to one another, it can not incorporate some physically important processes that are possible even within the limitation of the two- and three-cluster coupling model. These are the sequential transfer processes, a typical diagram of which is shown in Fig 20. If we succeed in incorporating systematically these processes into the MTCC model, the d+α states in particle channel 1 and 5 are unified. This can be explained in Fig. 20. The process corresponding to the left-hand side of the dashed line is involved in Z_{54} in the MTCC processes, but the process corresponding to the right-hand side of the dot-dashed line is included in Z_{21}. Hence, the d+α state between the dashed and the dot-dashed lines should be uniquely defined. This will eliminate the restriction in the MTCC model, expressed by Eq. (4.14). In other words, a new coupling scheme between the three-cluster partitions (n,p,α) and (n,d,^{3}He) is introduced via the d+α state between the dashed and the dot-dashed lines in Fig. 20, which is expected to cause conspicuous influence on the elastic scattering observables. The next subsection will be devoted to the consideration of such an extention of the MTCC model.

Summing up the application to the d-α elastic scattering, MTCC effects are clearly shown at large angles in the cross

section and the analyzing powers. To reproduce the experimental data, it is necessary not only to improve two-cluster interactions but also to extend the theoretical framework of the MTCC model.

4.3 An extention of the MTCC model

A physically important diagram missing from the MTCC model is the process of sequential transfer. In Fig. 21, we show a typical diagram for the MTCC model of Fig. 9. Since we observe Rule 2, the only possible process is the exchange of one cluster at a time back and force between the interacting pair and the spectator, but never the process in which two or more particles are exchanged in one direction as shown in Fig. 20. Theses sequential transfer processes may have important influence on scattering observables for some reactions.

In this subsection, we describe the method which enable us to incorporate sequential transfer processes into the MTCC model within the two- and three-cluster approximation. We name such an extension of the MTCC model the Multi Two- and Three-Cluster coupling (MTTC) model. The general description of the method for the system of six nucleons has been given in Ref. 42. Here, we restrict ourselves to a typical type of sequential transfer processes as shown in Fig. 20, where the d+α state intervene between two successive particle exchanges. As discussed in § 4.2.2, this type of processes is expected to remove the restriction in the MTCC model expressed by Eq. (4.14).

First, we investigate the basic assumption which causes this restriction. As mentioned in § 4.1, in Fig. 11, the d+α state is included in both process (a) and process (b). The α particle in process (b) can break up into n and ^{3}He, while in process (a) it can not. This restriction imposed on the spectator α in process

(a) is due to Rule 2. Now, let us introduce a process where this spectator α breaks up into n and ^{3}He. This is shown in Fig. 22, where the neutron is exchanged between the α particle and the interacting pair (p,n). This process can be decomposed into process (a) and process (b) in Fig. 23, where $(n,p)_b$ represents the deuteron and $(n,p)_c$ the continuum states of the interacting pair (p,n). Here, it should be noticed that physically process (a) is the same as a part of Z_{65} in the MTCC model, which is shown in Fig. 24. To be consistent with the inclusion of Z_{65}, and to remain within the two- and three-cluster model, we should allow process (a) in Fig. 23. If we identify $(n,p)_b$ and α in Fig. 23 (a) with d and the bound state of $(n,^3He)$ in Fig. 24, we can treat this diagram in exactly the same manner as the allowed diagrams. The process of Fig. 23 (b) can not be treated in the three-cluster model, because it contains a four-cluster diagram. All of the above considerations hold similarly for the spectator d in Fig. 11 (b). Thus we replace Rule 2 by the following rule.

Rule 2' All vertices with continuum states of the interacting pair as daughters are forbidden.

Under this rule, together with Rule 1, we can introduce sequential transfer processes as shown in Fig. 20 within the two- and three-cluster coupling model. This unifies the d+α states in particle channel 1 and 5 in the MTCC model depicted in Fig. 9.

In order to implement the above idea, the re-definition of channels is necessary. The inclusion of the process in Fig. 23

(a) raises the problem of double counting, because this process is the same as a part of Z_{65} in the MTCC model. In the MTCC model, this problem is settled by imposing Rule 2, since then the process in Fig. 23 (a) becomes forbidden. In the MTTC model, it is resolved by the following re-definition of channels. Let us write again the definition of particle channel 1 and 5 in the MTCC model,

$$(N_2,N_3) + \alpha \quad \text{(particle channel 1)} ,$$
$$(N\ ,A\ ) + d \quad \text{(particle channel 5)} ,$$

where the parentheses indicate interacting pairs. These channels are replaced by

$$(N_2,N_3)_c + \alpha \quad (\text{ channel } 1_c\ ) ,$$
$$(N\ ,A\ )_c + d \quad (\text{ channel } 5_c\ ) ,$$
$$d + \alpha \quad (\text{ channel } 7\ ) ,$$

where $(\ N_2,N_3\ )_c$ and $(\ N\ ,\ A\ )_c$ denote only the continuum states of interacting pairs (N_2,N_3) and (N,A) respectively. Other channel are the same as in the MTCC model. By extracting the d+α state from both particle channels 1 and 5 in the MTCC model, the possibility of double counting is removed.

By imposing both Rule 1 and Rule 2', and by using the re-defined channels, we can describe the MTTC processes in the same manner as Eq. (4.3) in the MTCC model. In solving the equation, the differences from the MTCC calculation are the use

of the propagator of re-defined channels 1_c, 5_c and 7, and the use of two-cluster verticies $\alpha \to N + A$ and $d \to N_2 + N_3$. These quantities are obtained by the following procedures. Let us symbolize the above verticies by $P \to Q + R$. First, we introduce the separable representation of a two-cluster potential between Q and R for angular momentum eigenstates,

$$V(p', p) = \lambda\, g(p')\, g(p) \quad , \tag{4.23}$$

from which it follows

$$t(p', p\,;\, \sqrt{s}) = g(p')\, \tau(\sqrt{s})\, g(p) \tag{4.24}$$

Here s is the square of the two-body total energy in the CM system, and

$$\tau(\sqrt{s}) = \left[\lambda^{-1} - \int dp\, p^2\, \frac{g(p)^2}{\sqrt{s} - \tilde{E}(p) + i\varepsilon} \right]^{-1} , \tag{4.25}$$

where $\tilde{E}$ includes the rest mass. The t-matrix is determined by fitting the scattering data corresponding to the Q+R scattering as well as reproducing the bound state energies of Q and R. Then, we decompose it into the bound state pole part t_b and the continuum state part t_c,

$$t = t_b + t_c \quad , \tag{4.26}$$

and express both t_b and t_c in separable forms:

$$t_b = f(p')\ \tau_b(\sqrt{s})\ f(p) \tag{4.27}$$

where

$$\tau_b(\sqrt{s}) = 1/(\sqrt{s} + i\varepsilon - m) \tag{4.28}$$

The continuum state part t_c is defined by Eq. (4.26). In general, its separable representation requires a multi-rank form,

$$t_c = \sum_{i,j} h_i(p')\ \tau_c^{ij}(\sqrt{s})\ h_j(p) \quad . \tag{4.29}$$

These equations define the propagators τ_b and τ_c and the form factors $f(p)$ and $h_i(p)$, which are required as inputs to the MTTC calculation.

Thus we can incorporate sequential transfer processes as shown in Fig. 20 in a consitent manner. In general, the MTTC model can include all possibble processes within the limitation of two- and three-cluster coupling model.

§ 5 Summary and conclusions

In this paper, we propose two alternative versions of connected kernel theories of nuclear reactions, which are called the MTCC model and the MTTC model. In these models, various reaction processes, elastic, inelastic, rearrangement and breakup processs, are treated in a unified manner in compliance with the unitarity requirement. In the MTCC model, the scattering processes are represented by a superposition of three-cluster processes where a number of important three-cluster partitions are coupled to one another. Each of the three-cluster partitions is treated as a Faddeev system and is coupled to others via two-cluster rearrangement processes. Other reaction processes that are weakly coupled to the scattering state can be incorporated into the two-cluster processes as absorption effects. By the use of multi-channel two-cluster interactions of separable form, we formulate these processes in a set of one-variable integral equations for reaction amplitudes similar to the Amado-Lovelace form. The MTCC model is an important extension of the three-body Faddeev approach in that it can treat a wide class of nuclear reactions. It has the advantage over the existing N-body connected kernel theories in that it is practicable. The MTTC model, an extension of the MTCC model, includes the process of sequential transfer so that it can treat all possible processes within the limitation of the two- and three-cluster approximation.

The simplest application to nuclear reactions of the MTCC

model is the calculation of scattering processes in which only one three-cluster partition is considered, but with absorption effects in two-cluster subsystems. This an immediate extension of the three-body Faddeev approach and we name it the absorption model. In §§ 3 and 4, we apply the absorption model and the MTCC model to the d-α elastic scatterings at E_d= 21 and 56 MeV. We choose these scatterings for the following reasons. The d-α scattering at relatively low incident energies ($E_d \lesssim 20$ MeV) have been studied well in terms of Faddeev formalism, where the scattering processes are represented by the three-cluster partition (N,N,α). This model has succeeded in explaining surprisingly well the cross sections and analyzing powers at low energies. However, at higher energies, there have been only a few limited analyses since the effective approach has not yet been established. This is due to the fact that at higher energies various reaction channels are open, and for realistic analyses it is necessary to incorporate the effects of these channels in addition to the deuteron breakup. Indeed, the data for analyzing powers at 56 MeV show the conspicuous diffraction-like patterns that is expected to be caused by the coupling to various reaction channels. Thus, while at 21 MeV we can check our models by comparison with the previous results of pure three-body calculations, at 56 MeV we can investigate the many-body effects reflected in the scattering observables according to our sophisticated models.

In the analysis of the absorption model, we take the three-cluster partition (N,N,α). As expected, at 21 MeV the

absorption model reproduces the experimental results well and improves previous three-body calculaons. However, at 56 MeV the absorption model can not reproduce the notable structures of analyzing powers as seen in the data, although absorption effects are apparent at large angles. The cause of such disagreement with the data should be ascribed to the basic assumption of the absorption model that the scattering state are represented by one three-cluster partition (N,N,α), and that the effects of other reaction processes are weak enough to be incorporated into the (N,α) subsystem as absorption effects. There are evidences that the three-cluster partitions (n,d,^{3}He) and (p,d,^{3}H) are strongly coupled to the scattering state at higher energies. For example, the reaction cross sections of p+α → d+^{3}He above the threshold amount to 50 per cent of the total reaction cross sections of p+α scatterings. This fact suggests that we should take the three-cluster partitions (n,d,^{3}He) and (p,d,^{3}H) into consideration to reproduce the experimental results at 56 MeV.

The MTCC model enables us to treat these three-cluster partitions explicitly. Since the main aim in the present MTCC calculation is to investigate the effects of the coupling to the three-cluster partitions, we utilize simplified two-cluster interactions for coupled Faddeev systems (n,d,^{3}He) and (p,d,^{3}H). The results of preliminary calculation for the d-α elastic scattering at E_d= 56 MeV exhibit notable oscillations in the tensor analyzing powers, and the coupling effects to the newly added three-cluster partitions are clearly seen at large angles. These facts indicate that it is indispensable to include the

couplings among relevant three-cluster partitions for the analyses of the d-α scattering in this energy region to be realistic.

A physically important diagram missing from the MTCC model is the process of sequential transfer. In § 4.2.3 and § 4.3, we show that the introduction of sequential transfer processes amounts to inducing new coupling shemes between three-cluster partitions in the MTCC model. For certain reactions, it can exert an important influence on scattering observables. This can be accomplished in the MTTC model.

Acknowledgements

The author would like to thank Professor S. Takagi, Professor T. Sawada and Dr. T. Ueda for the collaboration throughout the present work and for continuous encouragements. Especially, he is most grateful to Professor T.Sawada and Dr. T. Ueda for many critical discussions and advices, and for careful reading through the manuscript.

He wishes to express his deep gratitude to Dr. Y. Koike for proposing many interesting subjects on few-body reactions, kind advices, encouragements and the co-work on the absorption model.

He is also thankful to the members of Department of Applied Mathematics, Faculty of Engineering Science, Osaka University, for their various supports and encouragement.

The numerical calculations for this work have been carried out on the Computer system at the Computation Center of Osaka University. They have been financially supported in part by Research Center for Nuclear Physics, Osaka University.

Appendix A

Non-orthogonality terms and effective interactions

For simplicity, let us consider the case of two coupled rearrangement channels such as the (N,α) and (d,^{3}He) channels in the N-α scattering. The Hamiltonian of the system can be expressed as

$$H = H_i + V_i + K_i \quad , \tag{A.1}$$

where H_i is the cluster-internal Hamiltonian, V_i is the cluster-external interaction, and K_i is the relative kinetic energy operator between the center-of-mass of two clusters in channel i. Let χ_i be the eigenstate of H_i with the eigenvalue e_i. By assumption, the wave function Ψ of the system is expressed as a superposition of χ_1 and χ_2:

$$\Psi = \psi_1\chi_1 + \psi_2\chi_2 \quad . \tag{A.2}$$

Substituting Eq. (A.2) into the Schrödinger equation $(H-e)\Psi = 0$, we find the following set of coupled equations for ψ_1 and ψ_2:

$$\begin{aligned} [(e-e_1)-K_1]|\psi_1\rangle &= V_{11}|\psi_1\rangle + V_{12}|\psi_2\rangle \quad , \\ [(e-e_2)-K_2]|\psi_2\rangle &= V_{21}|\psi_1\rangle + V_{22}|\psi_2\rangle \quad , \end{aligned} \tag{A.3}$$

where we have defined the 2×2 coupling interaction V by

$$V_{11} = (\chi_1|V_1|\chi_1), \quad V_{22} = (\chi_2|V_2|\chi_2), \tag{A.4a}$$

$$V_{12}|\psi_2\rangle = (\chi_1|H-e|\chi_2\psi_2\rangle, \quad V_{21}|\psi_1\rangle = (\chi_2|H-e|\chi_1\psi_1\rangle, \tag{A.4b}$$

where V_{12} and V_{21} are non-local. The interaction V defined above is manifestly hermitian. It is important to realize that V_{12} and V_{21} contain the non-orthogonality terms. Equation (A.4b) can be rewritten as

$$V_{12}|\psi_2\rangle = (\chi_1|V_2|\chi_2\psi_2\rangle - (\chi_1|[(e-e_2)-K_2]|\chi_2\psi_2\rangle, \tag{A.5a}$$

$$V_{21}|\psi_1\rangle = (\chi_2|V_1|\chi_1\psi_1\rangle - (\chi_2|[(e-e_1)-K_1]|\chi_1\psi_1\rangle \ . \tag{A.5b}$$

The non-orthogonality terms are the second terms on the right-hand sides. Notice that they contribute only off the energy shell. Since χ_1 and χ_2 are two-cluster states of different compositions, their overlap becomes null at the asymptotic region. Therefore, the non-orthogonality terms are of short range, and so is the coupling interaction V without the Coulomb interctions. From Eqs. (A.3) and (A.4), we obtain the following Lippmann-Schwinger equation for Ψ:

$$\Psi = \Phi + G_0 \, V \, \Psi \ , \tag{A.6}$$

where

$$\Psi = \begin{pmatrix} \psi_1 \\ \psi_2 \end{pmatrix} , \qquad \Phi = \begin{pmatrix} \phi_1 \\ 0 \end{pmatrix} , \tag{A.7}$$

ϕ_1 being the incident wave in channel 1. Here, $G_0(e)$ is diagonal and is given by

$$G_0(e) = \begin{pmatrix} G_0^{(1)}(e) & 0 \\ 0 & G_0^{(2)}(e) \end{pmatrix} , \tag{A.8}$$

where

$$G_0^{(i)}(e) = [(e-e_i)-K_i+ i\varepsilon]^{-1} . \tag{A.9}$$

Had we defined the coupling potential in terms of the cluster-external interactions alone without the non-orthogonality terms, then we would have obtained, instead of Eq. (A.3),

$$[(e-e_1)-K_1]|\psi_1\rangle+(\chi_1|(e-e_2)-K_2|\chi_2\psi_2\rangle= V_{11}|\psi_1\rangle +W_{12}|\psi_2\rangle ,$$

$$[(e-e_2)-K_2]|\psi_2\rangle+(\chi_2|(e-e_1)-K_1|\chi_1\psi_1\rangle= W_{21}|\psi_1\rangle +V_{22}|\psi_2\rangle ,$$

where the coupling interactions are

$$W_{12}|\psi_2\rangle=(\chi_1|V_2|\chi_2\psi_2\rangle \quad \text{and} \quad W_{21}|\psi_2\rangle=(\chi_2|V_1|\chi_1\psi_1\rangle .$$

Notice that the non-orthogonality terms now appear on the left-hand sides. Thus, the "free" Green function acquires non-diagonal elements. Besides, the coupling potential on the

right-hand sides of the above equations is non-hermitian. In contradistinction to this, we have transferred the burden of the non-orthogonality of χ_1 and χ_2 to the off-shell property of the coupling interaction in Eqs (A.3) and (A.6). In fact, the non-orthogonality terms should be regarded as a part of the coupling interaction since they arise due to the overlap between χ_1 and χ_2. This makes the free Green function diagonal and the interaction hermitian. Since the non-orthogonality effects are already in the off-shell part of the interaction, we should treat χ_1 and χ_2 as if they were orthogonal to each other in order to avoid double counting. We might simply say that we have chosen the representation in which χ_1 and χ_2 are orthogonal.

Appendix B

Separable optical potential with coupling effects

In this appendix, we derive Eq. (3.2) and prove that $t_{opt} = t_{11}$. From Eq. (A.6), we eliminate channel 2 and obtain

$$\psi_1 = \phi_1 + G_0^{(1)}(e)\, V_{opt}\phi_1 \ , \qquad (B.1)$$

where the "optical potential" V_{opt} is given by

$$V_{opt} = V_{11} + V_{12}[1 - G_0^{(2)}(e)V_{22}]^{-1}\, G_0^{(2)}(e)V_{21} \ . \qquad (B.2)$$

Using Eq. (2.5) here, we find

$$V_{opt} = \lambda|g_1\rangle\, [1 + \lambda\langle g_2|\xi\rangle]\, \langle g_2| \ , \qquad (B.3)$$

where

$$|\xi\rangle = [\ 1 - \lambda\, G_0^{(2)}(e)|g_2\rangle\langle g_2|\ ]^{-1} G_0^{(2)}(e)|g_2\rangle \ . \qquad (B.4)$$

Equation (B.4) leads to the following integral equation for $|\xi\rangle$:

$$|\xi\rangle = G_0^{(2)}(e)|g_2\rangle + \lambda\, G_0^{(2)}(e)|g_2\rangle\langle g_2|\xi\rangle \ . \qquad (B.5)$$

From this we find

$$\langle g_2|\xi\rangle = [\ 1 - \lambda\, \langle g_2|G_0^{(2)}(e)|g_2\rangle\ ]^{-1}\langle g_2|G_0^{(2)}(e)|g_2\rangle \ . \qquad (B.6)$$

Substituting this expression into Eq. (B.3), we obtain

$$V_{opt} = |g_1\rangle \lambda_{opt}(e) \langle g_1| \tag{B.7}$$

with

$$\lambda_{opt}(e) = [\ \lambda^{-1} - \langle g_2|G_0^{(2)}(e)|g_2\rangle\ ]^{-1} \ . \tag{B.8}$$

This is Eq. (3.2). Now, using Eq. (B.7), the Lippmann-Schwinger equation

$$t_{opt} = V_{opt} + V_{opt}\ G_0^{(1)}(e)\ t_{opt} \tag{B.9}$$

is easily solved, and the result is

$$\begin{aligned} t_{opt} &= |g_1\rangle [\ \lambda_{opt}^{-1}(e) - \langle g_1|G_0^{(1)}(e)|g_1\rangle\ ]^{-1}\langle g_1| \\ &= |g_1\rangle [\ \lambda^{-1} - \sum_{i=1}^{2} \langle g_i|G_0^{(i)}(e)|g_i\rangle\ ]^{-1}\langle g_1| \ . \end{aligned} \tag{B.10}$$

This proves the assertion made near the end of § 3.1.

Appendix C

Unitary relation in the MTCC model

In this appendix, we derive the unitarity relation in the MTCC model for the d-α scattering depicted in Fig 9. The derivation is based on Ref. 43. We start from the matrix form of Eq. (4.3), namely

$$X(E) = Z(E) + Z(E)\tau(e)X(E) \quad , \tag{C.1}$$

where E is the total energy and e represents the energy of two-cluster subsystems which is related to E by energy conservation. The square matrices Z(E) and τ(e) are symmetric, which follows from the symmetric properties of Born amplitudes and propagators:

$$Z_{\alpha\beta}(\vec{q}_\alpha,\vec{q}_\beta;\ E) = Z_{\beta\alpha}(\vec{q}_\beta,\vec{q}_\alpha;\ E) \quad , \tag{C.2}$$

$$\tau_{\alpha\beta}(e) = \tau_{\beta\alpha}(e) \quad . \tag{C.3}$$

Hence, from Eq. (C.1) we obtain

$$X(E) = Z(E) + X(E)\tau(e)Z(E) \quad . \tag{C.4}$$

Both Eqs. (C.1) and (C.4) can be solved for Z(E) to derive

$$Z(E) = X(E)\ [1 + \tau(e)X(E)\ ]^{-1} \tag{C.5}$$

and

$$Z(E) = X(E)\,[1 + X(E)\tau(e)]^{-1} \quad . \qquad (C.6)$$

We now let $E^+=E+i\varepsilon$ in (C.5) and $E^-=E-i\varepsilon$ in (C.6), and subtract the equations with the result

$$\begin{aligned} Z(E^+)-Z(E^-) = \; & X(E^+)[1+\tau(e^+)X(E^+)]^{-1} \\ & - [1+X(E^-)\tau(e^-)]^{-1}\, X(E^-) \quad . \end{aligned} \qquad (C.7)$$

Multiplying (C.7) from the left by $[1+X(E^-)\tau(e^-)]$ and from the right by $[1+\tau(e^+)X(e^+)]$, we finally have

$$\begin{aligned} & X(E^+)-X(E^-) \\ & \quad = [Z(E^+)-Z(E^-)] + X(E^-)\tau(e^-)[Z(E^+)-Z(E^-)] \\ & \quad + [Z(E^+)-Z(E^-)]\tau(e^+)X(E^+) \\ & \quad + X(E^-)[\tau(e^+)-\tau(e^-)]\, X(E^+) \\ & \quad + X(E^-)\tau(e^-)[Z(E^+)-Z(E^-)]\tau(e^+)X(E^+) \quad . \end{aligned} \qquad (C.8)$$

Now we limit ourselves to the case that the total energy E is below the lowest three-body breakup thresholds. Then, $Z(E^+)$ and $Z(E^-)$ are real:

$$Z(E^+) = Z(E^-) = Z(E) \quad . \qquad (C.9)$$

Therefore Eq. (C.8) is reduced to

$$X(E^+)-X(E^-) = X(E^-)[\tau(e^+)-\tau(e^-)]\, X(E^+) \quad . \qquad (C.10)$$

Here, we take matrix elements of Eq. (C.10) in momentum space into explicit consideration, then

$$\begin{aligned} & X_{\alpha\beta}(\vec{q}_\alpha,\vec{q}_\beta;\, E^+)-X_{\alpha\beta}(\vec{q}_\alpha,\vec{q}_\beta;\, E^-) \\ &= \sum_{\gamma,\delta} \int d\vec{q}\; X_{\alpha\gamma}(\vec{q}_\alpha,\vec{q};\, E^-)\, [\tau_{\gamma\delta}(E^+ - h^2q^2/2\mu^\gamma)-\tau_{\gamma\delta}(E^- - h^2q^2/2\mu^\gamma)] \\ &\qquad \times X_{\delta\beta}(\vec{q},\vec{q}_\beta;\, E^+) \quad . \qquad (C.11) \end{aligned}$$

Now, we impose another restriction that no two-body channels are open except the d+α channel at energy E. From Eq. (C.11) it follows that

$$\begin{aligned} & X_{\alpha\beta}(\vec{q}_\alpha,\vec{q}_\beta;\, E^+)-X_{\alpha\beta}(\vec{q}_\alpha,\vec{q}_\beta;\, E^-) \\ &= -\pi \sum_{\gamma=1,5} \rho(q_0) \int d\Omega_{\vec{q}_0}\; X_{\alpha\gamma}(\vec{q}_\alpha,\vec{q}_0;\, E^-)\, X_{\gamma\beta}(\vec{q}_0,\vec{q}_\beta;\, E^+) \quad , \qquad (C.12) \end{aligned}$$

where we denote by $\vec{q}_0$ the incident relative momentum between d and α, and $\rho(q_0)$ is defined by

$$\rho(q_0) = \mu^\gamma\, q_0\, /h^2 \quad . \qquad (C.13)$$

Using the fact that Z(E) is real and that $X_{\alpha\beta}(E^+) = X^*_{\alpha\beta}(E^-)$, we obtain

$$\mathrm{Im}\; X_{\alpha\beta}(\vec{q}_\alpha,\vec{q}_\beta;\, E^+)$$

$$= -\pi \sum_{\gamma=1,5} \rho(q_0) \int d\Omega_{\vec{q}_0} X^*_{\gamma\alpha}(\vec{q}_\alpha, \vec{q}_0; E^+) X_{\gamma\beta}(\vec{q}_0, \vec{q}_\beta; E^+) \ . \quad (C.14)$$

Thus we obtain the unitarity relation (C.14). From Eq. (C.14) we can derive

$$\text{Im } (X_{11}+X_{15}+X_{51}+X_{55})$$

$$= -\pi \rho(q_0) \int d\Omega_{\vec{q}_0} [|X_{11}+X_{15}|^2 + |X_{51}+X_{55}|^2] \ , \quad (C.15)$$

where the labels for momenta are suppressed. From Eq. (C.15) the expression Eq. (4.14) for the d-α elastic scattering cross section follows.

Appendix D

Definition of isospin states and symmetric properties of Born amplitudes and propagators in the MTCC model for the d-α elastic scattering

To derive the symmetric properties expressed by Eq. (4.15), we consider explicitly the isospin states in particle channels depicted in Fig. 9. Let us denote the isospin state in particle channel j by $|I_j\rangle$. The states $|I_j\rangle$ (j=1,6) are defined as follows.

$$|I_1\rangle = \frac{1}{\sqrt{2}} [\ (np)\alpha - (pn)\alpha\ ] \qquad (D.1)$$

$$|I_2\rangle = \frac{1}{\sqrt{2}} [\ (p\alpha)n - (n\alpha)p\ ] \qquad (D.2)$$

$$|I_3\rangle = \frac{1}{\sqrt{2}} [\ (n\alpha)p - (p\alpha)n\ ] \qquad (D.3)$$

$$|I_4\rangle = \frac{1}{\sqrt{2}} [\ (d\ ^3He)n - (d\ ^3H)p\ ] \qquad (D.4)$$

$$|I_5\rangle = \frac{1}{\sqrt{2}} [\ (^3He\ n)d - (^3H\ p)d\ ] \qquad (D.5)$$

$$|I_6\rangle = \frac{1}{\sqrt{2}} [\ (n\ d)^3He - (p\ d)^3H\ ] \qquad (D.6)$$

Here, two particles inside the parenthesis indicate the interacting pair and another particle is the spectator, according to the definition of particle channels depicted in Fig. 9. From the definitions (D.1), (D.2) and (D.3), we can derive the isospin

coupling coefficients included in the Born amplitudes Z_{12} and Z_{13}:

$$\langle I_1 | I_2 \rangle = 1 \quad , \quad \langle I_1 | I_3 \rangle = -1 \quad . \tag{D.7}$$

These relations, together with the identity of nucleons N_2 and N_3, lead to the symmetric property for the Born amplitudes:

$$Z_{12} = -Z_{13} \quad . \tag{D.8}$$

Next, the overlaps $\langle I_2 | I_4 \rangle$ and $\langle I_3 | I_4 \rangle$ included in the propergators τ_{24} and τ_{34} respectively are explicitly shown as

$$\langle I_2 | I_4 \rangle = \frac{1}{\sqrt{2}} \left[\langle (p\alpha)n | (d^3He)n \rangle + \langle (n\alpha)p | (d^3H)p \rangle \right] \tag{D.9}$$

and

$$\langle I_3 | I_4 \rangle = \frac{1}{\sqrt{2}} \left[-\langle (p\alpha)n | (d^3He)n \rangle - \langle (n\alpha)p | (d^3H)p \rangle \right] . \tag{D.10}$$

from which it follows that

$$\tau_{24} = -\tau_{34} \quad . \tag{D.11}$$

References

1) N.Austern, Direct nuclear reaction theories (Wiley, New York,1970).

2) P.E.Hodgson, Nuclear reactions and nuclear structure (Clarendon, Oxford, 1971).

3) N.Austern, C.M.Vincent and J.P.Farrell Jr., Ann. of Phys. 114 (1978) 93.

4) M.Yahiro, M.Nakano, Y.Iseri and M Kamimura, Prog. Theor. Phys. 67 (1982) 1467.

5) T.sawada and K.Thusima, Prog. Theor. Phys. 76 (1986) 440.

6) L.D.Faddeev, Soviet Physics JEPT 12 (1961) 1014.

7) See, for example, Modern Three-Hadoron Physics, ed. by A.W.Thomas (Springer-Verlag, Berlin, 1977), and the references are therein.

8) E.O.Alt, P.Grassberger and W.Shandhas, Nucl. Phys. B2 (1967) 167.

9) B.Charnomordic, C.Fayard and G.H.Lamot, Phy. Rev. C15 (1977) 864.

10) Y.Koike, Prog. Theor. Phys. 59 (1978) 87; Nucl. Phys. A301 (1978) 411; A337 (1980) 23.

11) P.Doleshall, G.Bencze, M.Bruno, F.Cannata and M.D'Agostino, Phys. Lett. 152B (1985) 1.

12) K.Hahn, E.W.Schmid and P.Doleshall, Phys. Rev. C31 (1985) 325.

13) J.M.Lambert, P.A.Treado, P.G.Roos, N.S.Chant, A.Nadasen, I.Slaus and Y.Koike, Phys. Rev. C26 (1982) 357.

14) K.Miyagawa, Y.Koike, T.Ueda, T.Sawada and S.Takagi, Prog. Theor. Phys. 74 (1985) 1264.

15) R.Frick, H.Clement, G.Graw, P.Schiemenz and N.Seichert, Phys. Rev. Lett. 44 (1980) 14.

16) K.Nishimura, H.Shimizu, K.Imai, T.Ichihara, N.Matsuoka, K.Hatanaka, H.Sakai, T.Saito, K.Hosono, K.Kondo and A.Okihana, Nucl. Phys. A432 (1985) 378.

17) O.Y.Yakubowskii, Sov. J. Nucl. Phys. 5 (1967) 937;
P.Grassberger and Shandhas, Nucl. Phys. B2 (1967) 181;
I.H.Sloan, Phys. Rev. C6 (1972) 1945;
G.Bencze, Nucl. Phys. A210 (1973) 568;
E.F.Redish, Nucl. Phys. A225 (1974) 165;
T.Sasakawa, Phys. Rev. C17 (1978) 2015, 2026.

18) D,J,Kouri and F.S.Levin, Nucl. Phys. A253 (1975),395;
W.Tobocman, Phys. Rev. C12 (1975) 746,1146.

19) J.M.Greben and F.S.Levin, Nucl. Phys. A325 (1979) 145.

20) E.F.Redish, Nucl. Phys. A235 (1974) 82.

21) T.Ueda, Phys. Lett. 141B (1984) 157.

22) R.D.Amado, Phys. Rev. 132 (1963) 485;
R.Aaron, R.D.Amado and Y.Y.Yam, Phys. Rev. 136B (1964) 650;
R.Aaron and R.D.Amado, Phys. Rev. 150 (1966) 857;
C.Lovelace, Phys. Rev. 135B (1964) 1225.

23) G. Bencze and P.Doleshall, Phys. Lett. 32B (1970) 539.

24) V.M.Krasnopol'sky and V.I.Kukulin, Sov. J. Nucl. Phys. 20 (1975) 470;
V.I.Kukulin, V.G.Neudatchin, I.T. Obukhovski and Yu.F.Simonov, Clusters as Subsystems in Light Nuclei

(Vieweg & Sohn, 1983).

25) J.H. Hetherington and L.H.Schick, Phys. Rev. B925 (1965) 137.

26) R.G.Newton, Scattering theory of waves and particles (McGraw-Hill, New york, 1966), p522.

27) H.H.Hackenbroich, P.Heiss and Le-Chi-Niem, Nucl. Phys. A221 (1974) 461;
M.Yahiro and M.Kamimura, Prog. Theor. Phys. 65 (1981) 2051;
H.Kanada, T.Kaneko, S.Saito and Y.C.Tang, Nucl. Phys. A444 (1985) 209.

28) H.Nakamura, Nucl. Phys. A208 (1973) 207; A223 (1974) 59.

29) Houdayer, N.E.Davison, S.A.Elbakr, A.M.Sourkes, W.T.H.van Ores and A.D.Backer, Phys. Rev. C18 (19789 1985;
D.C.Dodder, G.M.Hale, N.Jarmie, J.H.Jett, P.W.Keaton, Jr.,R.A.Nisley and K.Witte, Phys. Rev. C15 (19779 518.

30) G.R.Plattner, A.D.Backer and H.E.Conzett, Phys. Rev. C5 (1972) 1158.

31) Cited in J.P.Svenne, J.Birchall and J.S.C.Mckee, Phys. Lett. 119B (1982) 269.

32) A.C.Phillips, Nucl. Phys. A107 (1968) 207.

33) R.T.Chahill and I.H.Sloan, Nucl. Phys. A165 (1971) 161.

34) G.A.Baker,Jr., Essentials of Pade Approximants (Academic press, New York, 1975).

35) M.Ishikawa, Dissertation, University of Tsukuba, Jan. 1983.

36) M.Ishikawa, S.Seki, K.Furuno, Y.Tagishi, M.Sawada, T.Sugiyama, K.Matsuda, T.Murayama, N.X.Dai, J.Sanada and Y.Koike, Phys. Rev. C28 (1983) 1884.

37) A.M.Sourkes, A.Houdayer and W.T.H.van oers, R.F.Carlson and R.E.Brown, Phys. Rev. C13 (1976) 451.

38) I.R.Afnan and A.W.Thomas, Modern Three-Hadoron Physics, ed. by A.W.Thomas (Springer-Verlag, Berlin, 1977), p14.

39) P.A.Schmelzbach, W.Gruebler, R.E.White, V.König, R.Risler and P.Marmier, Nucl. Phys. A197 (1972) 273.

40) I.Y.Barit and V.A.Sergeev, Sov. J. Nucl. Phys. 13 (1971) 708.

41) T.A.Tombrello, R.J. Spiger and A.D.Backer, Phys. Rev. 154 (1967) 935.

42) K.Miyagawa, T.Ueda, T.Sawada and S.Takagi, Nucl. Phys. A459 (1986) 93.

43) R.Aaron, Modern Three-Hadoron Physics, ed. by A.W.Thomas (Springer-Verlag, Berlin, 1977), p171.

Table 1

The state (ℓ_1,j) of the N-α channel, and the values of ℓ_2 and the potential parameters that reproduce the p-α phase shifts and absorption coefficients of Refs 29 and 30. For β_1, β_2, κ and λ, see Eqs. (2.5), (3.1) and (3.3). For the second component in Eq. (3.1), κ is understood to have the dimension $fm^{-2(\ell_2-\ell_1)}$.

(ℓ_1,j)	ℓ_2	$\beta_1(fm^{-1})$	$\beta_2(fm^{-1})$	κ	$\lambda(MeVfm^{-(\ell_1+1)})$
S 1/2	2	1.5711	1.8641	0.98227	-13683
p 3/2	1	1.6326	2.5726	0.39775	-4201.3
p 1/2	1	1.3240	0.65885	0.60572×10^{-3}	-620.25
d 5/2	2	2.9940	1.3015	0.54632×10^{-3}	-0.12858×10^{7}
d 3/2	0	2.8033	2.4166	0.29224×10^{-3}	-0.55874×10^{6}
f 7/2	3	2.2255	1.3723	0.37643×10^{-3}	-0.19468×10^{7}
f 5/2	3	1.6560	1.7831	0.82947	-0.22683×10^{6}

Table 2

The values of the potential parameters of coupled $^2S_{1/2}$-$^4D_{1/2}$ partial waves in the (N,d) system. The first channel is assigned to the $^2S_{1/2}$ channel and the second to the $^4D_{1/2}$ channel. For β_1, β_2, κ and λ, see Eqs. (2.5), (3.1) and (3.3). For the second component in Eq. (3.1), κ is understood to have the dimension $fm^{-2(\ell_2-\ell_1)}$.

$\beta_1(fm^{-1})$	$\beta_2(fm^{-1})$	κ	$\lambda(MeVfm^{-(\ell_1+1)})$
4.1332	1.3488	0.44437	-5305.4

Table 3

The values of the potential parameters of $^1S_0$ partial wave in the (N,A) system. For β_1, β_2, λ_1 and λ_2, see Eqs. (4.22) and (4.23).

$\beta_1(fm^{-1})$	$\beta_2(fm^{-1})$	$\lambda_1(MeVfm^{-1})$	$\lambda_2(MeVfm^{-1})$
0.36956	0.38028	-84.713	68.025

Figure captions

Fig. 1 The compex z plane into which the Riemann surface of a two-channel t-matrix is mapped. The parentheses indicate whether k_1 and k_2 are positive, nagative, imaginary or negative imaginary, respectively. The numbers in each square bracket denote the quadrants to which k_1 and k_2 belong in each complex plane.

Fig. 2 The N-α pase shifts and absorption coefficients obtained by the parameter values listed in Table 1. The dots are the data points of Ref. 29. For the $d_{3/2}$ state, the triangles and the squares are the data taken from Ref. 30.

Fig. 3 The d-α elastic scattering cross sections and vector and tensor analyzing powers at E_d(Lab)=21 MeV. The experimental points are taken from Ref. 35. The solid lines are with full effects of absorption and the Pauli exclusion. The results without absorption effects are given by the dashed lines, and those without the Pauli exclusion are shown by the dot-dashed lines. The NN potential utilized is the YY7 of Ref. 32.

Fig. 4 The results for the d-α elastic scattering at E_d(Lab)=56 MeV. The data are taken from Ref. 16. See the caption of FIg. 3 for other details.

Fig. 5 Comparison of the results for the d-α elastic scattering at E_d=21 MeV calculated by using the YY7 and YY0 potentials. The results are shown by the solid and

dashed lines, respectively, for the YY7 and YY0.

Fig. 6 Comparison of the results for the d-α elastic scattering at E_d=56 MeV calculated by using the YY7 and YY0 potential. See the caption of Fig. 5.

Fig. 7 Comparison of the results for the d-α elastic scattering at E_d=21 MeV calculated by using the YY7 and 2T4 potentials. The results are shown by the solid and dashed lines, respectively, for the YY7 and 2T4.

Fig. 8 The results of the d-α elastic scattering without the f-waves in the (N,α) subsystem (dashed lines) are compared with those including the f-waves (solid lines) at E_d(lab)=56 MeV.

Fig. 9 The schematic diagram of the MTCC model as applied to a simplified model of the d-α scattering. For detailed explanation, see the text.

Fig. 10 The diagramatic representation of Eq. (4.3). For detailed explanation, see the text.

Fig. 11 Two-body processes involved in the (d,α) system in (a) particle channel 1 and (b) particle channel 5 of Fig. 9.

Fig. 12 A lowest order diagram of transition from particle channel 1 to 6.

Fig. 13 The lowest order two-body process for p+α → d+^{3}He.

Fig. 14 Two possible processes obtained by repracing the two-body process p+α → d+^{3}He in Fig. 12 by Fig. 13. The vertical lines connecting two particle lines represent interactions. The time runs from left to right.

Fig. 15 The lowest order diagram from particle channel 1 to

particle channel 1 (process (a)) and from particle channel 5 to particle channel 1 (process (b)).

Fig. 16 The phase shifts of $^2S_{1/2}$ and the mixing parameters in the coupled $^2S_{1/2}$-$^4D_{1/2}$ partial waves of N-d scattering, which are obtained by the parameter values listed in Table 2. The dots are the data taken from Ref. 39.

Fig. 17 The N-^{3}He phase shifts of $^1S_0$ partial wave obtained by the parameter values listed in Table 3. The dots are the data points of Ref. 40.

Fig. 18 The results for the d-α elastic scattering at E_d(Lab)=56 MeV. The solid and dashed lines correspond to two possible choice of the sign of τ_{24}. The dot-dashed line are pure three-body calculations given in Fig. 4 (with no absorption).

Fig. 19 The differntial cross sections for ^{3}He(d,d)^{3}He at the center of mass angle 90.0 , obtained by the simplified potential for the coupled (N_2,α) and (d,A) system, which is mentioned in § 4.2.2. The solid circles are the data taken from Ref. 41.

Fig. 20 A typical diagram for a sequential trnsfer. The time runs from left to right.

Fig. 21 A typical diagram of the MTCC process of Fig. 9.

Fig. 22 An example of diagrams which includes breakup of the spectator α.

Fig. 23 The process of Fig. 22 is decomposed into process (a) and process (b).

Fig. 24 A part of the processes included in Z_{65}. See Fig. 9 for particle channels.

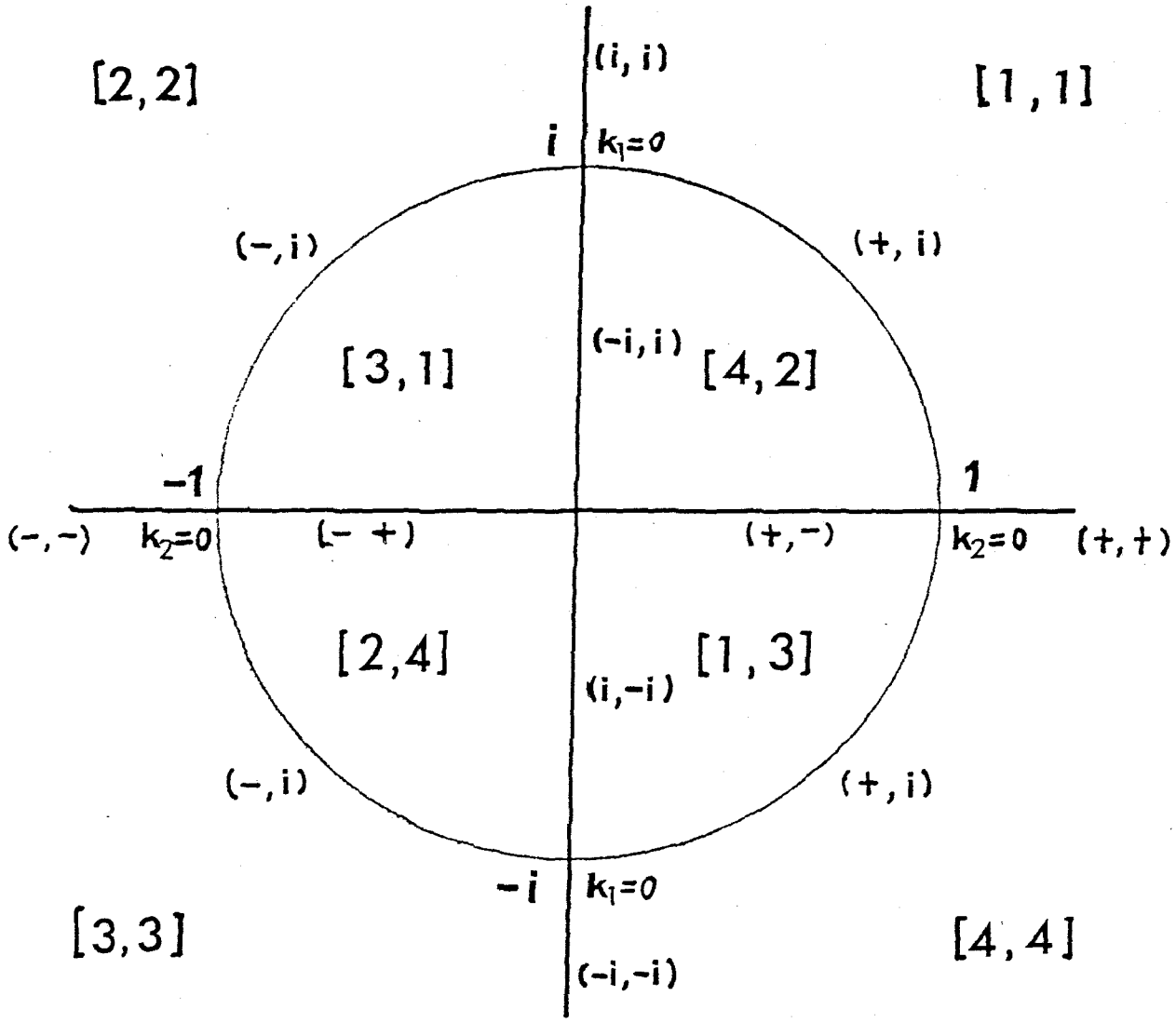

Fig. 1

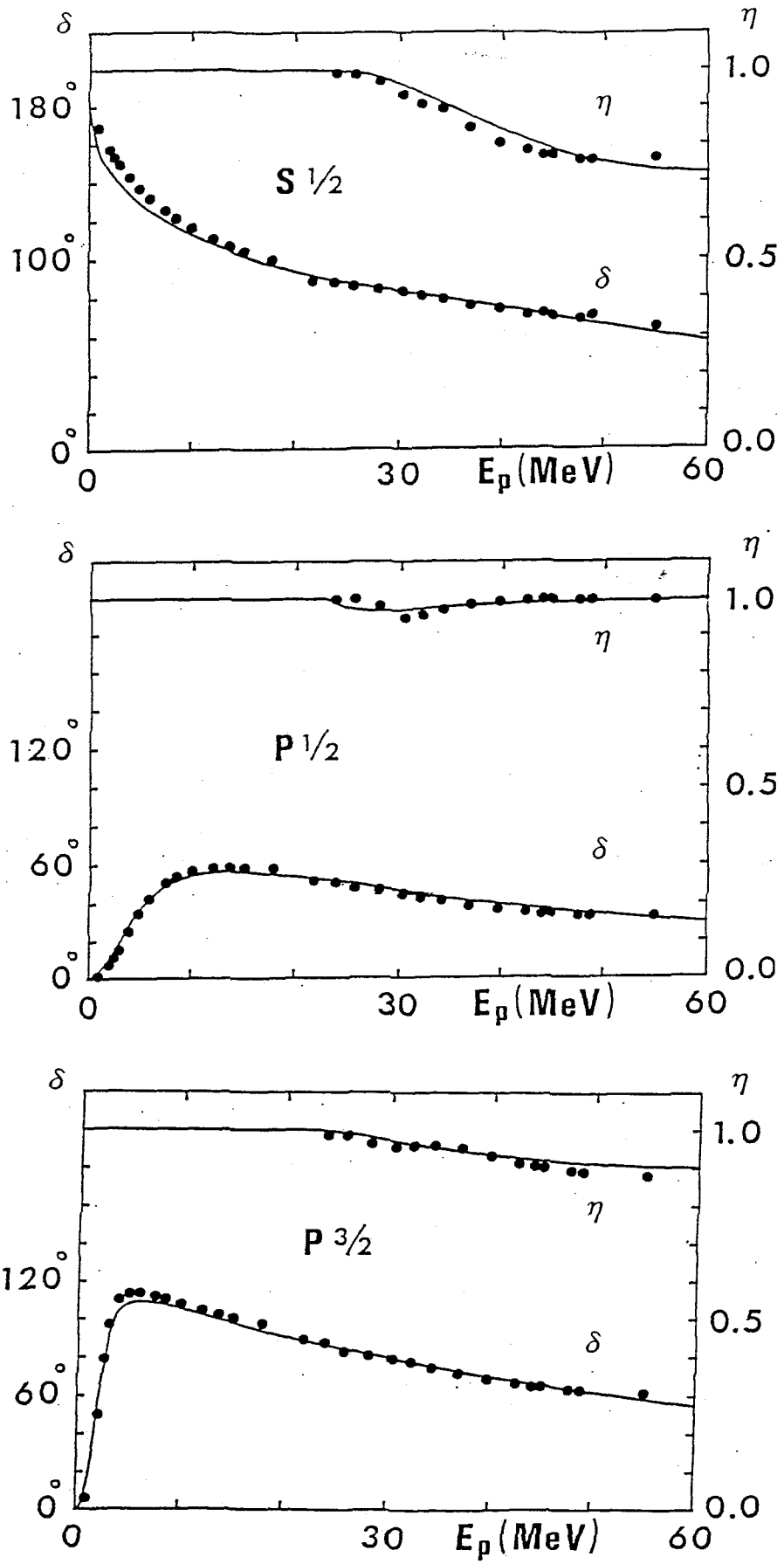

Fig. 2

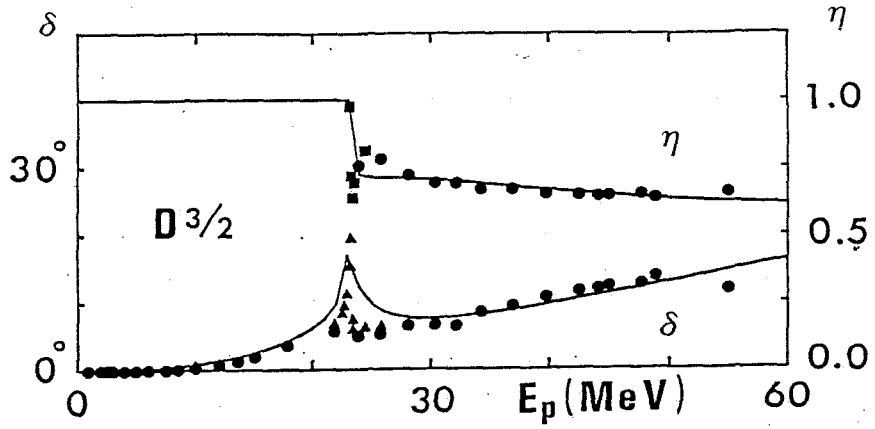
δ
η
30°
0°
1.0
0.5
0.0
D 3/2
η
δ
0
30
Ep(MeV)
60

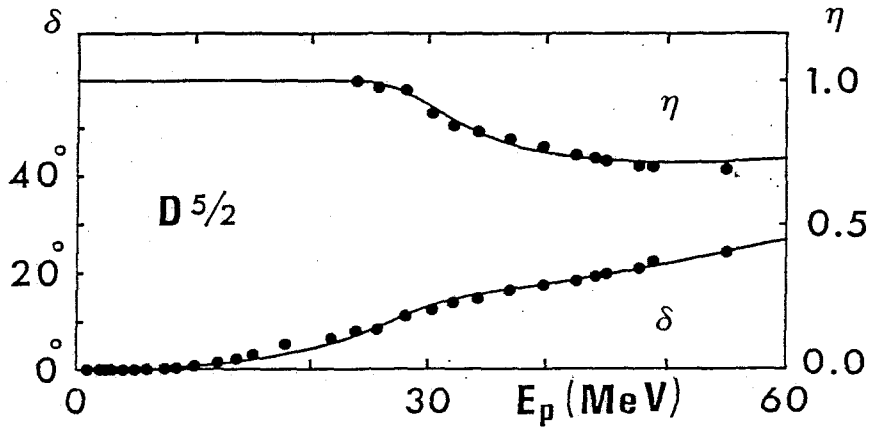
δ
η
40°
20°
0°
1.0
0.5
0.0
D 5/2
η
δ
0
30
Ep(MeV)
60

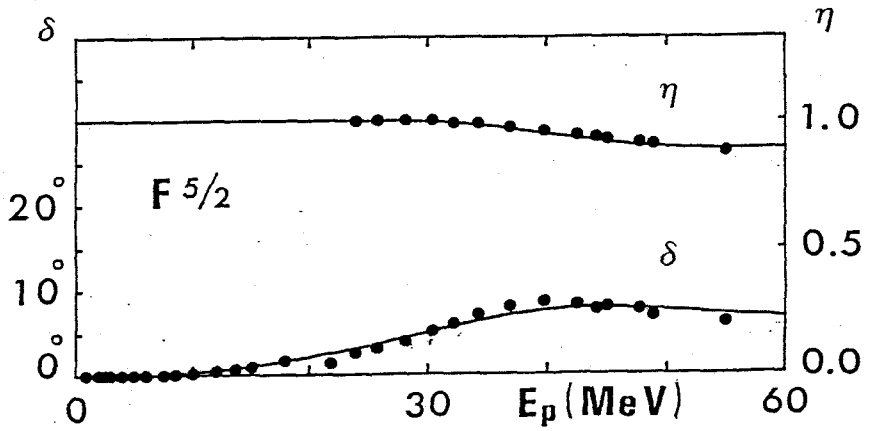
δ
η
20°
10°
0°
1.0
0.5
0.0
F 5/2
η
δ
0
30
Ep(MeV)
60

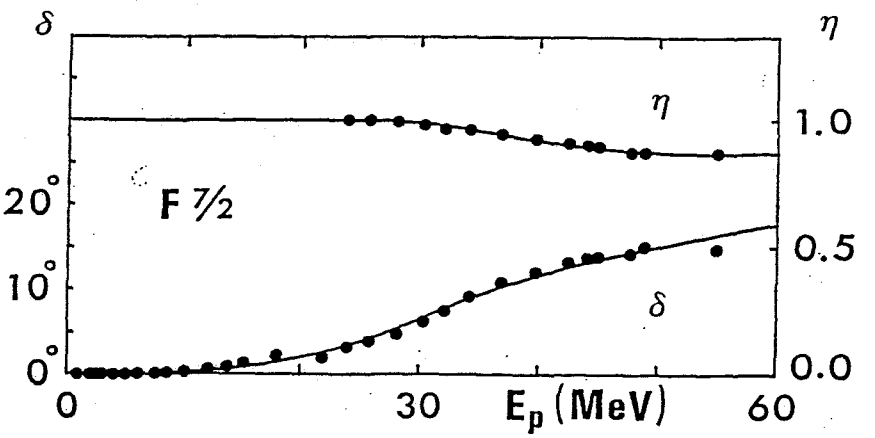
δ
η
20°
10°
0°
1.0
0.5
0.0
F 7/2
η
δ
0
30
Ep(MeV)
60

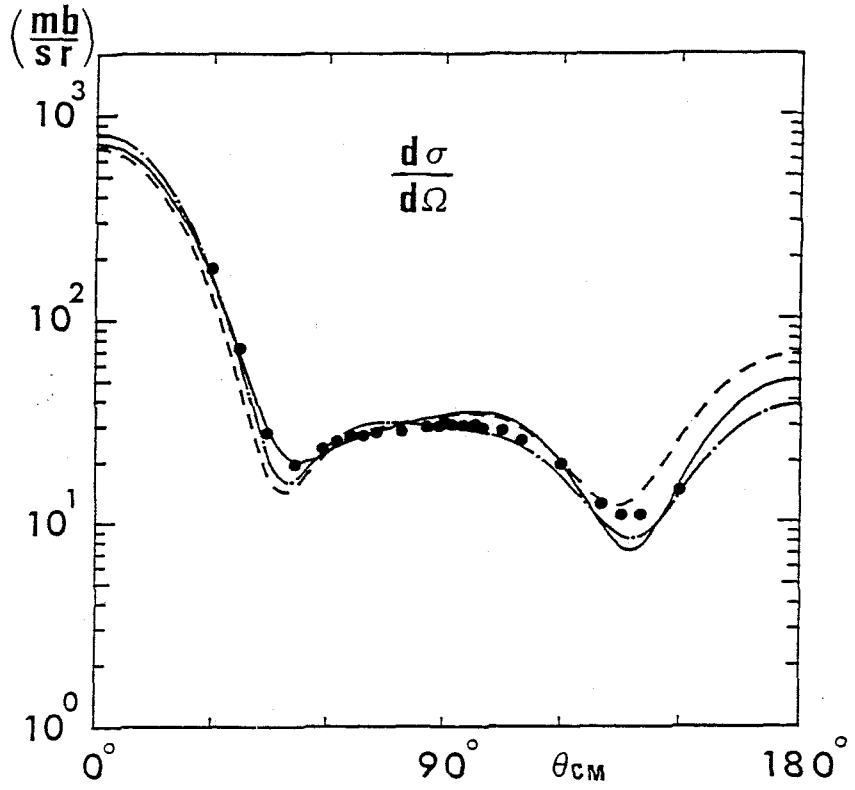

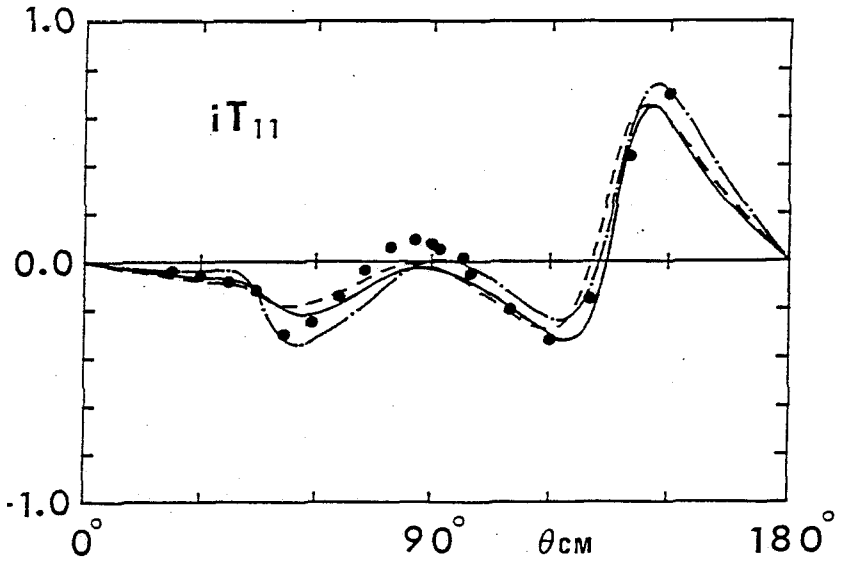

Fig. 3

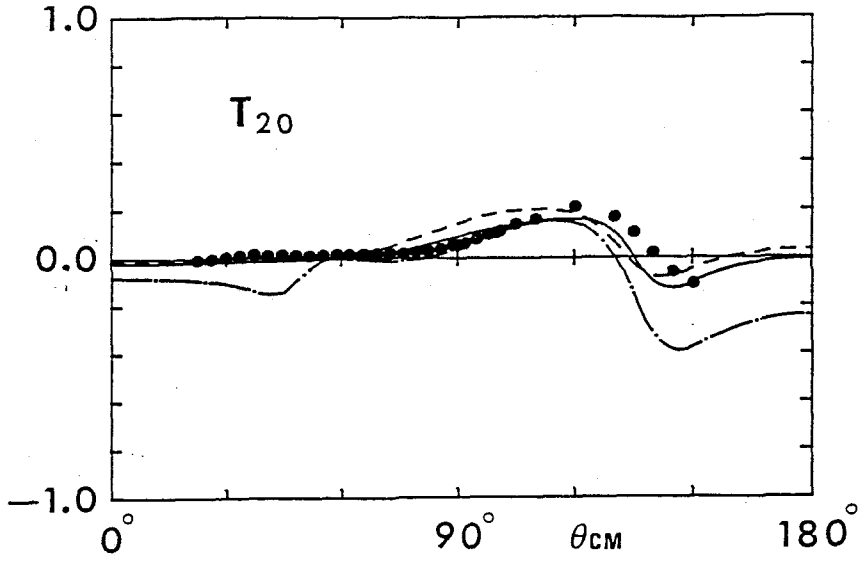
1.0
T_{20}
0.0
−1.0
0°
90°
θcm
180°

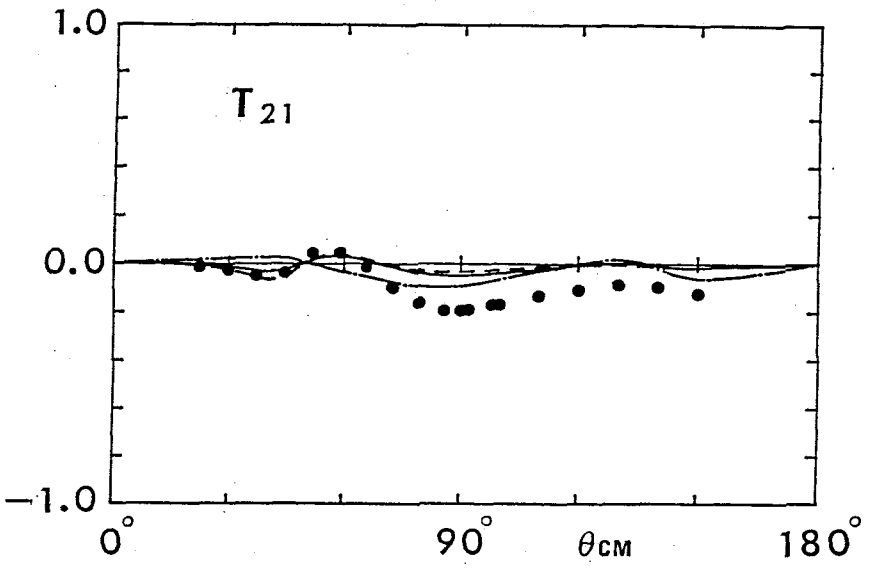
1.0
T_{21}
0.0
−1.0
0°
90°
θcm
180°

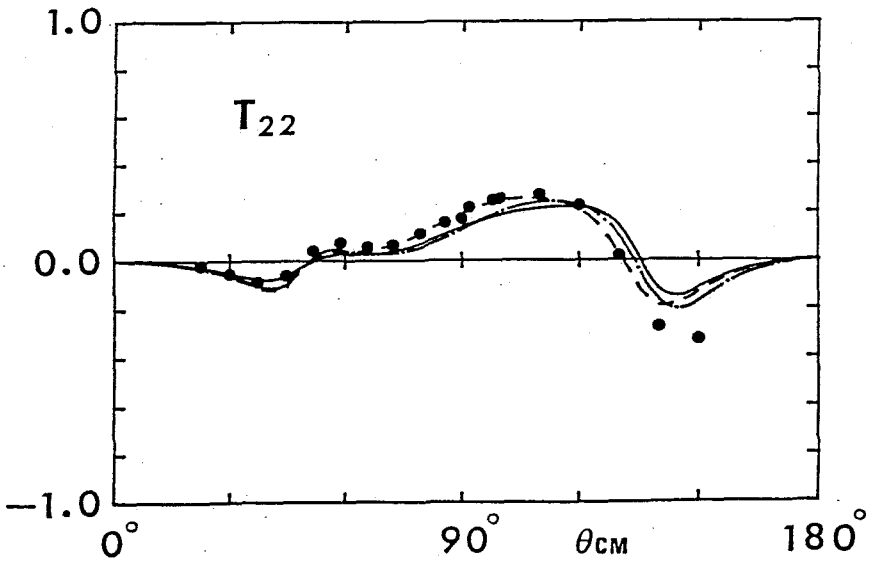
1.0
T_{22}
0.0
−1.0
0°
90°
θcm
180°

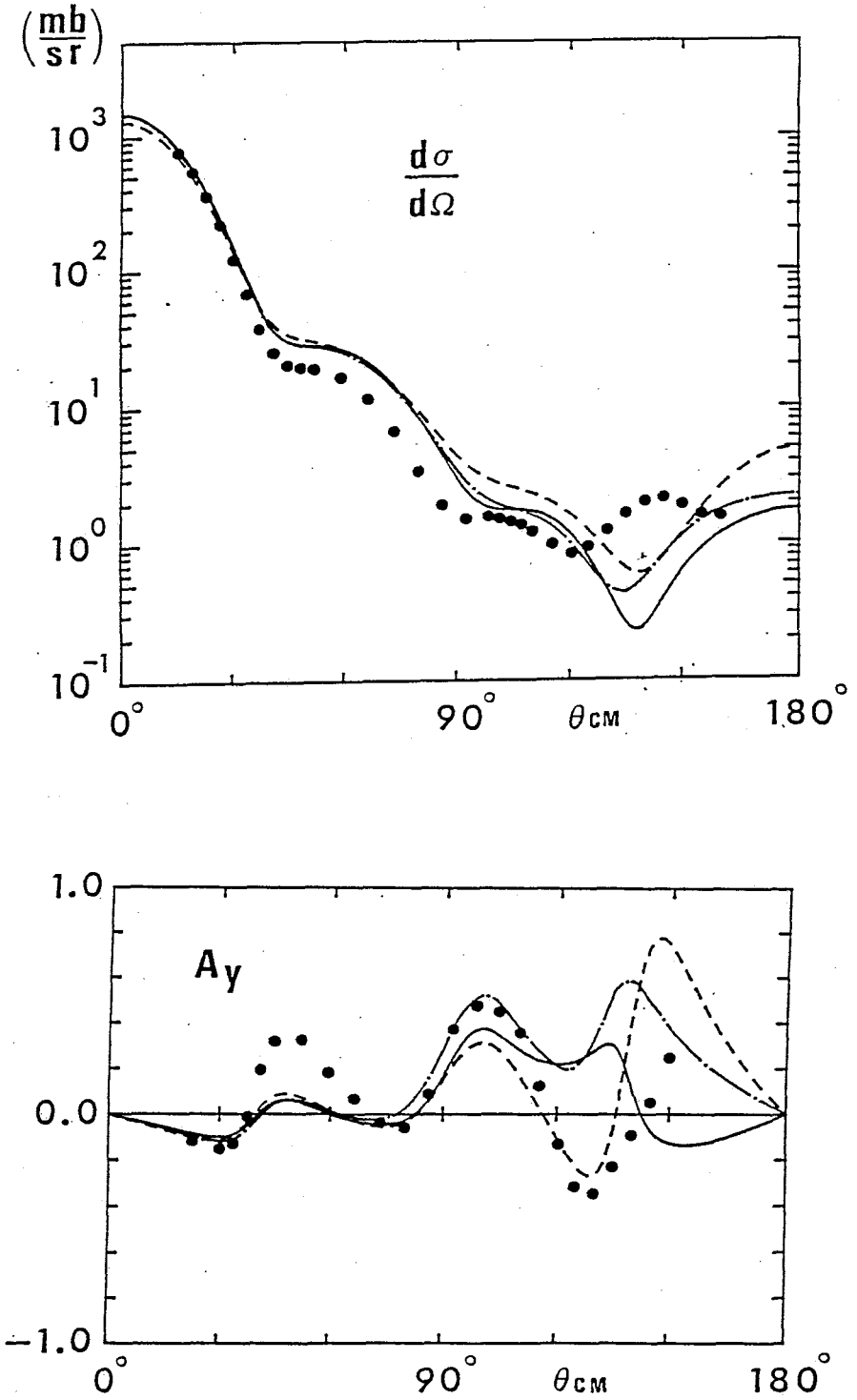

Fig. 4

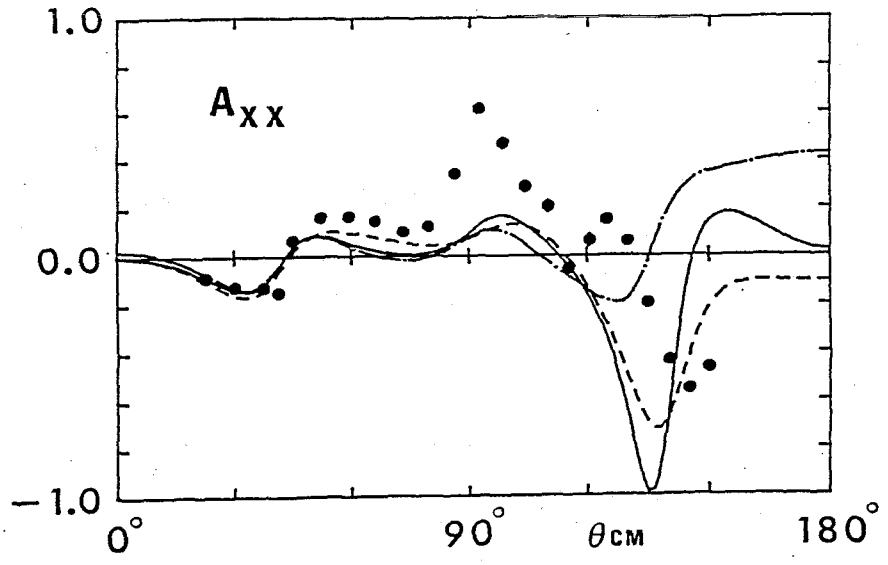
1.0
A_{xx}
0.0
−1.0
0°
90°
θcm
180°

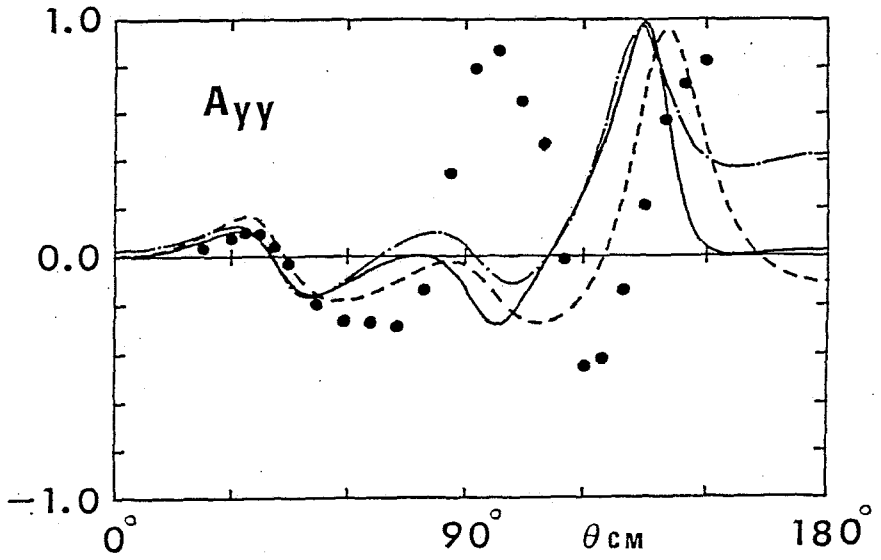
1.0
A_{yy}
0.0
−1.0
0°
90°
θcm
180°

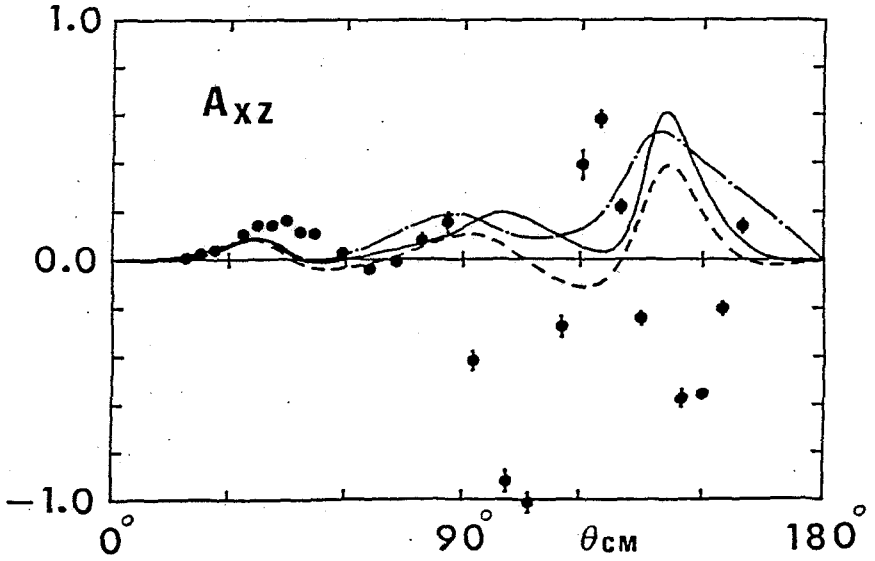
1.0
A_{xz}
0.0
−1.0
0°
90°
θcm
180°

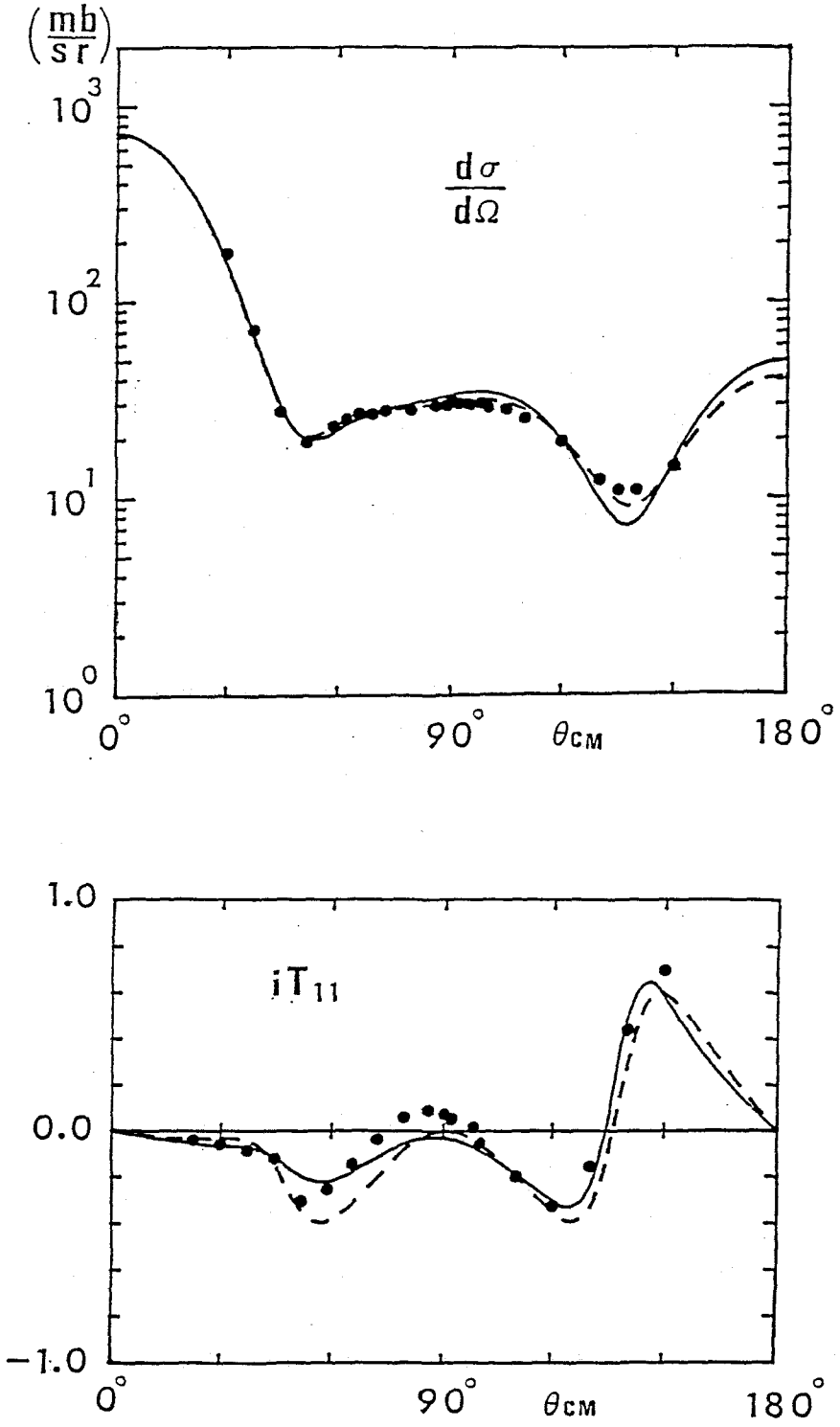

Fig. 5

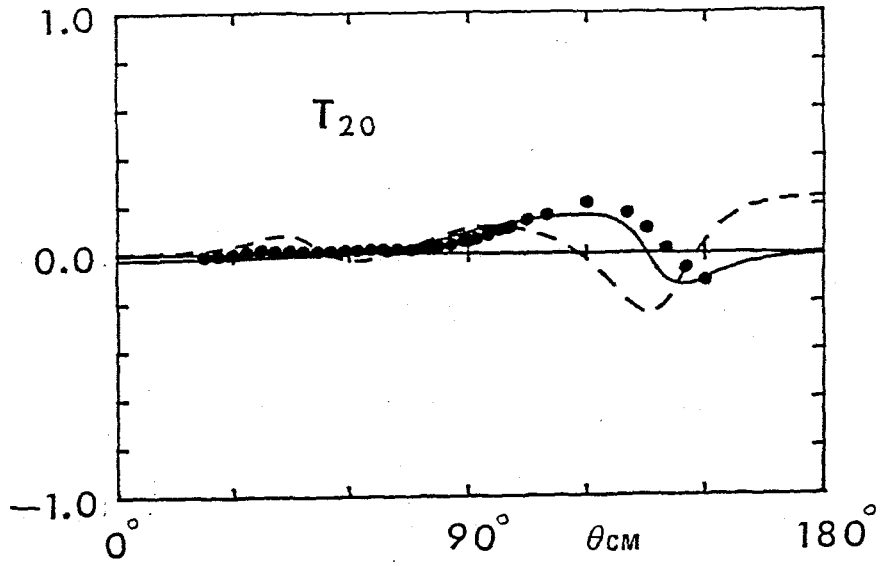
1.0
T_{20}
0.0
−1.0
0°
90°
θ_{CM}
180°

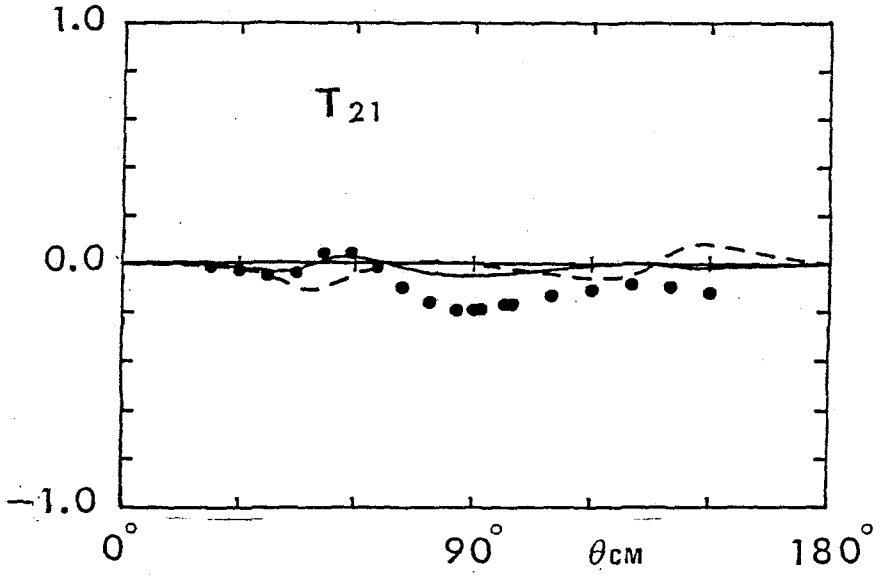
1.0
T_{21}
0.0
−1.0
0°
90°
θ_{CM}
180°

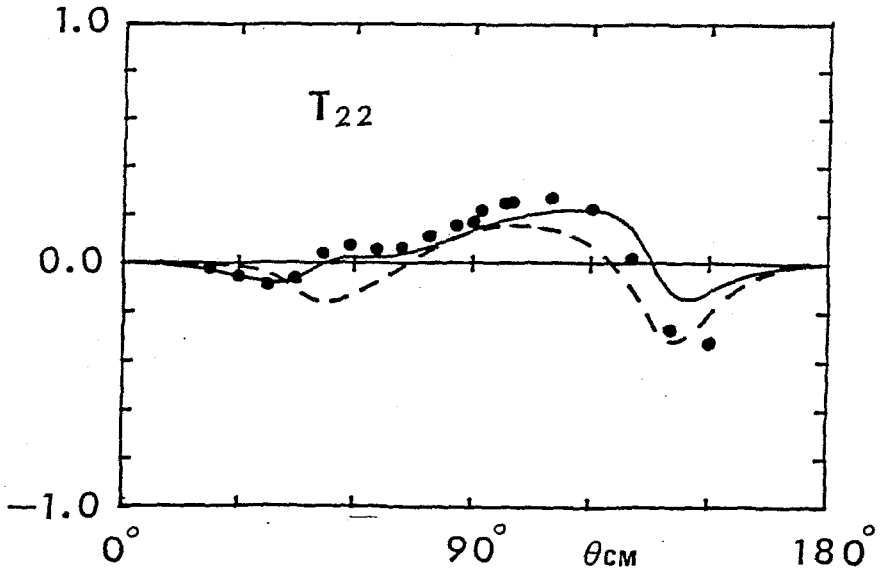
1.0
T_{22}
0.0
−1.0
0°
90°
θ_{CM}
180°

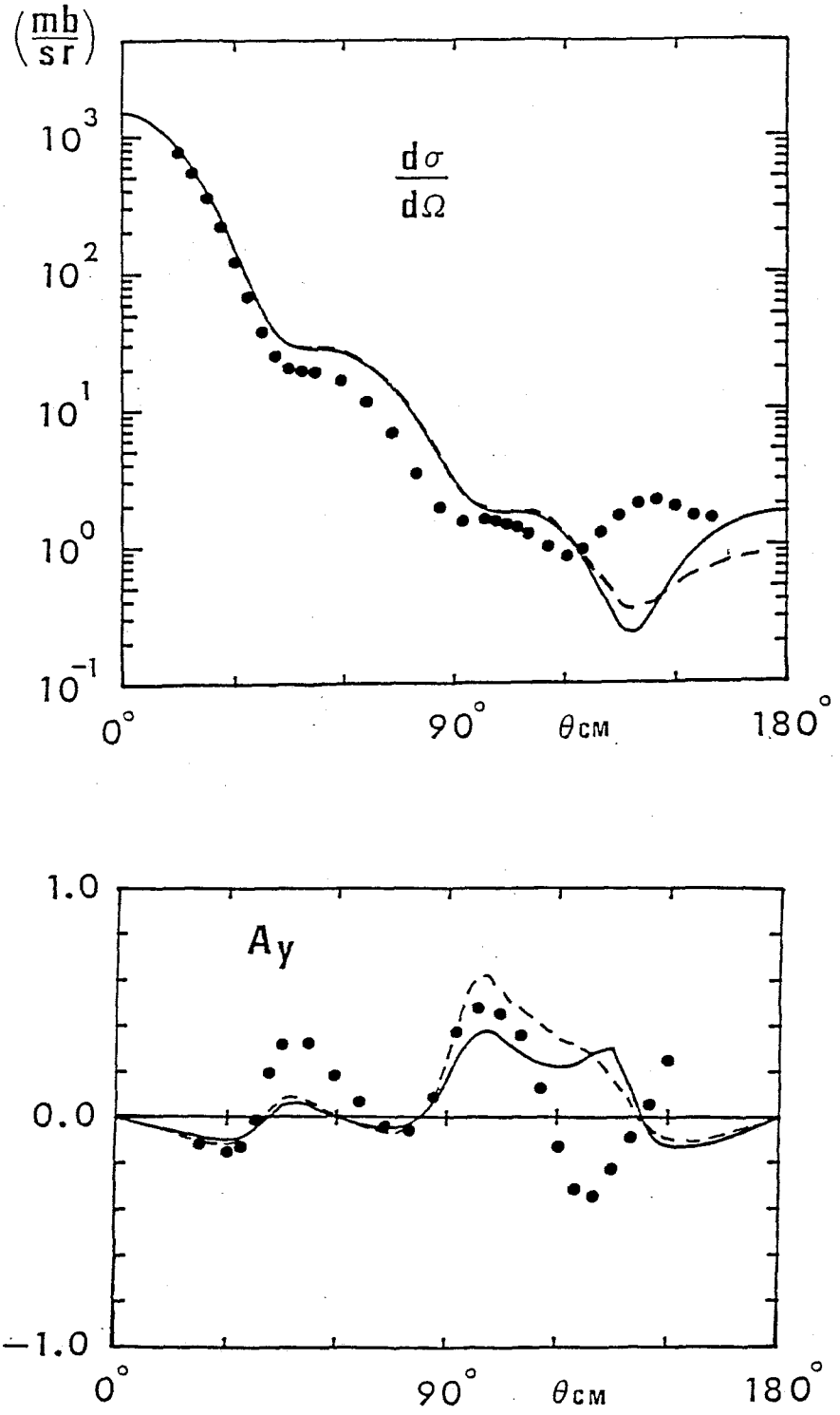

Fig. 6

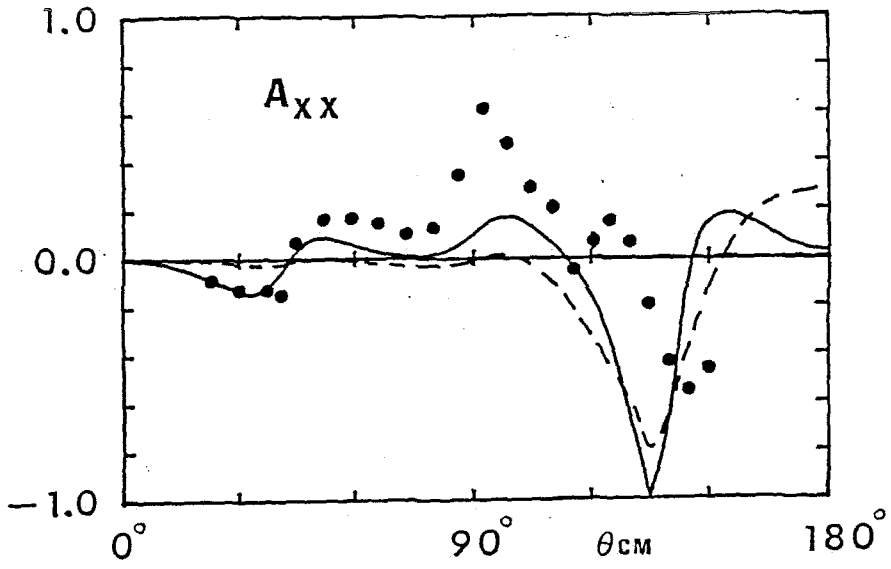
1.0
A_{xx}
0.0
−1.0
0°
90°
θcм
180°

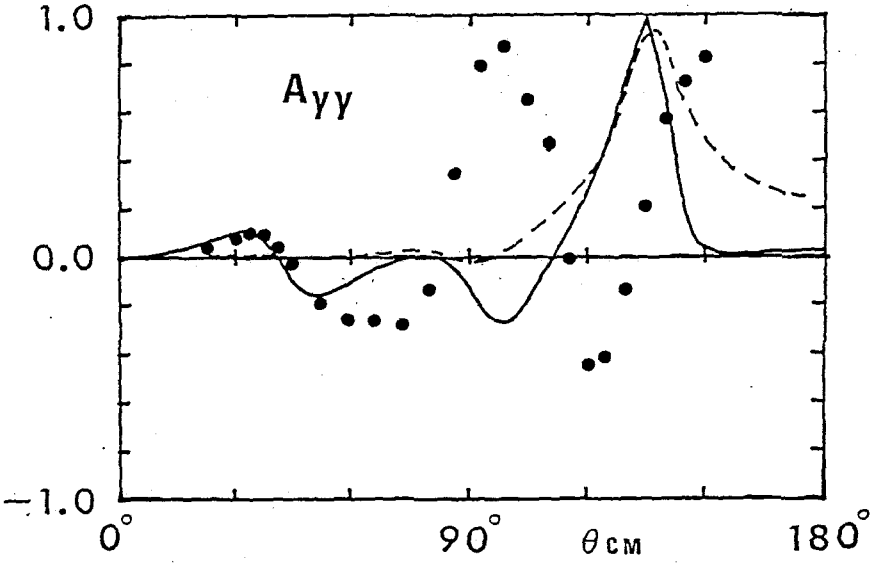
1.0
A_{yy}
0.0
−1.0
0°
90°
θcм
180°

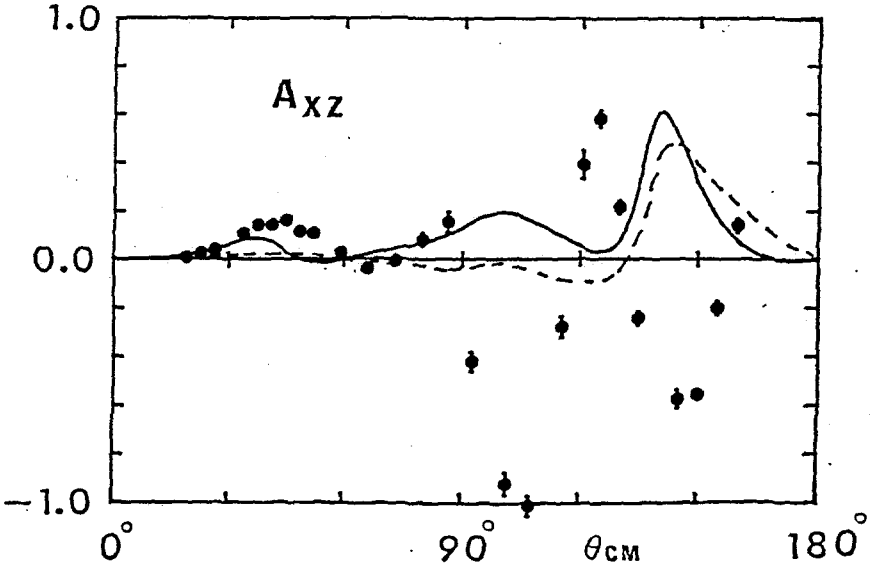
1.0
A_{xz}
0.0
−1.0
0°
90°
θcм
180°

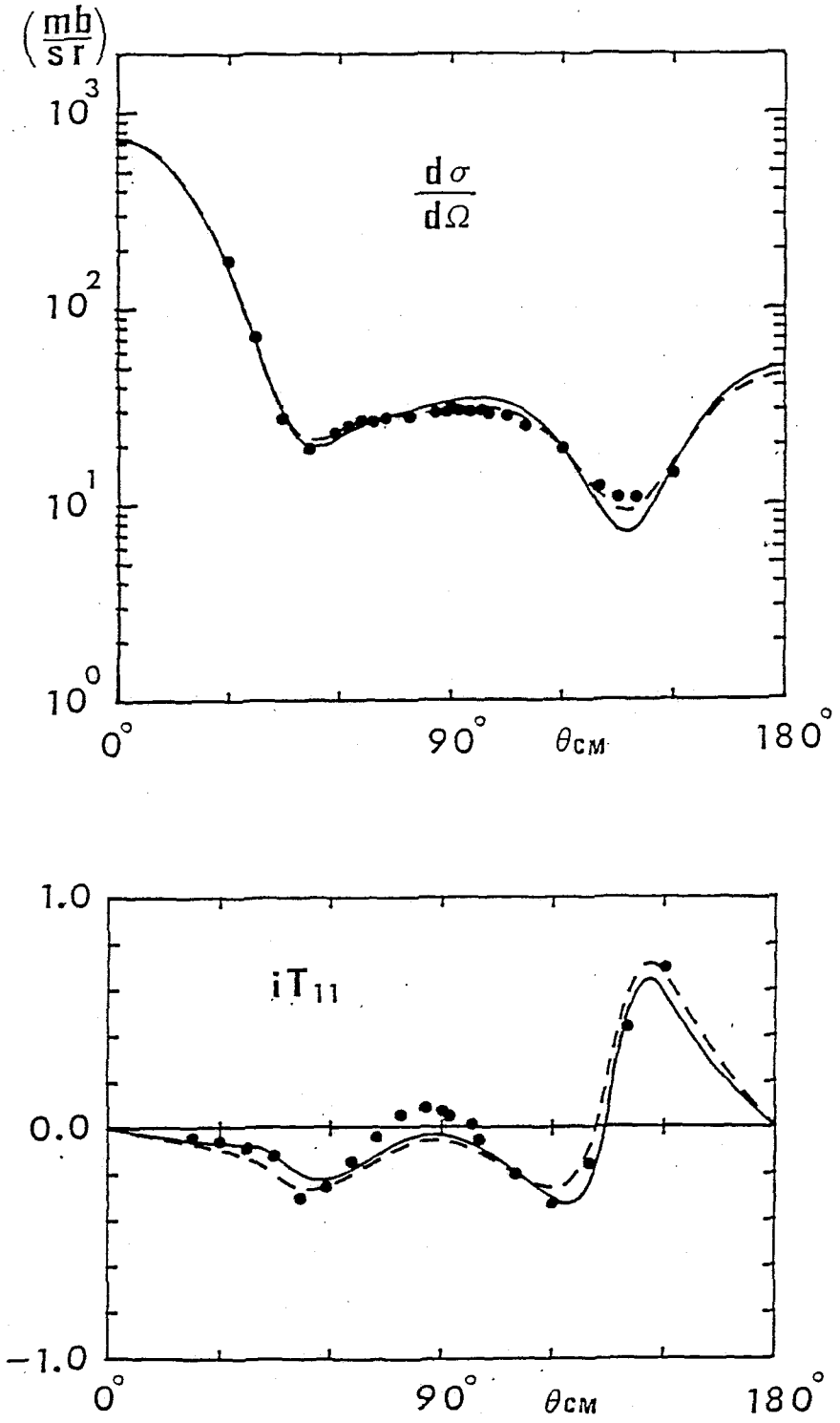

Fig. 7

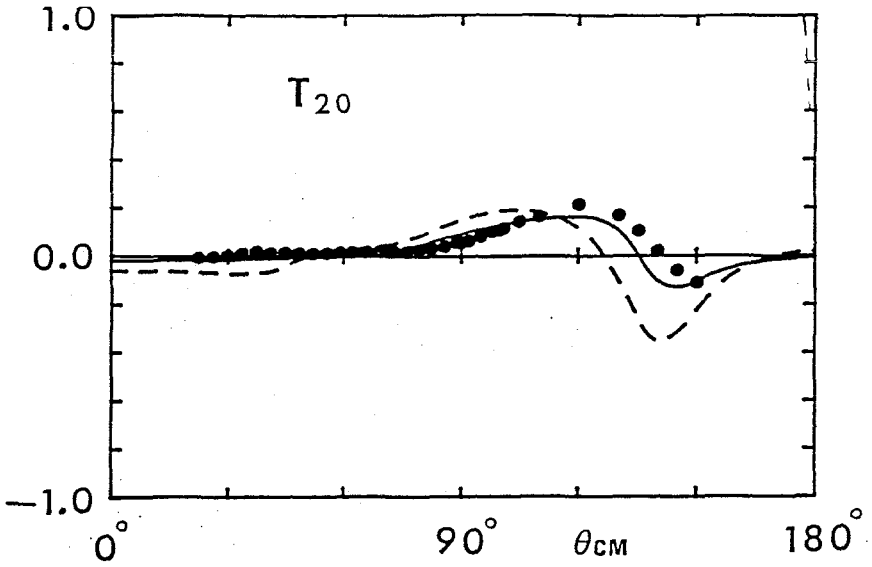
1.0
T_{20}
0.0
−1.0
0°
90°
θ_{CM}
180°

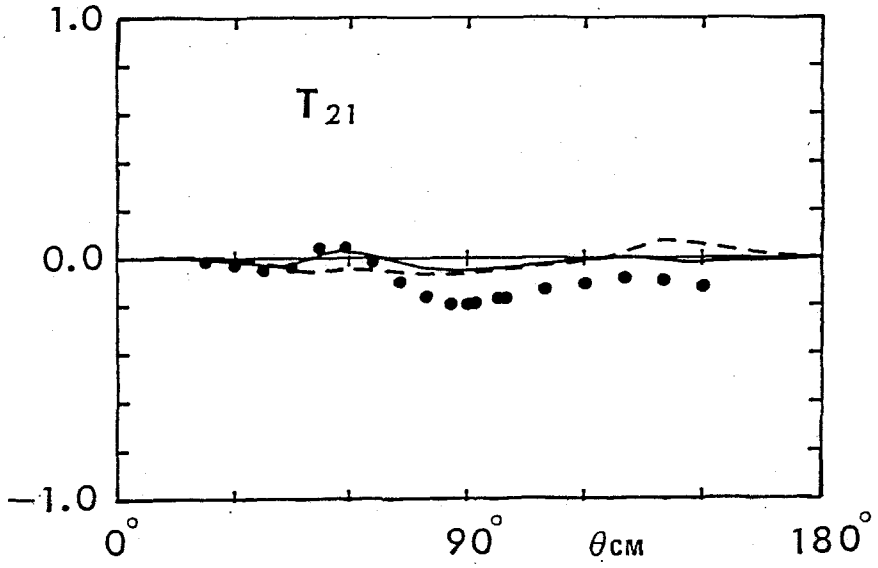
1.0
T_{21}
0.0
−1.0
0°
90°
θ_{CM}
180°

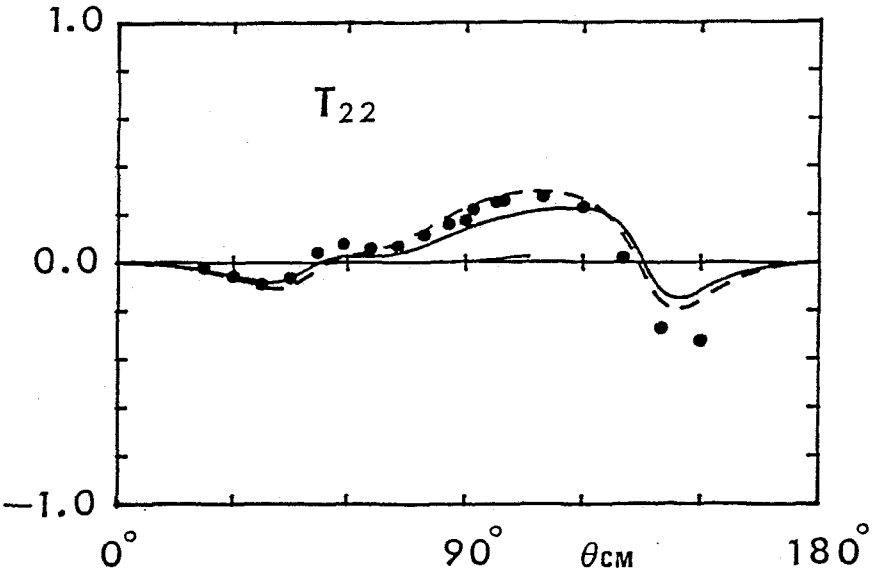
1.0
T_{22}
0.0
−1.0
0°
90°
θ_{CM}
180°

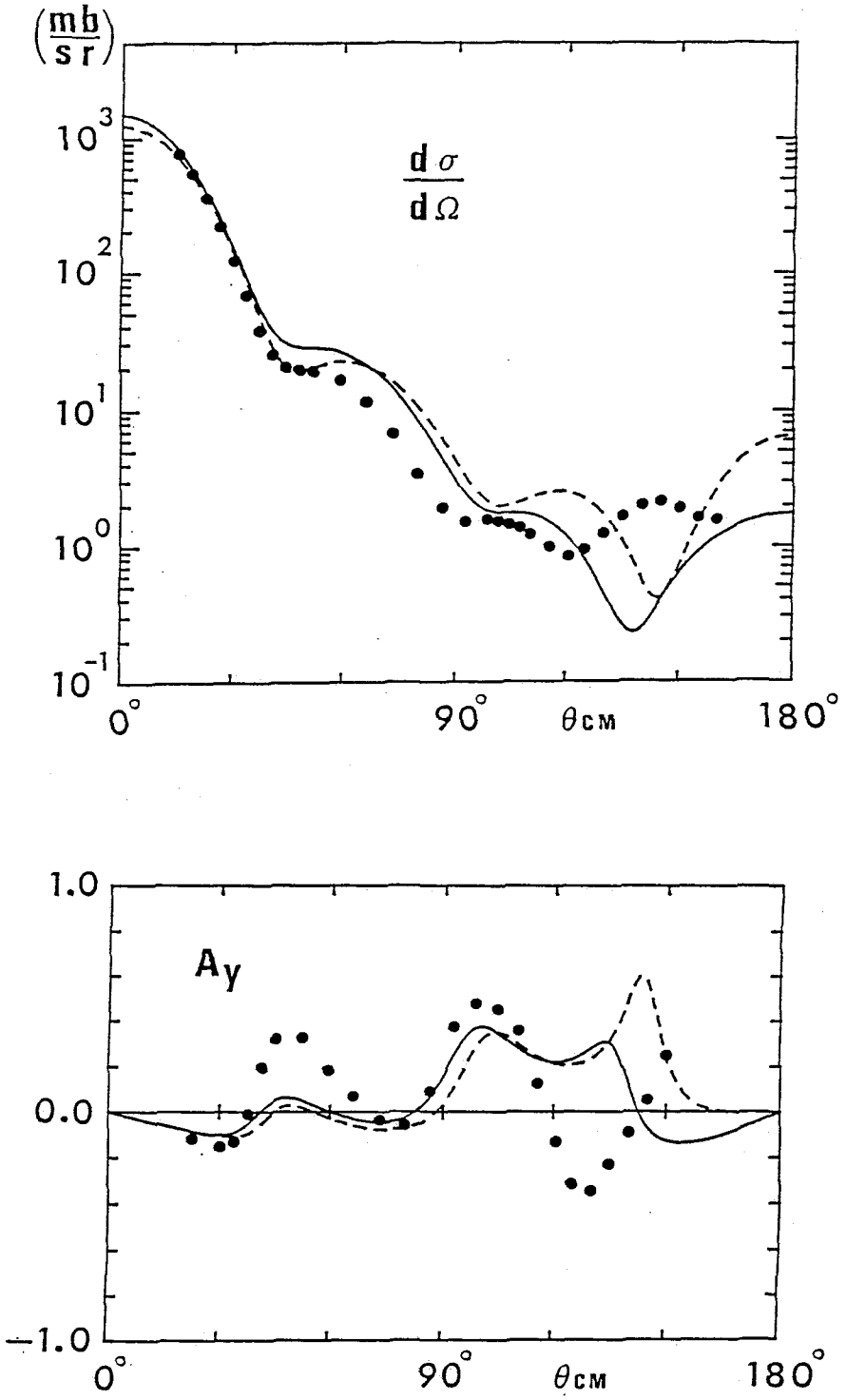

Fig. 8

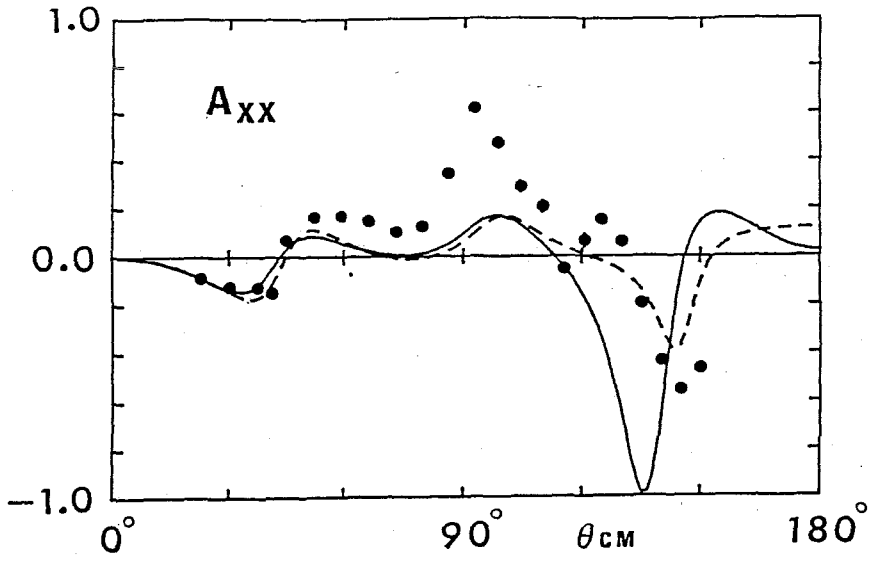
1.0
A_{xx}
0.0
−1.0
0°
90°
θсм
180°

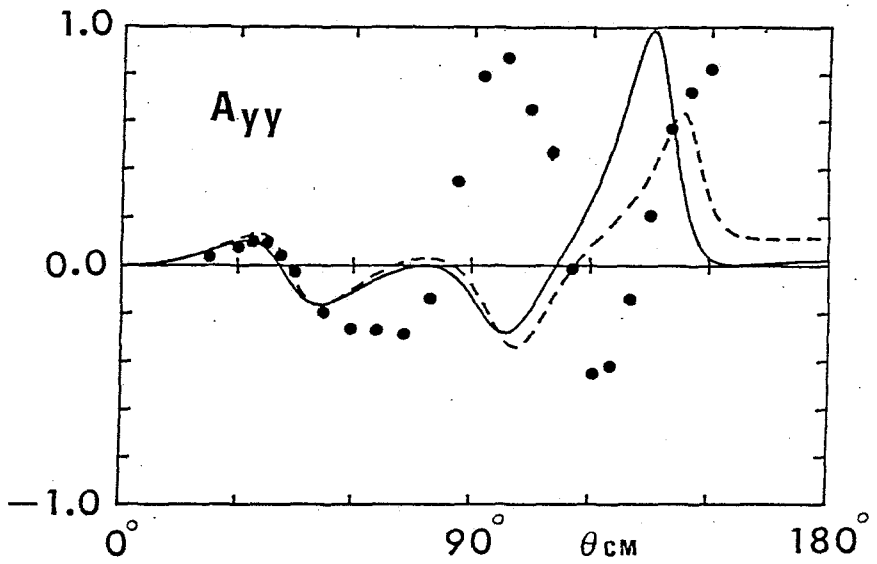
1.0
A_{yy}
0.0
−1.0
0°
90°
θсм
180°

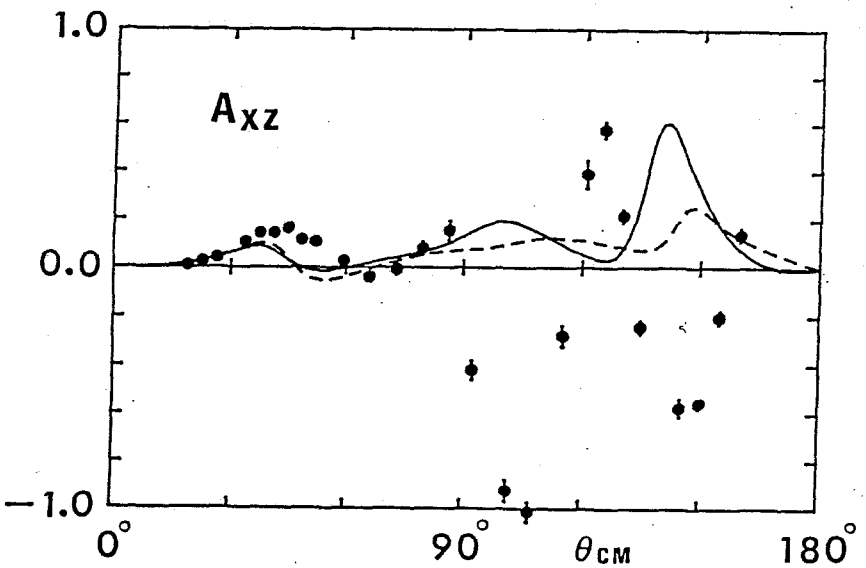
1.0
A_{xz}
0.0
−1.0
0°
90°
θсм
180°

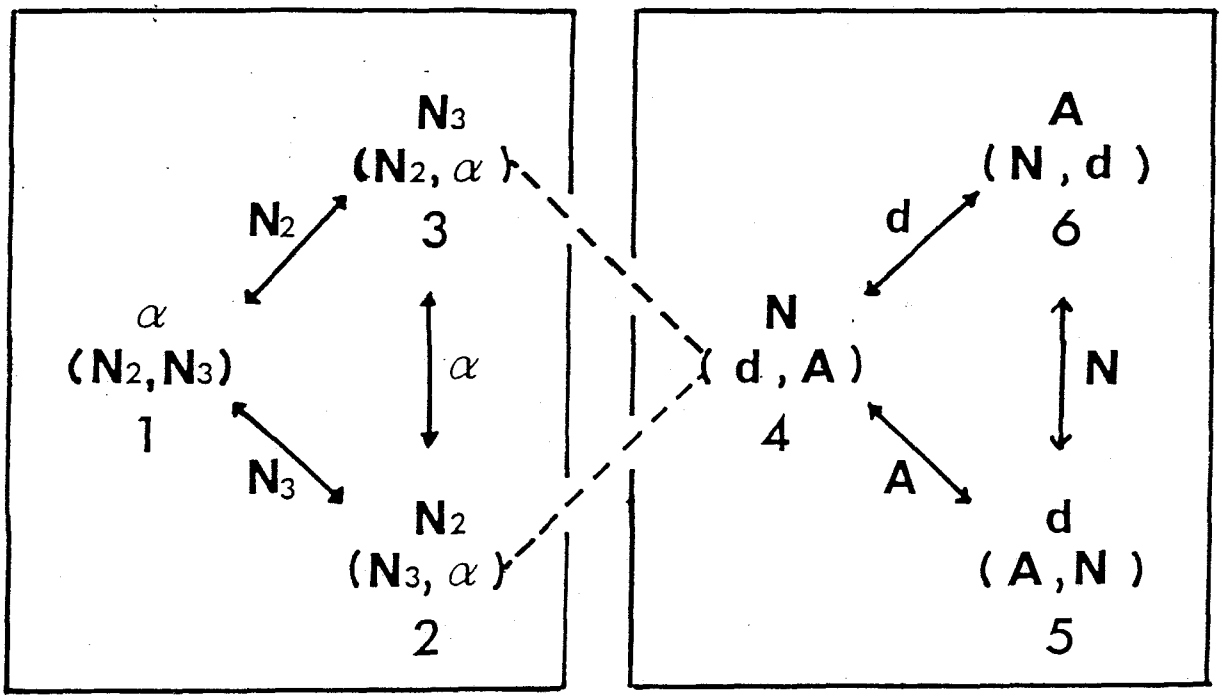

Fig. 9

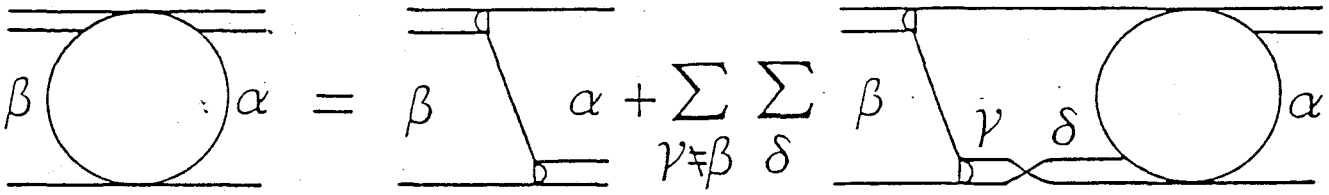

Fig. 10

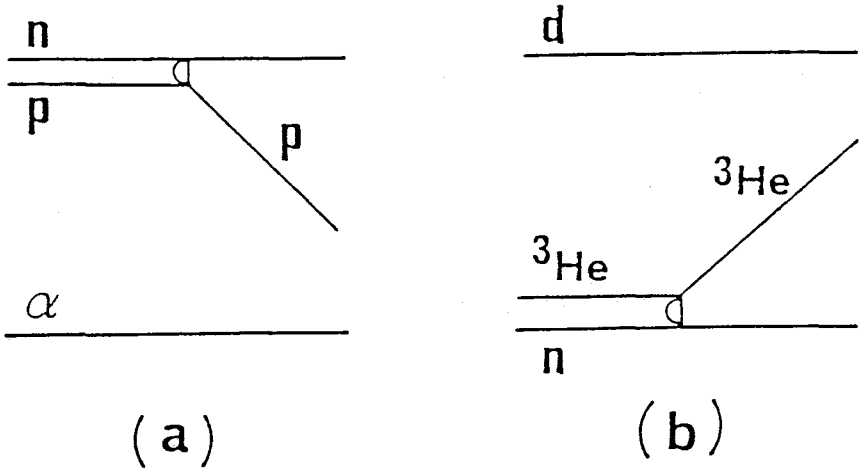

Fig.11

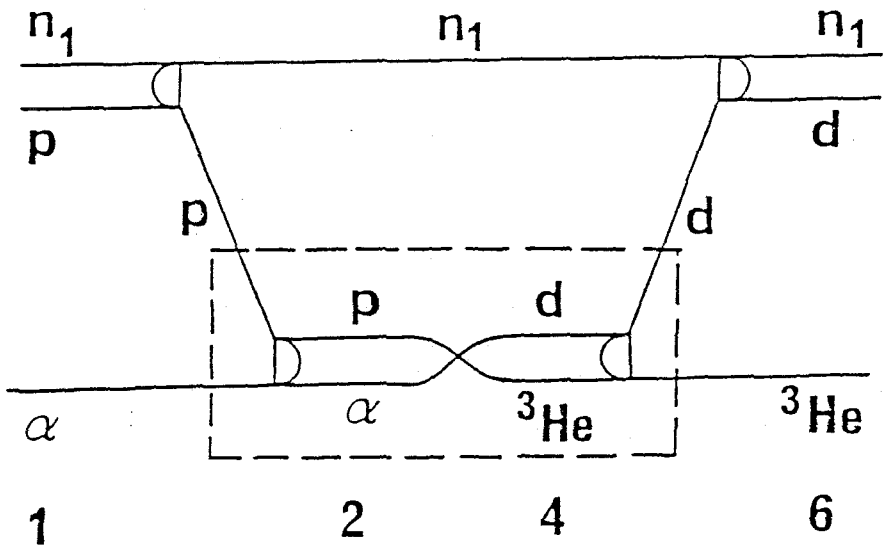

Fig. 12

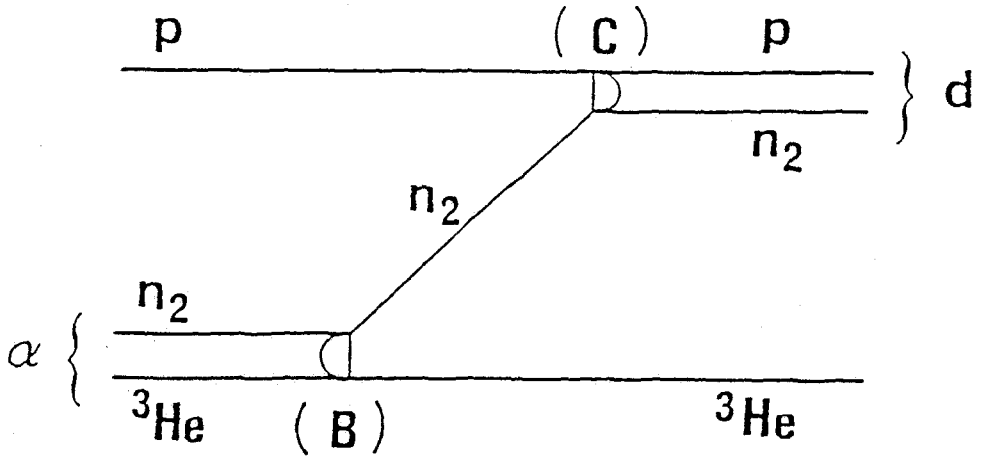

Fig. 13

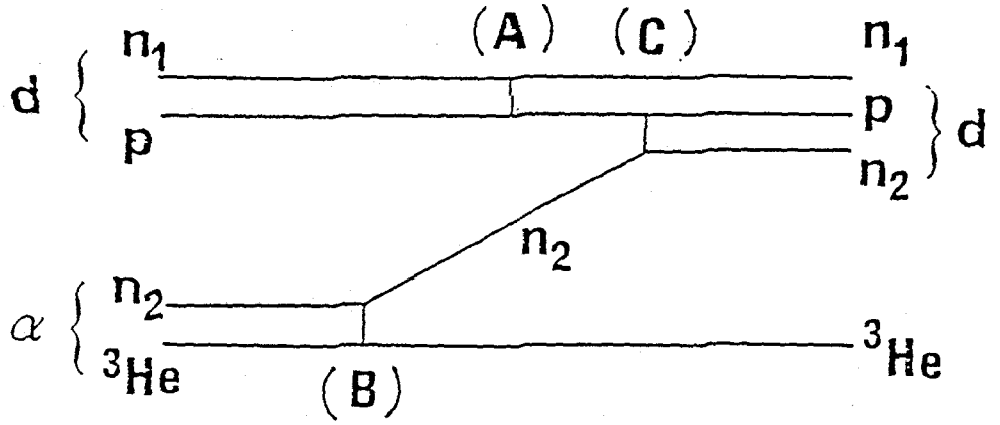

(a)

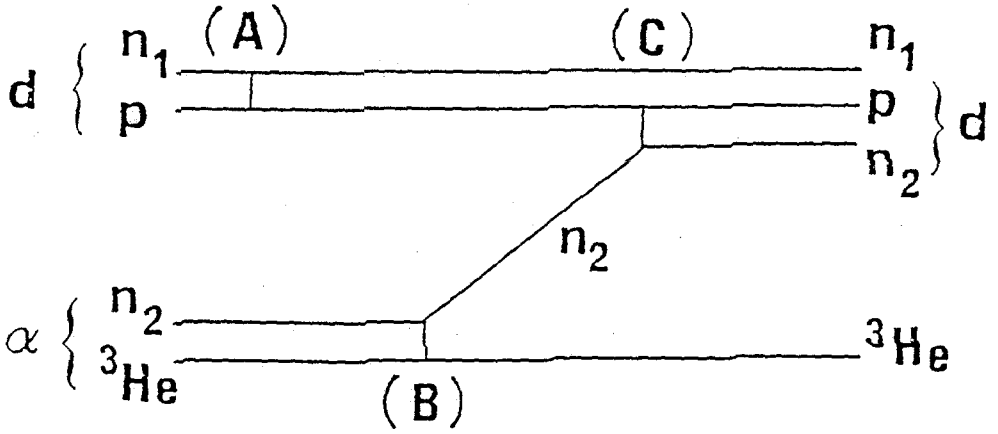

(b)

Fig. 14

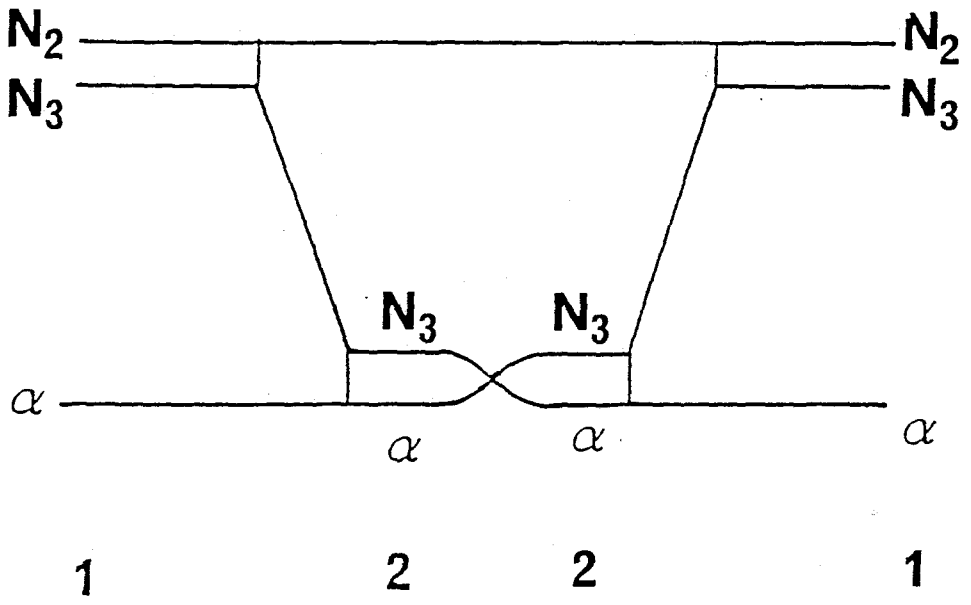

(a)

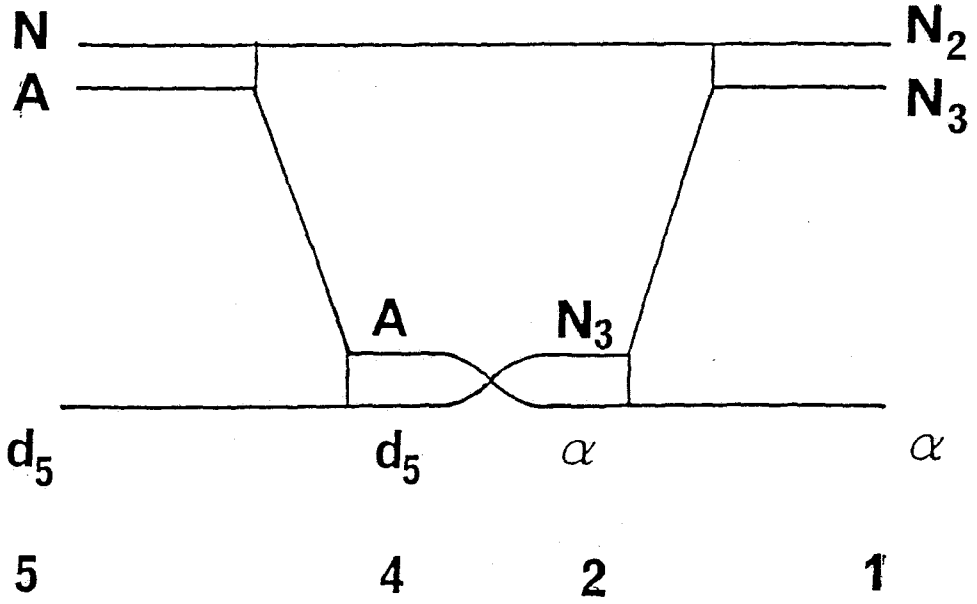

(b)

Fig. 15

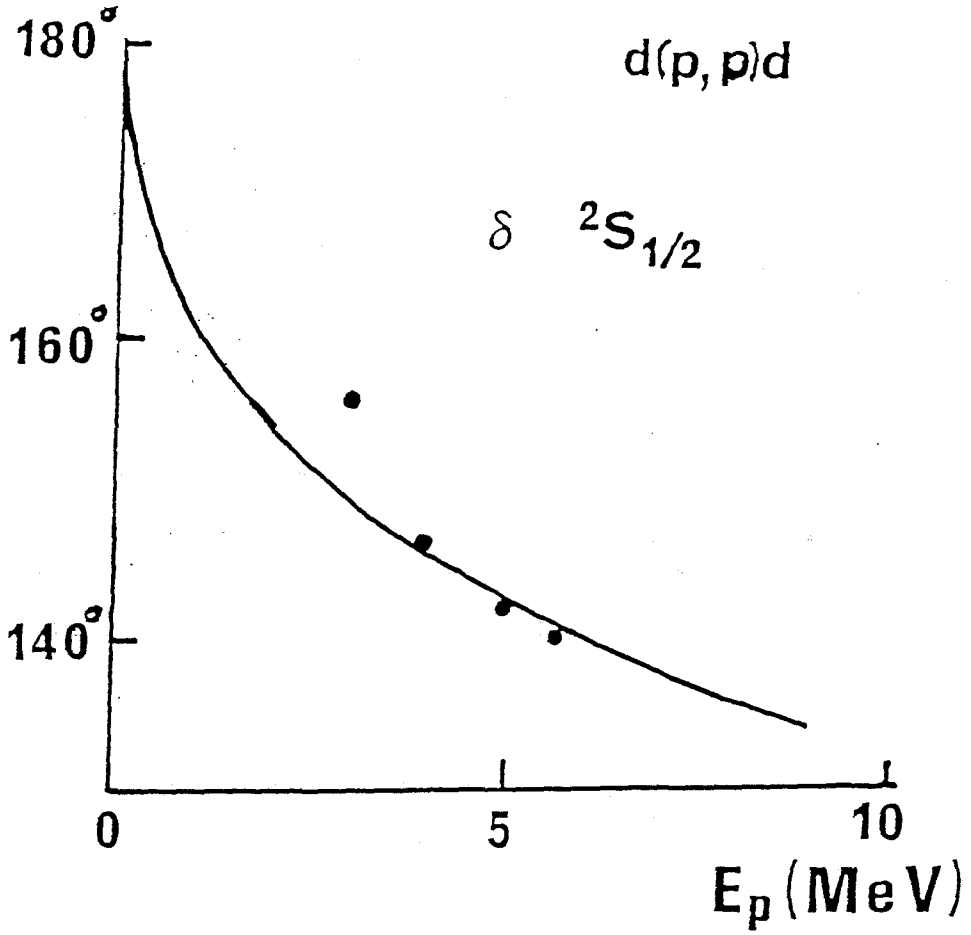

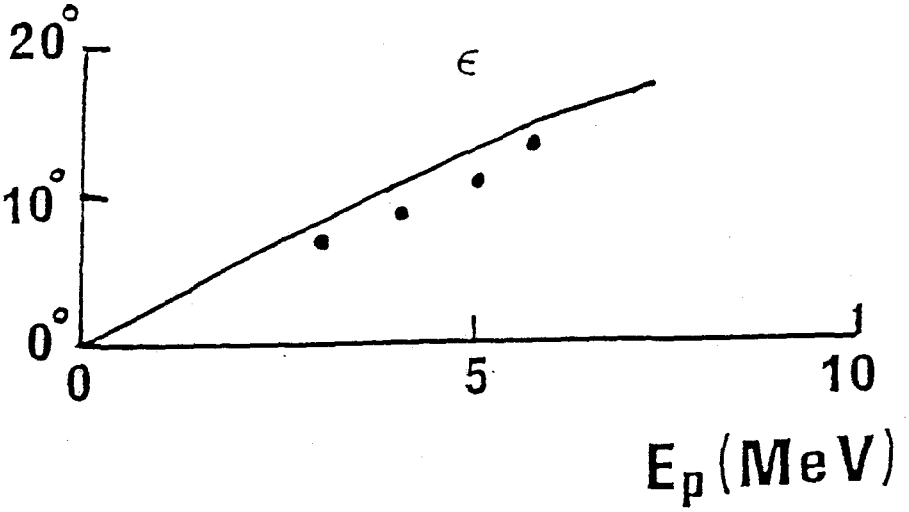

Fig. 16

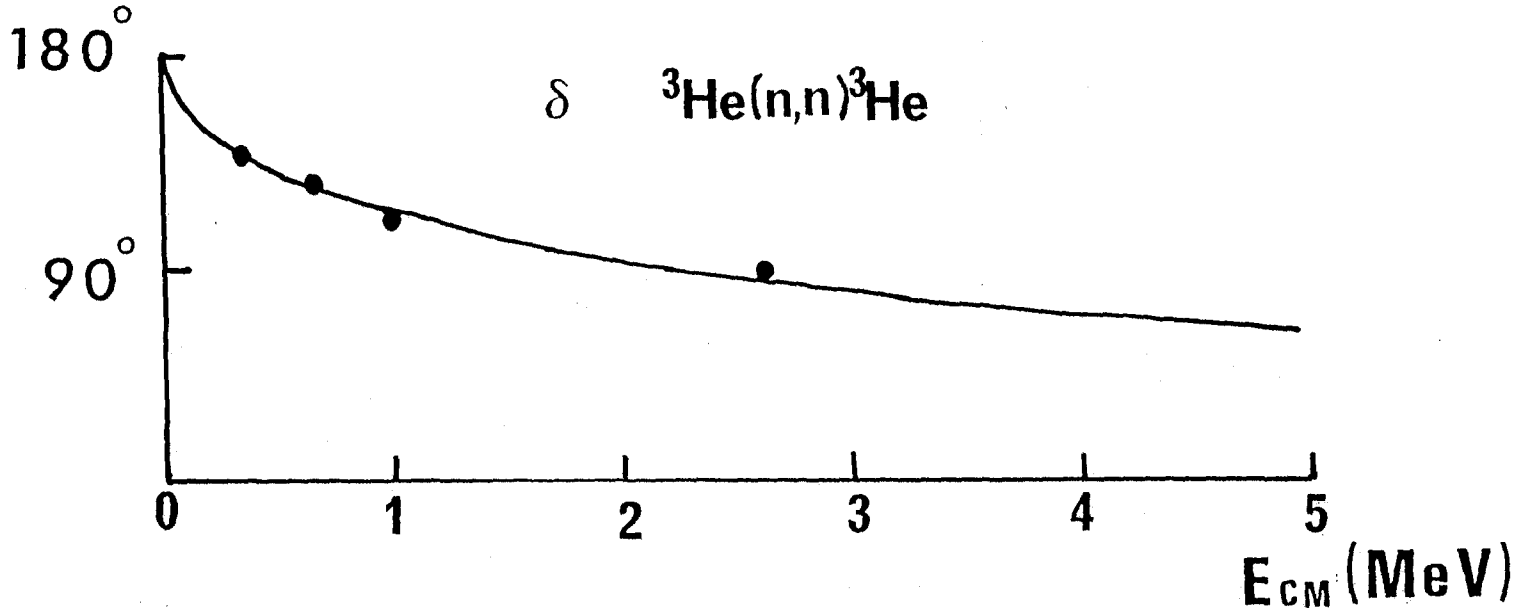

Fig. 17

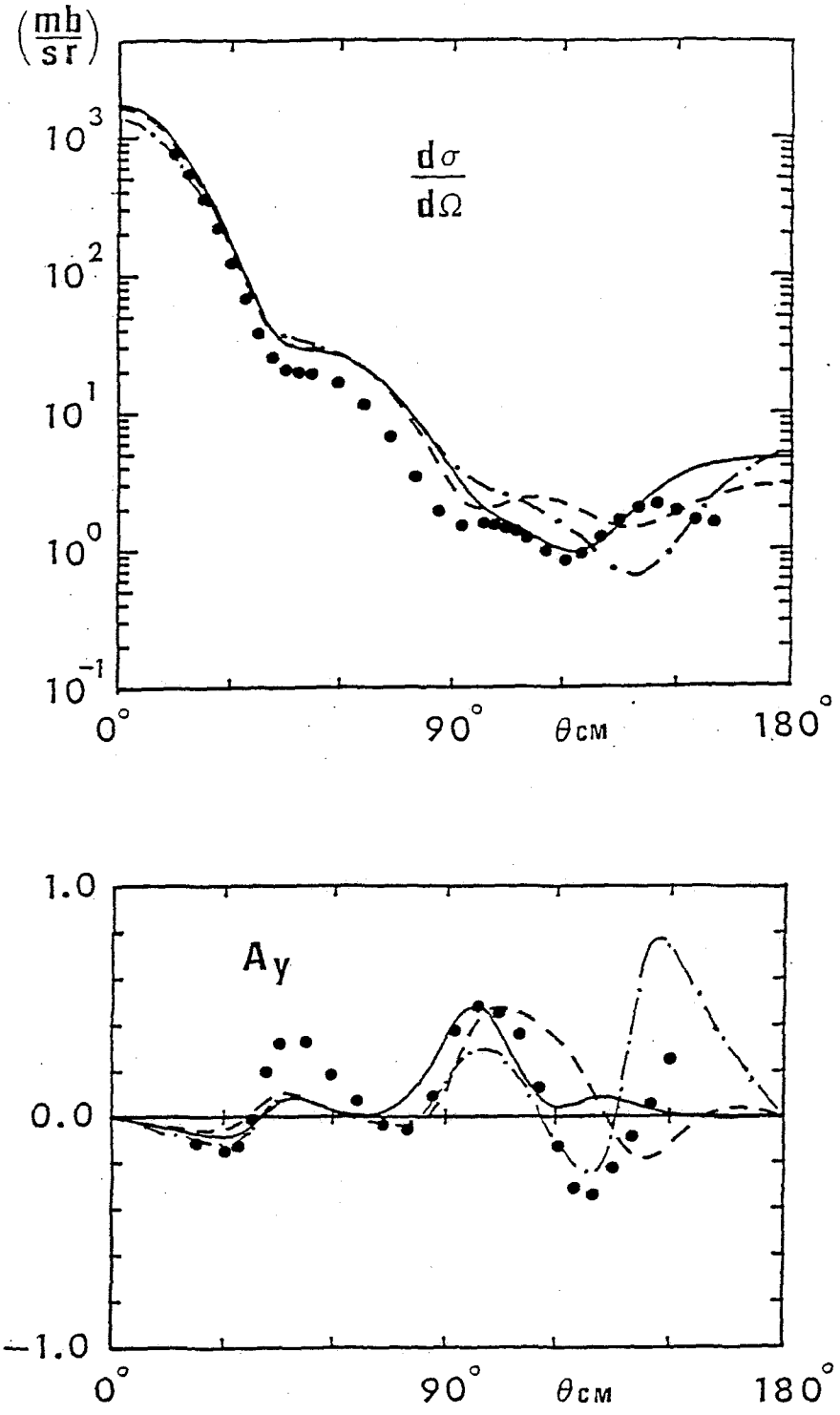

Fig. 18

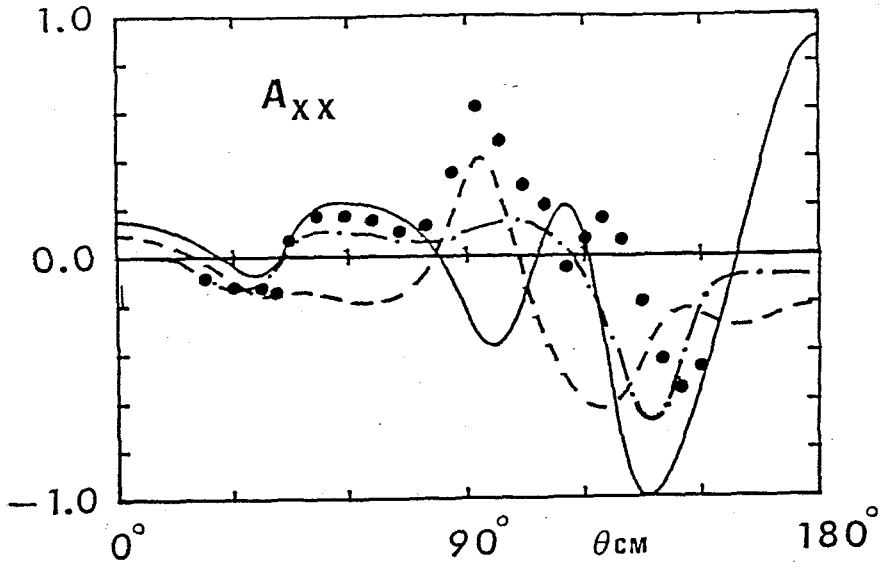
1.0
A_{xx}
0.0
−1.0
0°
90°
θсм
180°

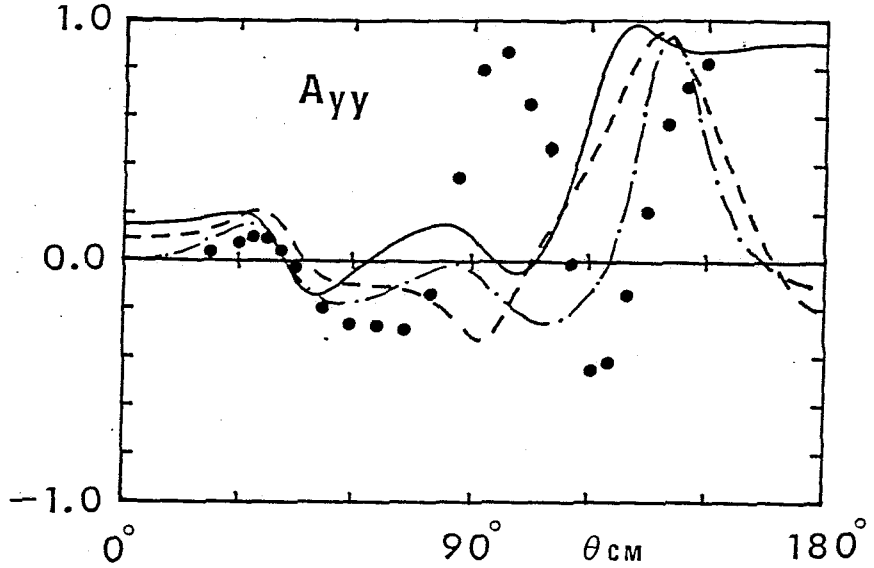
1.0
A_{yy}
0.0
−1.0
0°
90°
θсм
180°

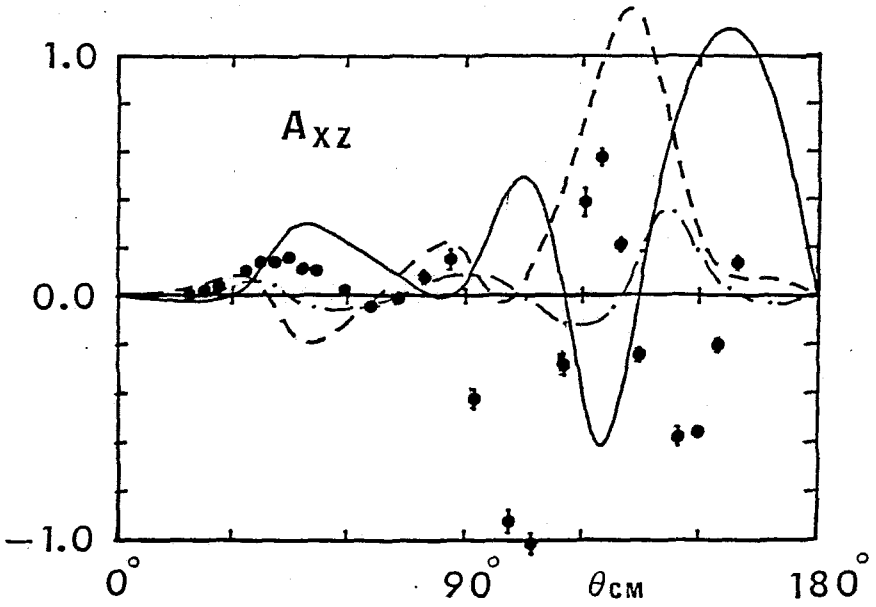
1.0
A_{xz}
0.0
−1.0
0°
90°
θсм
180°

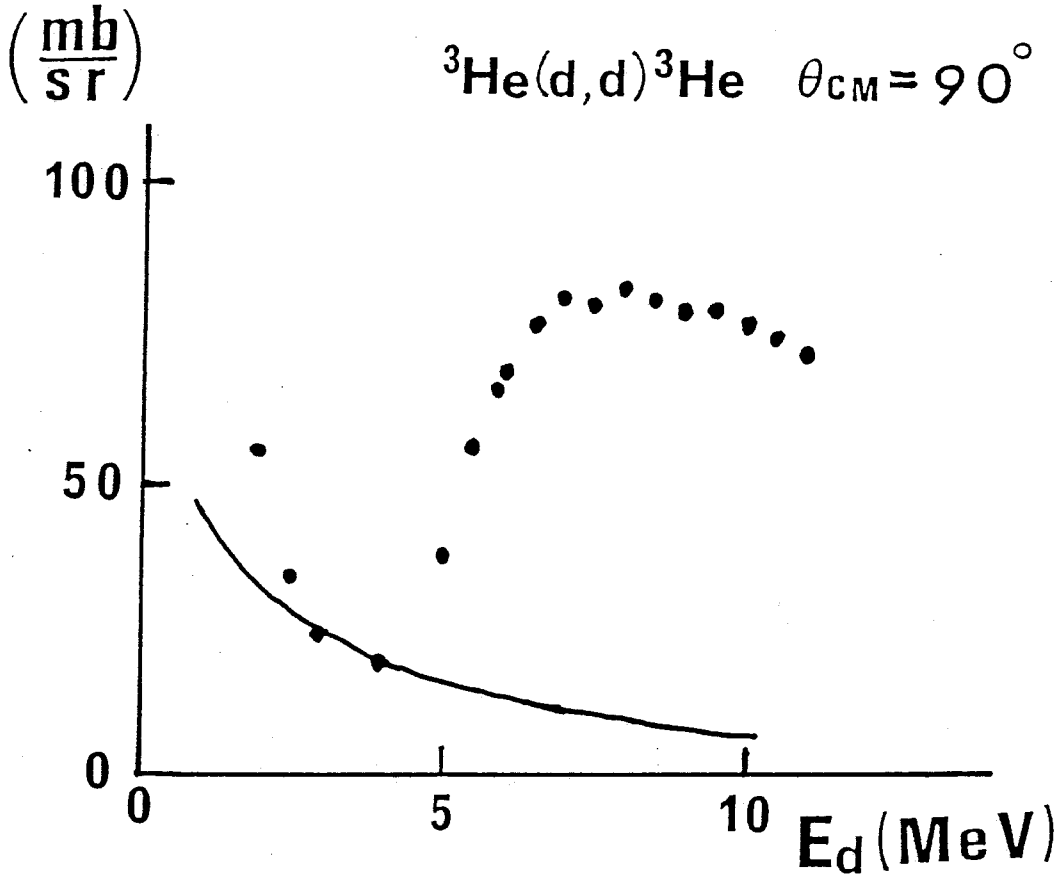

Fig. 19

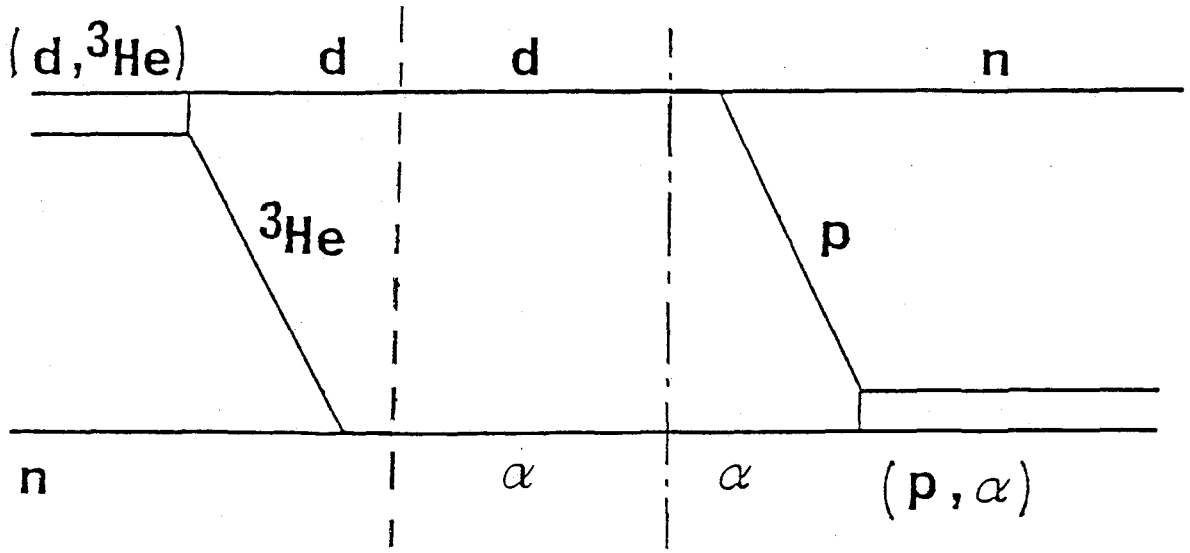

Fig. 20

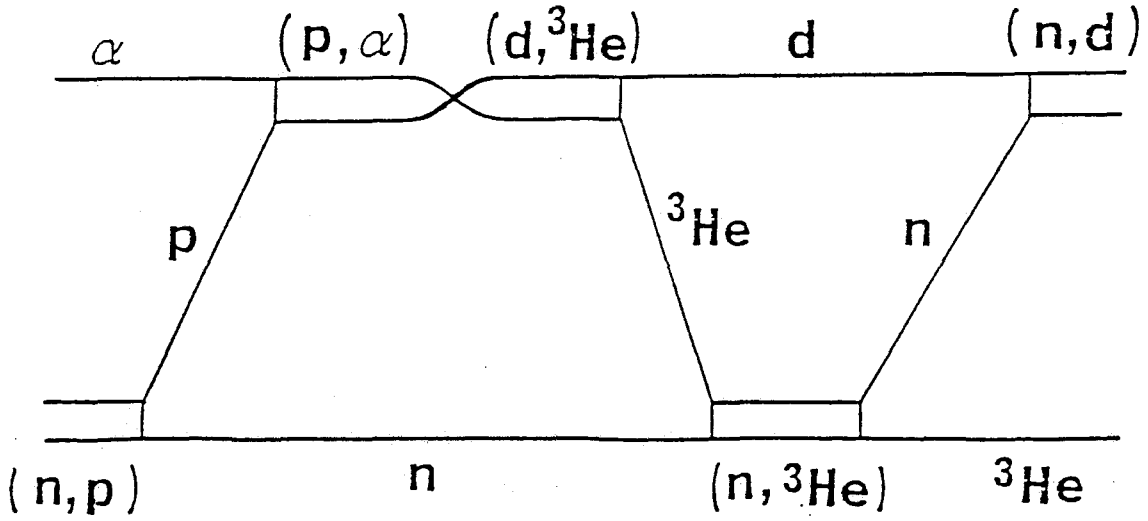

Fig. 21

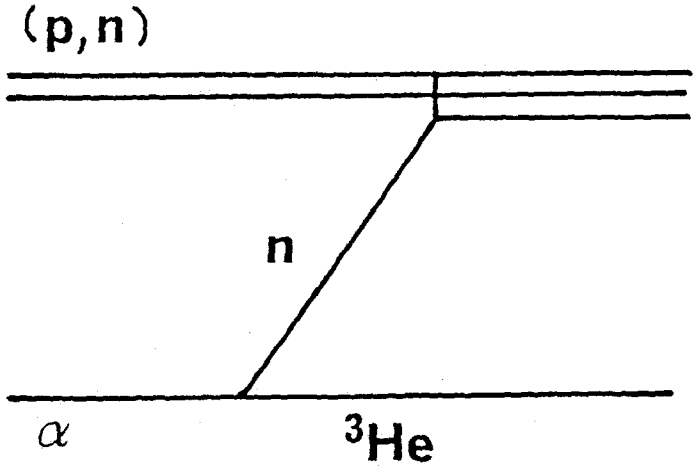

Fig. 22

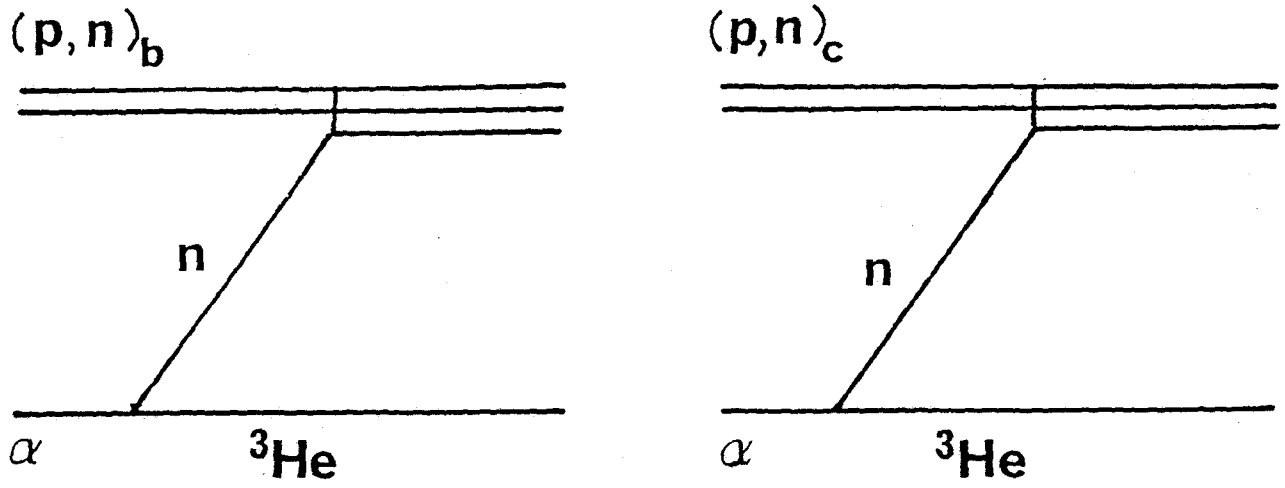

(a) (b)

Fig. 23

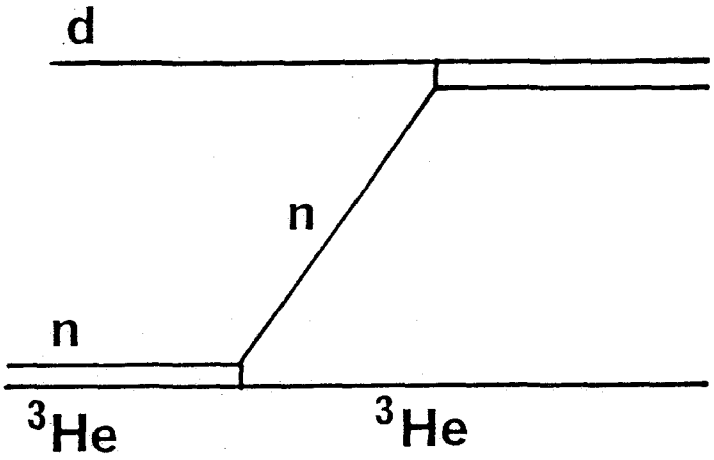

Fig. 24